

Review

Application of Electrospun Nanofibers for Fabrication of Versatile and Highly Efficient Electrochemical Devices: A Review

Seyedeh Nooshin Banitaba ¹  and Andrea Ehrmann ^{2,*} 

¹ Textile Engineering Department, Amirkabir University of Technology, Tehran 1591634311, Iran; nooshin_bt@yahoo.com

² Faculty of Engineering and Mathematics, Bielefeld University of Applied Sciences, 33619 Bielefeld, Germany

* Correspondence: andrea.ehrmann@fh-bielefeld.de

Abstract: Electrochemical devices convert chemical reactions into electrical energy or, vice versa, electricity into a chemical reaction. While batteries, fuel cells, supercapacitors, solar cells, and sensors belong to the galvanic cells based on the first reaction, electrolytic cells are based on the reversed process and used to decompose chemical compounds by electrolysis. Especially fuel cells, using an electrochemical reaction of hydrogen with an oxidizing agent to produce electricity, and electrolytic cells, e.g., used to split water into hydrogen and oxygen, are of high interest in the ongoing search for production and storage of renewable energies. This review sheds light on recent developments in the area of electrospun electrochemical devices, new materials, techniques, and applications. Starting with a brief introduction into electrospinning, recent research dealing with electrolytic cells, batteries, fuel cells, supercapacitors, electrochemical solar cells, and electrochemical sensors is presented. The paper concentrates on the advantages of electrospun nanofiber mats for these applications which are mostly based on their high specific surface area and the possibility to tailor morphology and material properties during the spinning and post-treatment processes. It is shown that several research areas dealing with electrospun parts of electrochemical devices have already reached a broad state-of-the-art, while other research areas have large space for future investigations.

Keywords: electrolytic cells; batteries; fuel cells; supercapacitors; electrochemical solar cells; sensors



Citation: Banitaba, S.N.; Ehrmann, A. Application of Electrospun Nanofibers for Fabrication of Versatile and Highly Efficient Electrochemical Devices: A Review. *Polymers* **2021**, *13*, 1741. <https://doi.org/10.3390/polym13111741>

Academic Editor: Francesco Lufrano

Received: 28 April 2021

Accepted: 24 May 2021

Published: 26 May 2021

Publisher's Note: MDPI stays neutral with regard to jurisdictional claims in published maps and institutional affiliations.



Copyright: © 2021 by the authors. Licensee MDPI, Basel, Switzerland. This article is an open access article distributed under the terms and conditions of the Creative Commons Attribution (CC BY) license (<https://creativecommons.org/licenses/by/4.0/>).

1. Introduction

Electrochemical devices have been part of our lives for a long time. They enable storing energy in batteries [1–3], supercapacitors [4–6], or fuel cells [7–9], can be used as sensors in healthcare and biotechnology [10–12], or gain solar energy [13–15].

One of the possibilities to increase the efficiency of such electrochemical devices is increasing the contact area between the different parts of the electrochemical devices, typically electrodes and electrolyte, by nanostructuring the electrodes [16–18]. Besides diverse physical and chemical methods, such a nanostructure can be achieved unambiguously by the textile technology of electrospinning.

Electrospinning belongs to the primary spinning techniques and enables spinning continuous nanofibers with typical diameters in the range of some ten to some hundred nanometers [19–21]. Recently, the needleless and needle-based electrospinning techniques are becoming more and more sophisticated, with modifications of both electrodes as well as with the support of other physical processes, such as Corona-electrospinning or magnetic-field-assisted electrospinning [22–25].

Typical applications of electrospun nanofiber mats can be found in the areas of biotechnology and biomedicine [26–29], implant scaffolds [30], micropollutant elimination [31], nanoparticle delivery [32], oil/water separation [33,34], air and water filtration [35–38], and electrochemical cells [39]. This review gives an overview of the aforementioned kinds

of electrochemical cells in which electrospun nanofiber mats are applied. As Figure 1 shows, publications about electrospun nanofiber mats used in these electrochemical cells are increasing from year to year for most sub-topics. Batteries including nanofiber mats are apparently most often investigated, while electrolytic cells based on electrospun nanofiber mats are relatively scarce and most recently did not show increasing numbers anymore. Unexpectedly, in spite of the recent ongoing discussions on fuel cells, supercapacitors have outpaced them in research during the last years. Electrochemical solar cells are only scarcely investigated. Electrochemical sensors, finally, are steadily increasing on a relatively low level. This short overview already shows that electrochemical devices based on nanofiber mats still belong to the topics in which there is much space left for new research approaches, especially in the area of electrolytic cells.

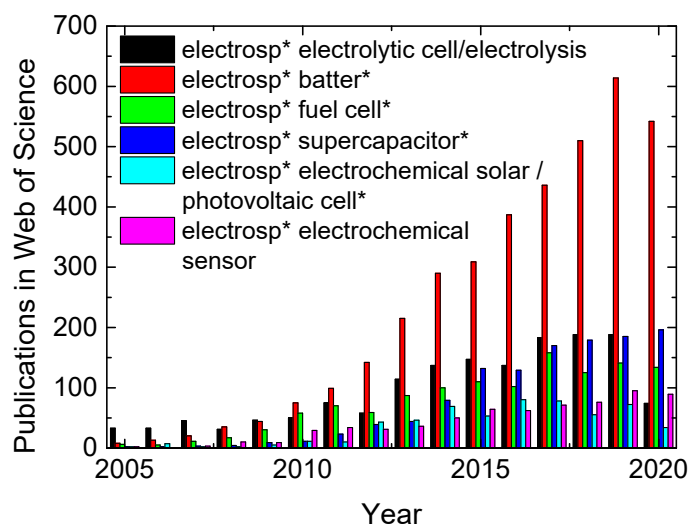


Figure 1. Publications reporting on electrospun nanofiber mats applied in electrochemical cells, found in the Web of Science during the last decades. Data accessed on 18 March 2021.

2. Electrospinning Process

The electrospinning technique has been identified as a versatile and highly efficient method for fabrication of continuous nanofibers from polymer solution or melt. Generally, an electrospinning set-up contains a high voltage power supplier, a feeding pump, a spinning apparatus (such as spinneret), and a rotational/constant collector. In electrospinning procedure, ultrathin fibers are fabricated in an electrical field created between the collector and spinneret by applying a high voltage. The applied voltage, the distance between the spinneret and collector, the feeding rate, the spinneret inner diameter, and the collector speed belong to the common electrospinning parameters which can influence morphology of the electrospun membranes as well as fiber diameters. Fiber orientation, pore size distribution, and membrane porosity are significant morphology features of the electrospun membranes. Apparently, the morphology characteristics and fiber diameter should be tuned to obtain the most appropriate electrospun fibrous structure for the considered application [40–42]. As an example, fiber orientation may lead to production of an electrochemical biosensor with high sensitivity, while it can reduce ionic conductivity of an electrospun electrolyte applicable in lithium ion batteries [43,44].

Optimum electrospinning parameters should be determined for each polymer system as they vary from polymer to polymer. Overall, increasing the applied voltage up to a critical point causes formation of finer fibers due to more stretching of the electrospinning jet resulting from higher repulsion forces in it. On the other hand, thicker or beaded electrospun fibers can be obtained by exceeding the critical voltage as a result of higher velocity as well as smaller size of the Taylor cone [45]. The electrospinning distance should be recognized regarding the evaporation rate and deposition time of the electrospinning jet to gain a uniform membrane. A short electrospinning distance may lead to formation of

ribbon-like nanofibers with large diameters, whereas thick fibers are fabricated through a high electrospinning distance [46]. In addition, a critical flow rate is essential to obtain homogenous and beadless electrospun fibers. By increasing the feeding rate beyond the critical point, defective fibers with high diameters in a wide range and large pore sizes may be obtained [47]. Moreover, the receiver type and collector speed mainly influence the fibers' orientations and so the pore sizes. As the collector speed increases, fibers with higher orientation and less porosity and pore sizes are obtained [48].

Besides the apparatus adjustments, features of the polymer solution or melt influence the membrane morphology and fibers' diameter. The role of polymer solutions on various features of the electrospun membrane depends on their concentration, viscosity, and conductivity. Enhancement of the solution concentration up to a critical point provides more entanglement between the polymer chains which results in formation of beadless fibers with higher uniformity. Nevertheless, beaded and defective fibers can be obtained beyond the critical point due to drying of the polymer solution on the applied spinneret tip. Notably similar trends have been observed for the viscosity impact on the obtained electrospun fibers by numerous researchers. Furthermore, the electrospinning process highly depends on the Coulomb forces between the electrical field and accumulated charges on the solution surface. Therefore, a polymer solution with very low conductivity cannot be electrospun due to lack of charges which are essential for formation of the Taylor cone. In contrast, polymer solutions with conductivity beyond the critical point cannot also be processed because of spreading of the fibers in the electrospinning environment [49,50].

3. Electrolytic Cells

Electrolytic cells use electrical energy to decompose chemical compounds by electrolysis. They can be set up in different forms, e.g., with two-dimensional electrode stacks, spaced without a membrane and connected in a bipolar way [51]. Alternative designs include rotating electrodes to enhance mass transfer without pumping and porous, i.e., three-dimensional electrodes [51]. Possible applications include, e.g., electrochemical CO₂ reduction [52–54], heavy metal removal from wastewater by electrodeposition [55–57], nitrogen reduction [58], nitrate removal [59,60] or depolymerization of lignin into renewable aromatic compounds [61], to name just a few.

Due to their large surface-to-volume ration, electrospun nanofiber mats could be used in several of these electrolytic cells. Unexpectedly, this is not fully reflected by the recent literature which shows only few combinations of these two techniques amongst large numbers of papers dealing with one of the topics. Manesh et al. prepared poly(vinylidene fluoride)/poly(aminophenylboronic acid) (PVdF/PAPBA) electrospun composite nanofiber mats to be inserted into electrolytic cells; however, these were used to detect glucose, i.e., they worked as sensors and not as electrodes [62]. Many papers report about using an electrolytic cell to measure the conductivity of the spinning solution (e.g., [63–65]) or apply an electrolytic cell to perform electrochemical deposition on a nanofiber mat [66,67]. As most of the authors mention, the fiber and mat morphologies play an important role for this application. Usually, finer nanofibers, providing a higher specific surface, are preferred [62,63]. In addition, some electrospinning processes allow for producing nanofibers with pores or even with additional dendrite-like structures on the fiber surface [64] which further increases the specific surface and thus the contact area to the surrounding material.

Electrolysis based on electrospun nanofibers mats can, e.g., be found in some dye-degradation applications. Sun et al., for example, used activated carbon nanofibers modified with carbon nanotubes (CNTs) as electrodes for the electrochemical degradation of methyl orange (Figure 2) [68]. Li et al. prepared poly(acrylonitrile) (PAN) and Fe/PAN electrodes by electrospinning and reported an increase of the electrochemical degradation due to the higher specific surface area (SSA) and higher amount of mesopores [69]. Hwang et al. showed that carbon nanofibers, prepared by electrospinning followed by stabilization and carbonization, supported the toluene removal efficiency by electrolysis when used as cathodes or anodes [70].

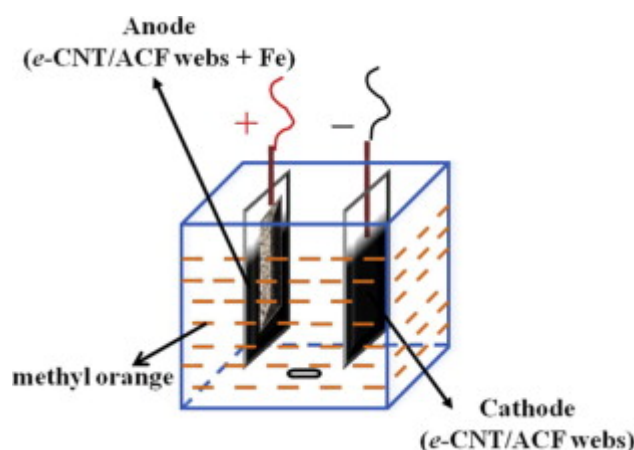


Figure 2. Scheme of the electrolytic cell used for methyl orange degradation. Reprinted from [68], with permission from Elsevier.

Degradation of organic particles was examined by Kim et al., using bisphenol A as a model substance. They prepared Sb-doped SnO_2 nanofibers by electrospinning SnCl_2 and SbCl_3 with polyvinylpyrrolidone (PVP) dissolved in a dimethylformamide (DMF) solution, partly with a shell containing RuO_2 , followed by calcination of the polymer. These materials were investigated as anodic materials for anodic oxidation of bisphenol A and found highly suitable for this application, with an eleven-fold faster organic oxidation than the reference of pure RuO_2 nanofibers combined with low noble metal content [71].

Recently, Chen et al. used electrospun polyethylene oxide (PEO)/ionomer/graphene oxide (GO) nanofiber mats for water dissociation and found high stability under repeated cycling, even for high current densities. These findings let the authors suggest such three-dimensional bipolar membranes for the application in CO_2 electrolysis devices where high current densities are applied [72].

The electrocatalytic activity of Pt- IrO_2 electrospun nanofibers in water electrolysis was investigated by Wang et al. [73]. They found that, for different ratios of Pt to Ir, these nanofiber mats showed better catalytic performance than commercial IrO_2 catalysts and at the same time reduced the amount of expensive Ir.

Mugheri et al. used NiO nanostructures deposited on MoS_2 nanofiber mats for water splitting. For electrospinning, the NiO nanostructures were inserted together with ammonium phosphomolybdate hydrate and PVP into a spinning solution. The nanofiber mat was afterwards calcinated at $500\text{ }^\circ\text{C}$ to remove the polymer. This electrocatalyst nanofiber mat showed good stability, durability, and high efficiency in the hydrogen evolution reaction [74].

Similarly, diverse other materials were electrospun by using different polymers as spinning agents and different metals to form the final nanofiber mat after calcination, and applied for electrocatalytic water splitting, i.e., hydrogen or oxygen evolution reaction. Some of these metals or metal oxides are Co_3O_4 [75], $\text{Co/Mo}_2\text{C}$ [76], and $\text{Ni}_3\text{V}_2\text{O}_8$ nanocube decorated nanofibers [77].

Other applications of nanofiber mats in electrolytic cells are, e.g., disinfection of water from bacteria by combining electrolysis with physical filtering through a PAN/polyurethane (PU)/polyaniline(PAni) nanofiber mat with embedded single-walled carbon nanotubes [78]; elimination of urea from wastewater by electrospun Ni/C nanofiber mats [79]; and N_2 fixation to NH_3 by the electrocatalytic nitrogen reduction reaction, e.g., by carbon nanofibers with embedded MnO nanocrystals [80].

As these examples show, electrospun nanofiber mats are mostly applied in electrocatalytic water splitting and degradation of dyes and other contaminants. This recent restriction on a relatively small range of research topics within the field of electrolytic cells suggests broadening the possible range of applications of nanofiber mats from diverse materials by further research in neighboring regions.

4. Batteries

Rechargeable or secondary batteries are electrochemical power sources commonly utilized in portable devices such as camcorders, mobile phones, laptops, and electric transportations. In general, batteries are comprised of one or more electrochemical cells. Positive electrode (cathode), negative electrode (anode), porous separator membrane, and ionic conductive electrolyte are the essential components for fabrication of each electrochemical cell. Lead-acid, nickel cadmium, and lithium ion belong to the well-known secondary batteries. However, lithium ion batteries (LIBs) have shown superior advantages compared with the other rechargeable ones. High specific energy density as well as small size and low mass are outstanding and distinctive characteristics of the LIBs [81,82].

Increasing progress in technology has forced researchers to design batteries with higher energy density, lighter weight, and more flexible structure. A basic LIB comprises of a lithium metal oxide electrode as cathode, a graphite-based anode, a porous polypropylene (PP) or polyethylene (PE) film as separator, and a lithium salt/solvent solution as electrolyte (Figure 3). Charge/discharge procedure of the LIBs is performed through chemical reactions. During the charge process, free lithium ions migrate from the cathode toward the anode, via diffusion into the ionic conductive electrolyte. Simultaneously, the electrons travel toward the anode through the external circuit and form LiC_6 compound in the anode material. Apparently, the reverse behavior takes place in the discharge step [81,82]. Over the past decades, most research in advanced development of LIBs has emphasized the use of electrospun fibers for fabrication of versatile and highly efficient components [83,84]. Recent progresses in the fabrication of electrospun cathode, anode, separator, and electrolyte are provided in the following section.

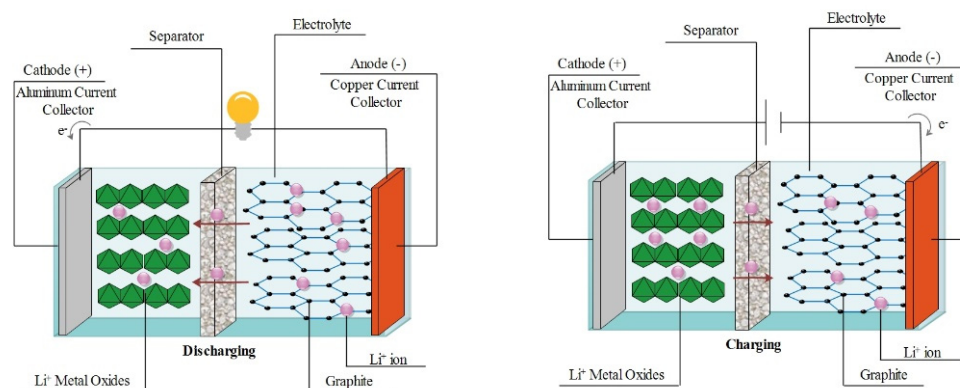


Figure 3. Schematic showing the intercalation mechanism in Li-ion batteries through charge and discharge. Reprinted from [85], with permission from Elsevier.

4.1. Electrospun Cathode Materials

Electrochemical performance of the batteries, such as potential window and storage capacity, is mostly affected by the cathode material. In fact, the number of extracted lithium ions from the cathode electrode determines the battery capacity. The energy could be stored in the cathode materials through two various conversion and intercalation techniques. In the conversion mechanism, lithium insertion and extraction are associated with changes in the crystalline structure of the applied cathode material, while the cathode structure acts as a host in the intercalation mechanism. So, the lithiation/delithiation can reversibly occur in the intercalation cathode materials. Notably, low electron conduction as well as high volume expansion have been reported as challenges linked with the conversion cathode materials. Therefore, the intercalation cathode structures have received more attention from numerous researchers. Among various types of intercalation structures (transition metal oxides, chalcogenides, and poly anions), transition metal oxides and poly-anionic compounds have displayed superior characteristics such as higher energy

storage and greater operating voltage, while development of chalcogenide materials has been influenced by their irreversible structure [86,87].

Layered structures have been identified as the most widely applied electrode materials in the commercial LIBs. They are commonly presented by the chemical formula of LiXO_2 , where X could be Co, Mn, or Ni. This group of cathode materials was first introduced by discovering of LiCoO_2 in the 1990s. During discharging, LiCoO_2 hexagonal cells are formed in layered structures, whereas $\text{Li}_{1-x}\text{CoO}_2$ monoclinic phases are created as a result of Li^+ ion removal during the charging procedure. The structural instability of LiCoO_2 cathode material is a major drawback associated with these materials which has resulted in lower practical capacity ($140 \text{ mAh}\cdot\text{g}^{-1}$) compared with the reported theoretical capacity ($280 \text{ mAh}\cdot\text{g}^{-1}$). So, LiNiO_2 was introduced to address the low experimental storage capacity. However, poor thermal stability, along with low electrochemical activity restricts practical usage of the layered LiNiO_2 . Therefore, $\text{LiNi}_{0.5}\text{Mn}_{0.5}\text{O}_2$ was presented by Ohzuku et al. as a modified compound. Based on various analyses, this cathode material has revealed appropriate structural stability due to the existence of Mn^{4+} cations. In addition, it has represented a stable structure up to 300°C , which is a crucial function for being applied in commercial batteries. Moreover, it has shown superior storage capacity ($200 \text{ mAh}\cdot\text{g}^{-1}$) compared with the LiCoO_2 layered structure, although limitation of Li^+ ion extraction due to presence of Ni in the cathode material has caused synthesis and evaluation of $\text{LiCo}_x\text{Ni}_y\text{Mn}_{1-x-y}\text{O}_2$ ternary compound materials such as $\text{LiCo}_{1/3}\text{Ni}_{1/3}\text{Mn}_{1/3}\text{O}_2$ [85,88].

Spinel oxides with the general chemical formula of LiM_2O_4 (e.g., LiMn_2O_4) are another group of cathode materials. Compared with layered structures, they are safer and more affordable. Three-dimensional paths in such structures facilitate Li^+ ion diffusion and therefore enhance the rate capability. Nevertheless, capacity fading is a critical disadvantage associated with these materials. To overcome the aforementioned obstacle, doping mechanism has been widely reported to reduce Jahn-Teller active Mn^{3+} ions and thus to enhance the electrochemical characteristics. Mg, Ni, Cr, Al, and many more metal elements belong to the applied dopant materials. As an example, $\text{LiNi}_{0.5}\text{Mn}_{1.5}\text{O}_4$ compound has illustrated superior rate capability and wider potential window compared with LiMn_2O_4 spinel oxide structure [89,90].

Poly-anionic compounds, with the general chemical structure of $(\text{XO}_4)^{3-}$ ($\text{X} = \text{P}, \text{Si}, \text{S}$, etc.), have also received much attention as cathode material of Li-ion batteries. LiFePO_4 and LiMnO_4 are of the well-known poly-anionic cathode materials. This could be linked with their great power capability and proper structural stability. Nevertheless, low conductivity of the aforementioned materials has restricted their applications [91,92].

Synthesis of highly efficient cathode materials is considered as a key building block toward progress of energy storage systems with high power and proper capacity in the future. Numerous researchers have illustrated great potential of the electrospun structures as cathode material of the Li-ion batteries. Besides storage capacity, cycling stability is considered as an important parameter for determination of the efficiency and capability of a designed cathode material. Cycling durability is measured by calculation of the storage capacity in various cycles. Apparently, a more ideal battery structure would be obtained through increment of the cycling stability. Commercial LIBs normally show cycling stability during first 300 to 500 cycles (or about 2 to 3 years) [93,94]. As an example, electrospun LiCoO_2 fibers ($148 \text{ mAh}\cdot\text{g}^{-1}$) result in higher cyclic stability compared with the LiCoO_2 powders ($138 \text{ mAh}\cdot\text{g}^{-1}$) [95]. Notably, the enhanced capacity of the nanofibrous structures could also be further improved through modification of the electrospun fibers by coating methods. In addition, electrospun LiM_2O_4 structures provide faster diffusion of the lithium ions as well as the promoted cycling stability. In fact, the highly porous structure of the electrospun fibers leads to reduction of the degradation rate during charging/discharging processes [96,97]. Moreover, presence of the carbon nanofibers in the poly-anionic compounds such as LiFePO_4 compensates the poor ionic conductivity of this category of cathode materials and causes approaching a more appropriate rate capability [98]. The

most recent approaches in fabrication of electrospun fibers applicable as cathode materials are summarized in Table 1.

Table 1. The most recent approaches toward fabrication of nanofibrous cathodes.

Material	Capacity (mAh·g ⁻¹)	Cycling Stability	Autor (Year)	Ref.
Li ₂ CoTi ₃ O ₈ /TiO ₂	82 at 0.1 C	83% after 25 cycles	Kap et al. (2020)	[99]
LiFePO ₄ nanocrystals/carbon nanofibers (CNFs)	152 at 0.5 C	98.2% after 500 cycles	Cao et al. (2020)	[100]
V ₂ O ₅ /GO	342 at 0.5 C	80% after 20 cycles	Ahmadian et al. (2020)	[101]
Li ₂ MnTiO _{4+z}	210 at 0.1 C	95.3% after 100 cycles	Vu et al. (2020)	[102]
LiFe _{0.8} Mn _{0.2} PO ₄ /C	169.9 at 0.1 C	160 after 200 cycles	Chen et al. (2020)	[103]
LiFe _{0.4} Mn _{0.6} PO ₄ /CNFs	133.5 at 1 C	138.8 after 100 cycles	Yang et al. (2020)	[104]

4.2. Electrospun Anode Materials

Intercalation-, conversion-reaction-, and alloying-reaction-based materials are various categories which have been applied as anodes of LIBs. In the intercalation group, the Li⁺ ions are placed between the layers of the utilized anode material. Graphite is the most well-known intercalation-based anode structure. In the low voltage range (<0.25 V), high capacity of 360 mAh·g⁻¹ along with 100% discharge/charge efficiency have been recorded for this anode structure, whereas most of the electrolyte solvents (e.g., ethylene carbonate (EC), propylene carbonate (PC), and so on) are decomposed between 0.5 and 0.7 V, resulting in the formation of a solid–electrolyte interface (SEI) layer. It is worth noting that proper ionic conductivity, low electrical conductivity, and great stability are the essential characteristics of the ideal SEI layer. Overall, poor capacity is a major drawback associated with the graphite anode materials [105,106].

Surface-to-volume ratio enhancement of the applied anode material is an effective method toward providing more accommodations for the Li⁺ ions. Therefore, various studies have been devoted to fabrication of carbonaceous nanomaterials. PAN is the most common precursor for synthesis of electrospun carbon fibers. This could be linked with the simple fabrication procedure, proper mechanical characteristics, and affordable cost. However, environmental concerns associated with DMF, an essential solvent for dissolving PAN polymer, has led to investigation for new precursor resources including lignin, polyvinyl alcohol (PVA), and many more [105,106]. Kim et al. [107] reported a large capacity of 450 mAh·g⁻¹ derived from the electrospun PAN nanofibers. In another attempt, Chen et al. [108] introduced a large capacity of 1150 mAh·g⁻¹ at 0.1 A·g⁻¹ for a hollow CNT/CNF composite. In addition, Culebras et al. [109] claimed a high capacity of 611 mAh·g⁻¹ after 500 cycles for a CNF mat obtained from lignin/poly(lactic acid) (PLA) precursor. Moreover, Nan et al. [110] revealed a large capacity of 841 mAh·g⁻¹ for a carbon nanofiber membrane synthesized from a PVA precursor. Notably, fabrication of porous and hollow CNFs could result in enhancement of the discharge capacity through increment of the Li⁺ ions' spaces. Further, it causes easier interaction between electrode and electrolyte components by reduction of the distances between ions and electronics [111].

Conversion-reaction-based anode materials work based on the faradic reaction. Metal oxides (e.g., Co₃O₄, Cu₂O, etc.), metal nitrides (M_xN_y, where M is Ni, Fe, Mo, etc.), metal sulfides (M_xS_y, where M is Ni, Fe, Mo, etc.), and metal phosphides (Li_xM_yP₄, where M is V, Cu, Ti, etc.) are of the conversion-reaction-based structures. These kinds of anode structures are able to provide capacity in the range from 350 mAh·g⁻¹ (Cu₂S) to 1800 mAh·g⁻¹ (MnP₄). Despite the high capacity, the conversion-reaction-based materials suffer from low potential, poor cycling durability, and high volume changes during extraction and insertion of the Li⁺ ions. In order to suppress volume changes of the conversion-reaction-based anode structures, fabrication of porous nanomaterials has received wide attention. Existence of pores in such materials manages the volume changes during lithiation/dilithiation processes through providing sufficient spaces for extraction and contraction of the applied anode material. In addition, combination of these materials with the carbonaceous structures has been claimed as another effective method for control of the volume changes [105,106]. Zhang et al. [112] reported a large capacity of 835 mAh·g⁻¹ at 0.2 A·g⁻¹ after 100 cycles

for a $\text{Mn}_3\text{O}_4/\text{CNF}$ composite membrane. In addition, a CoO/CNF three-dimensional mat revealed large discharge capacity of $853.5 \text{ mAh}\cdot\text{g}^{-1}$ after 100 cycles [113]. Moreover, electrospun NiO fibers have exhibited a discharge capacity of $784 \text{ mAh}\cdot\text{g}^{-1}$ at $0.08 \text{ A}\cdot\text{g}^{-1}$ [114].

Alloying-reaction-based materials have been considered as the third category of anode structures. Various metals which are able to be alloyed with lithium (such as Se, S, etc.) are classified in this group. During the charging procedure, lithium ions make an alloy with the applied alloying-reaction-based structures. The aforementioned class of anode structures could reveal various capacities based on the applied alloying metal ranging from $660 \text{ mAh}\cdot\text{g}^{-1}$ (Sb) to $4200 \text{ mAh}\cdot\text{g}^{-1}$ (Si). The major drawback linked with this materials are volume changes during insertion and extraction of the lithium ions, which could be suppressed by size reduction of the applied particles as well as combination with the carbonaceous materials [105,106]. Jang et al. [115] revealed a discharge capacity of $560 \text{ mAh}\cdot\text{g}^{-1}$ after 80 cycles for an electrospun $\text{Co-Sn}/\text{CNF}$ composite. In addition, a high discharge capacity of $830 \text{ mAh}\cdot\text{g}^{-1}$ at $0.4 \text{ A}\cdot\text{g}^{-1}$ after 100 cycles was claimed for the Si/CNF three dimensional structure [116]. Furthermore, a SnS/CNF composite membrane presented $648 \text{ mAh}\cdot\text{g}^{-1}$ discharge capacity at $0.2 \text{ A}\cdot\text{g}^{-1}$ after 500 cycles [117]. Table 2 describes some of the most recent advancements carried out for the fabrication of highly efficient electrospun anodes.

Table 2. Summarization of some of the most recent approaches toward fabrication of nanofibrous anodes.

Material	Energy Storage Mechanism	Capacity ($\text{mAh}\cdot\text{g}^{-1}$)	Autor (Year)	Ref.
CNF	Intercalation	294 at $0.2 \text{ A}\cdot\text{g}^{-1}$	Li et al. (2020)	[118]
MnCo_2O_4		701 at $0.5 \text{ A}\cdot\text{g}^{-1}$	Zhu et al. (2020)	[119]
TiO_2/CNF	Conversion reaction	399	Su et al. (2020)	[120]
$\text{Fe}_3\text{O}_4/\text{CNF}$		1635 at $1 \text{ A}\cdot\text{g}^{-1}$	Liu et al. (2020)	[121]
$\text{Sn}_4\text{P}_3/\text{CNF}$		710	Ran et al. (2020)	[122]
P/CNF	Alloying reaction	730 at $0.1 \text{ A}\cdot\text{g}^{-1}$	Libérale et al. (2020)	[123]
Si/PCNF		1033 at $5 \text{ A}\cdot\text{g}^{-1}$	Tian et al. (2020)	[124]
$\text{SnP}_{0.94}/\text{CNF}$		750 at $0.1 \text{ A}\cdot\text{g}^{-1}$	Yadav et al. (2020)	[125]
SnSe/CNF	Conversion/Alloying reactions	405 at $1 \text{ A}\cdot\text{g}^{-1}$	Xia et al. (2020)	[126]
SnSe/N-doped CNF		460 at $0.2 \text{ A}\cdot\text{g}^{-1}$	Shaji et al. (2020)	[127]

4.3. Electrospun Separator

The separator is another essential key component of LIBs. Prevention of the contact between positive and negative electrodes and transportation of the Li^+ ions between the electrodes, along with retaining the liquid electrolyte are apparent responsibilities of this crucial element. Regarding the role of a separator part in LIBs, an ideal separator must provide sufficient ionic conductivity, wettability, and permeability. In addition, dimensional, thermal, and electrochemical stabilities are other vital characteristics of an appropriate separator. Porous PP or PE membranes are common structures utilized as separators in LIBs. However, poor conductivity as well as low wettability are the most well-known downsides associated with these kinds of separators. Among various techniques applied for the fabrication of ideal separators, electrospun membranes have revealed more appealing features. The highly porous structure of the nanofibrous mats, interconnected pores, and large surface-to-volume ratios of the electrospun fibers provide proper wettability and permeability for separators [128,129].

The electrospun separators are mainly divided into four classes, including: monolayer, multilayer, modified, and composite membranes. Monolayer separators are mainly fabricated from one polymeric precursor such as PVDF [130], polyimide (PI) [131,132], PAN [133,134], and so on, while multilayer membranes are obtained by sequential fabrication of various polymer precursors. In this method, appropriate advantages of the various polymers (such as thermal stability, dimensional stability, electrochemical performance, etc.) could be attained in one separator membrane. PVDF/poly(m-phenylene isophthalamide) (PMIA) [135], PVDF/polyethylene terephthalate (PET) [136], PVDF/PI [137], and poly-

sulfonamide (PSA)/PET [138] are some of the reported multilayer electrospun separators. Post-treatment of the electrospun fibrous membranes is a great technique for modification and improvement of various characteristics. Dip-coating [139,140], in situ polymerization [141,142], and atomic layer deposition [143] are significant modification methods. In such procedures, a material is introduced into the electrospun separator, which results in improvement of its final properties. Direct electrospinning of the combination of two polymer solutions (e.g., PAN/PU [144], PAN/Lignin [145], PSA/PVDF-HFP [146], and so on) or filler-loaded polymer solution (e.g., PAN/SiO₂ [147], PI/Al₂O₃ [148], Nylon6,6/TiO₂ [149], etc.) leads to the fabrication of composite separator membranes with enhanced hydrophilicity and heightened thermal stability. Besides the role of the polymer type, the morphology of the electrospun fibers also influences the obtained electrochemical behavior. As an example, fabrication of finer fibers results in increment of electrolyte uptake and so enhancement of the ionic conductivity. Therefore, the morphology of the electrospun fibers should be tuned to approach appropriate electrospun separators with proper electrochemical characteristics [150]. A summary of the recent progresses in the fabrication of electrospun separators is provided in Table 3.

Table 3. Recent approaches toward fabrication of electrospun separator applicable in Li-ion batteries.

Material	Porosity (%)	Tensile Strength (MPa)	Electrolyte Uptake (%)	Ionic Conductivity (mS·cm ⁻¹)	Autor (Year)	Ref.
PAN	67.7	11.3	478.2	1.97	Dong et al. (2020)	[151]
PAN/PBS	59.3	7.66	665	2.1	Wei et al. (2020)	[152]
PVA/ZrO ₂	78	14.5	350	2.19	Xiao et al. (2020)	[153]
PI/Al ₂ O ₃	81	-	912	-	Iaritphun et al. (2020)	[154]
PVDF-HFP/SiO ₂	89.7	5	483	-	Xu et al. (2020)	[155]
PVDF-HFP/PI	85.9	9.76	483.5	1.78	Cai et al. (2020)	[156]
PVDF-HFP/LAGP	-	-	215	3.18	Liang et al. (2021)	[157]
PVDF/TPP/CA	90	6.9	301	4.4	Chen et al. (2020)	[158]
PAN/HCNFs@PVDF/UiO-66	77.61	24.77	570.97	1.59	Fa et al. (2021)	[159]

4.4. Electrospun Electrolyte

Cycle life, power density, and safety of LIBs are influenced by their electrolyte elements. In batteries, the electrolyte component transports the Li⁺ ions between the electrodes to complete the charge and discharge cycles. In the commercial LIBs, liquid electrolytes, consisting of an organic solvent and a lithium salt, are mainly utilized to fabricate the electrochemical cells. However, flammability of the applied solvents requires metallic sealing for the battery, which results in the production of heavy, inflexible, and expensive cells. Solvent-free electrolytes have been widely recommended as a solution toward fabrication of lightweight, safe, and cost-effective batteries. In such electrochemical cells, the solid electrolyte structure supports the role of both electrolyte and separator. In fact, it prevents the contact between electrodes and transports the Li⁺ ions between them. All-solid-state electrolytes are generally synthesized based upon polymeric structures and inorganic solid materials [160,161].

Polymeric solvent-free electrolytes are synthesized based on dispersion of a lithium salt (LiBF₄, LiClO₄, LiTFSI, etc.) in a polymer matrix (e.g., PAN, PVDF, PEO, poly(methyl methacrylate) (PMMA), etc.). They are mainly fabricated in the formation of casted films. Poor ionic conductivity has been claimed as the main drawback of the polymeric electrolytes. Formation of polymer/salt crystalline phases has been introduced as one of the inhibitor parameters for Li⁺ ion movements during cycling processes. In such combinations, Li⁺ ions are transported between the electrodes through polymer chain local motions or hopping mechanism. So, reduction of the glass transition temperature as well as increment of the amorphous regions are key solutions for enhancement of the ionic conductivity of the polymer films [161,162]. Therefore, introduction of particulate fillers

(such as SiO₂ [163], Al₂O₃ [164], TiO₂ [165], and many more) and plasticizer molecules (such as EC, PC, etc.) into the polymer matrix have been reported as influential methods for enhancement of the ionic conductivity. Particulate fillers placed between polymer chains of the utilized polymer matrix cause reduction of the crystalline phases. Thus, the polymer chains would be able to move easily and so accelerate transportation of the Li⁺ ions. In addition, inserted fillers enhance ion pair dissociation of the applied lithium salts, which obviously influences the ionic conductivity [163–165]. In 2017, Freitag et al. reported higher conductivity of the electrospun solvent-free electrolytes in comparison with that of the casted ones. Based on this research, PEO/SN/LiBF₄ electrospun electrolyte could exhibit a high ionic conductivity of 0.2 mS·cm⁻¹ [166]. In a similar research, they showed a high ionic conductivity of 0.1 mS·cm⁻¹ for the electrospun PEO/SN/NaBF₄ membrane [167]. Higher ionic conduction of the solvent-free electrospun structures compared with that of the solution-casted membranes are linked with two main issues. First, small pores between the electrospun fibers are excellent pathways for transportation of the Li⁺ ions. Second, fast evaporation of the solvent during electrospinning procedure does not allow the polymer chains and lithium salts to form polymer/salt crystalline regions. So, concentration of the free lithium ions increases in the electrospun membranes, leading to enhancement of the ionic conductivity [43,168]. It is worth noting that electrochemical behavior of the electrospun mats highly depends on the morphology of the fabricated fibers. Based on the obtained results, ionic conductivity could be enhanced by reduction of the average fiber diameter to an optimum range. This may be linked with formation of tiny pores and so more ideal pathways for fast transportation of the Li⁺ ions. Nevertheless, further decrement in average diameter of the fabricated fibers could result in reduction of the ionic conductivity. This trend is attributed to formation of more crystalline regions in the structure of finer fibers as well as superior density of the electrospun fibrous mats containing thinner fibers [43,169]. A comparison between ionic conductivity of the electrospun and solution-casted electrolytes with similar chemical compositions is provided in Table 4.

Table 4. Ionic conductivity of the electrospun and solution-casted membranes with similar chemical compositions.

Material	Fabrication Method	Ionic Conductivity (mS·cm ⁻¹)	Author (Year)	Ref.
PEO/PC/LiClO ₄	Casting	1.7 × 10 ⁻³	Banitaba et al. (2019)	[170]
	Electrospinning	5 × 10 ⁻²		
PEO/Li(TFSI)	Casting	1 × 10 ⁻³	Walk et al. (2018)	[171]
	Electrospinning	4.4 × 10 ⁻³		
PEO/EC/LiClO ₄	Casting	8 × 10 ⁻³	Banitaba et al. (2020)	[169]
	Electrospinning	1.72 × 10 ⁻¹		
PEO/EC/LiClO ₄ /Al ₂ O ₃	Casting	4.4 × 10 ⁻³	Banitaba et al. (2019)	[172]
	Electrospinning	5.9 × 10 ⁻²		

Inorganic solid materials have also been evaluated as applicable all-solid-state electrolyte in the LIB structures. Crystalline structure of such materials facilitates fast migration of the Li⁺ ions between the positive and negative electrodes. Garnet-type, LISICON-like, NASICON-like, and Argyrodite are well-known inorganic solid structures which are able to reveal high ionic conductivity as high as the liquid electrolytes. As an example, lithium germanium phosphorous sulfide (Li₁₀GeP₂S₁₂), classified in the LISICON-like category, has shown a high ionic conductivity of 10 mS·cm⁻¹ at room temperature. Nevertheless, the existence of rare and expensive elements in the structure of inorganic solid materials, along with low flexibility, has restricted their practical usage. To overcome the aforementioned obstacles, several researchers have suggested applying electrospun inorganic solid materials as fillers in the polymeric membranes [173–175]. So, a high ionic conductivity of 0.25 mS·cm⁻¹ has been reported for a PEO-based polymeric membrane incorporated with the electrospun Li_{6.4}La₃Zr₂Al_{0.2}O₁₂ fillers [173]. In addition, ionic conductivity of a PAN-based casted film was enhanced up to 0.24 mS·cm⁻¹ through introduction of Li_{0.33}La_{0.557}TiO₃ nanofibers (Figure 4) [174]. Moreover, Liu et al. [175] have reported that

dispersion of well-oriented ceramic nanowires instead of random nanowires in a host polymer matrix could cause more ionic conductivity resulting from faster transportation of the Li^+ ions. Hence, morphological features play a key role to obtain ideal electrochemical nanofibrous components.

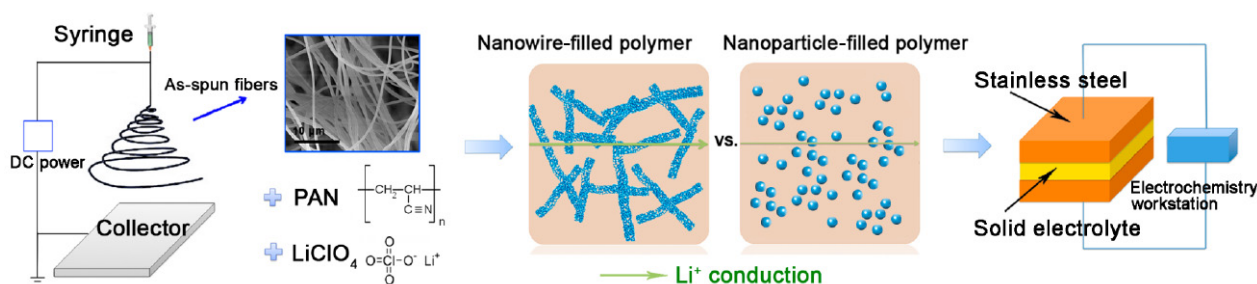


Figure 4. Schematic illustration of the synthesis of ceramic nanowire-filled polymer-based composite electrolytes, together with the comparison of possible lithium-ion conduction pathway in nanowire-filled and nanoparticle-filled composite electrolytes, and illustration of the electrode. Reprinted with permission from [174]. Copyright (2015) American Chemical Society.

So far, lithium secondary batteries have been widely utilized as energy storage devices in various applications. Regarding progress and development of technology, production of storage power tools with superior efficiency and improved function has been crucial. In order to achieve this significant aim, all battery components, including anode, cathode, separator, and electrolyte should be enhanced and augmented. In recent decades, the electrospinning technique has shown a great potential to approach versatile and highly efficient fibrous structures for designing advanced LIBs. Despite the reported advantages of electrospun components of LIBs, several drawbacks, such as poor mechanical strength, low electrical conductivity, and poor ionic conduction, have restricted their practical applications. Meanwhile, such downsides could be eliminated through further evaluation and modification of electrospun membranes. By addressing the mentioned challenges, fabrication of all-solid-state electrospun batteries comprising of nanofibrous electrodes along with nanofibrous electrolyte could be considered as the main trend in the near future.

5. Fuel Cells

Fuel cells are based on electrochemical reactions with an external source for the reacting material [176,177]. They have efficiencies around 40–85%, which is higher than those of turbine generators or a diesel engine and a capacity range comparable with photovoltaics or a turbine generator, making them highly interesting for rural areas with limited access to the public grid or for uninterruptible power supplies [177].

Technologically, they work by a reversed electrolysis reaction, creating electricity and heat by the reaction of oxygen and hydrogen to water. A fuel cell consists in principle of two electrodes, i.e., cathode and anode, separated by an electrolyte, and the external electric circuit used to gain energy from the cell. Depending on the kind of electrolyte, fuel cells are separated into alkaline, phosphoric acid, solid oxide, molten carbonate, direct methanol, and proton exchange fuel cells [178].

Similar to the aforementioned batteries, fuel cells can contain electrospun nanofiber mats for different purposes which will be presented in this section.

5.1. Electrospun Cathode Materials

Diverse studies investigated possibilities to prepare cathodes for fuel cells from electrospun nanofiber mats.

In proton exchange fuel cells, for example, the problem occurs that the water generated at the cathode is not properly transported at high current densities, resulting in so-called water flooding, and can in addition support corrosion of the carbon electrode, in this way reducing also the long-term stability [179]. To reduce this problem, Chung et al.

suggested introducing hydrophobic graphitized carbon nanofibers, achieved by annealing electrospun PAN nanofibers up to temperatures of 1000–2500 °C, into the cathode layer, resulting in water-free regions in the electrode, as depicted in Figure 5 [180]. They found highest peak power densities for a concentration of 45 wt.% graphitized carbon nanofibers by reducing water flooding [180]. Slack et al. suggested PVDF as a binder for Pt/C cathodes to reduce carbon corrosion accelerated stress [181]. They compared electrospun nanofiber cathodes with Nafion/PVDF and Nafion/poly(acrylic acid) (PAA) binders with a slurry cathode with neat Nafion and Nafion/PVDF binder and found that the presence of the hydrophobic PVDF reduced carbon loss and increased the binder strength [181]. In an earlier investigation, the group studied PtCo/C and Pt/C catalyst powders integrated in electrospun nanofibrous mats in comparison with conventional sprayed cathode membranes, again using Nafion/PAA as a binder, and found a higher initial performance as well as a superior long-term stability for the electrospun cathodes [182]. Similarly, Khandavalli et al. used PAA to reduce agglomerations of platinum on carbon catalyst particles in catalyst inks [183]. In another earlier work, Zhang et al. showed the advantages of electrospun nanofiber cathodes under low and high feed gas humidification with similar fiber composition [184]. Wei et al. used graphene-doped electrospun nanofiber mats for both cathode and anode and found high conductivity and great porosity of these electrodes, making them well suitable for fuel cells after Pt loading [185].

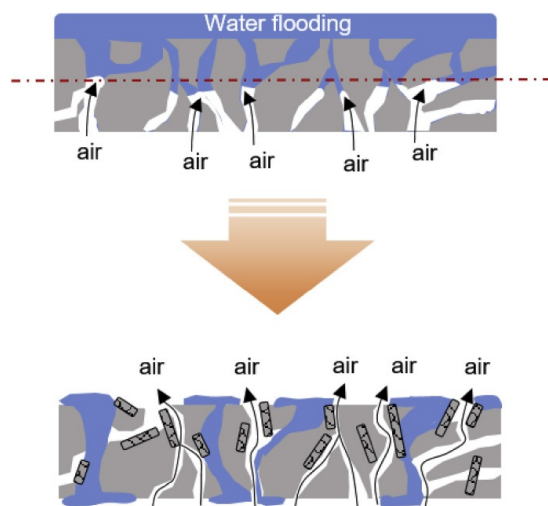


Figure 5. Improved water management due to graphitized carbon nanofibers incorporated in the cathode layer. Reprinted from [180], with permission from Elsevier.

Cathodes in direct methanol fuel cells can also be prepared by electrospinning. Membranes used in these fuel cells must combine high proton conductivity with low methanol permeability to avoid fuel from anode reaching the cathode, which is a problem for the typically used Nafion membranes [186]. Liu et al. compared sulfonated poly(ether ether ketone) (SPEEK) membranes, Nafion membranes, and SPEEK membranes doped with sulfonated carbon nanofibers (SCNFs) [187]. They found increased mechanical strength, proton conductivity, and decreased methanol permeability for SPEEK/SCNF composites, as compared to the other membranes. In a microfluidic fuel cell, working on formic acid as fuel and KMnO_4 as oxidant, Jindal et al. applied a CN_x nanofiber mat as cathode catalyst and found a power density similar to gold or platinum catalysts [188]. Electrospinning of CN_x nanofibers was performed by producing CN_x nanoparticles and spinning them with PAN, Nafion and carbon black powder from a DMF solution. In this way, usually a CN_x layer on PAN nanofiber was produced, bound by the Nafion dispersion, while sometimes nodes in the PAN nanofibers stemming from CN_x nanoparticles supported on carbon black were found [189]. Using an electrospun Fe-N/C nanofiber mat as catalyst for a direct methanol fuel cell, Mei et al. found the multi-scaled porous structure to be

beneficial for the cathode catalyst in a fuel cell [190] They concluded that while micropores helped accommodating active sites, the meso- and macropores supported oxygen supply to the active surfaces. In their study, high oxygen reduction reaction was found in acid media, combined with good stability and methanol tolerance.

While molten carbonate fuel cells scarcely contain electrospun nanofibrous cathodes, solid oxide fuel cells use them often. One of the problems of solid oxide fuel cells is the high operating temperature of typically 800 °C and higher when preparing solid oxide fuel cells based on an electrolyte from yttria-stabilized zirconia, resulting in relatively low lifetimes and high costs. To solve this problem, Zhi et al. suggest using a 3D nanofiber network as the cathode to reduce operation temperature to 750 °C [191]. They used an electrospinning solution of PAN in DMF, blended with $\text{La}_{0.58}\text{Sr}_{0.4}\text{Co}_{0.2}\text{Fe}_{0.8}\text{O}_3$, and heat treated the electrospun nanofibers at 800 °C to reach nanofibers with a perovskite structure. Further improvement was obtained by adding gadolinia-doped ceria into the 3D nanoporous network. In an earlier study, the group investigated yttria-stabilized zirconia nanofiber networks infiltrated with $\text{La}_{0.8}\text{Sr}_{0.2}\text{MnO}_3$ and found reduced polarization resistance in comparison to bulk cathodes from the same materials [192]. Enrico et al. used water instead of DMF for electrospinning a sol-gel solution to prepare $\text{La}_{0.6}\text{Sr}_{0.4}\text{Co}_{0.2}\text{Fe}_{0.8}\text{O}_{3-\delta}$ nanofibers [193]. After heat treatment of the nanofibers, they were applied on a $\text{Ce}_{0.9}\text{Gd}_{0.1}\text{O}_{1.95}$ electrolyte disk to prepare a symmetrical fuel cell which was investigated at temperatures of 550–950 °C and found to have low performance reduction for operation at 750 °C. A lower working temperature of 650 °C was achieved by using a composite cathode from electrospun $\text{La}_{0.8}\text{Sr}_{0.2}\text{Co}_{0.2}\text{Fe}_{0.8}\text{O}_{3-\delta}$ nanotubes/ $\text{Ce}_{0.8}\text{Gd}_{0.2}\text{O}_{1.9}$ [194]. Different materials were suggested by Ahn et al. who prepared $\text{Sm}_{0.5}\text{Sr}_{0.5}\text{CoO}_{3-\delta}$ and $\text{Gd}_{0.2}\text{Ce}_{0.8}\text{O}_{1.9}$ composite nanofibers by electrospinning and found a significant increase of the electrode performance as compared to pure $\text{Sm}_{0.5}\text{Sr}_{0.5}\text{CoO}_{3-\delta}$ cathodes [195]. The precursor-based one-step electrospinning process was found to be advantageous to prepare increased grain boundary density and maximum hetero-interfaces between both phases (Figure 6), which supports oxygen reduction reaction at the cathode and thus an increased fuel cell performance.

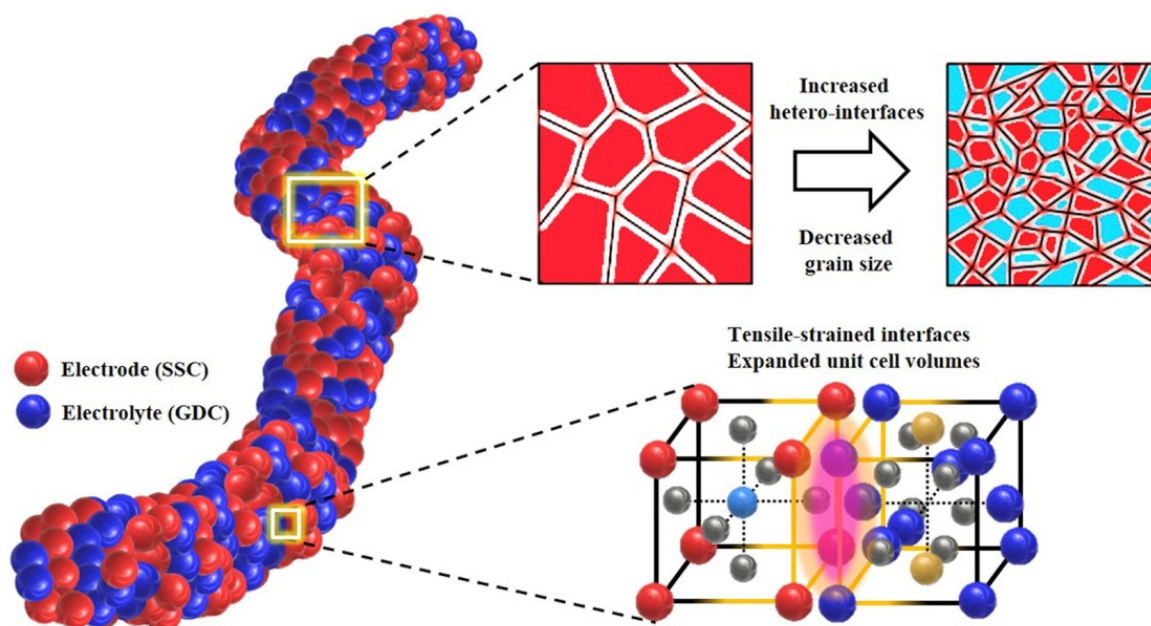


Figure 6. Schematic of electrode/electrolyte nanofiber from $\text{Sm}_{0.5}\text{Sr}_{0.5}\text{CoO}_{3-\delta}$ (SSC) and $\text{Gd}_{0.2}\text{Ce}_{0.8}\text{O}_{1.9}$ (GDC) with increased hetero-interface, decreased grain size, and expanded unit cell volumes. Reprinted from [195], with permission from Elsevier.

Phosphoric acid fuel cells belong to the most often used ones. Here, the electrolyte mainly contains phosphoric acid (H_3PO_4), a proton conductor delivering protons from the anode to the cathode [196]. In phosphoric acid fuel cells, again electrospun nanofiber mats can be applied as cathodes. Skupov et al., for example, modified cathodes for medium-temperature phosphoric fuel cells based on polybenzimidazole membranes [197]. They prepared PAN nanofiber mats from DMF, blended with carbon black and partly PVP, stabilized them in air and subsequently carbonized them at 900–1100 °C in vacuum. Afterwards, the nanofiber mats were partly loaded with Pt or Ni. These cathodes were found to show improved polarization values and increased catalytic activity due to the increased specific surface of the more porous nanofibers. Previously, the same group reported on gas diffusion electrodes for fuel cells, prepared by sequential oxidation and pyrolysis of electrospun nanofiber mats prepared from PAN, decorated with Pt [198]. Besides these few examples, phosphoric acid fuel cells are normally not prepared with nanofibrous cathodes.

Similarly, there are only few reports available on nanofibrous cathodes for alkaline fuel cells which use typically potassium hydroxide in water or nowadays an alkaline polymer membrane as the electrolyte. As an example, Uhm et al. prepared CNFs with embedded non-precious metals for the oxygen reduction reaction in alkaline ethanol fuel cells by electrospinning and subsequent carbonization [199]. They found that the Fe and Co metals supported nitrogen and oxygen incorporation on the CNF surface instead of directly being part of the oxygen reduction reaction.

Besides the possible applications of electrospun nanofiber mats as cathodes in fuel cells, the next sub-section gives a brief overview of applying nanofibrous materials as anodes.

5.2. Electrospun Anode Materials

An interesting application of nanofiber mats used as anodes in fuel cells is given by microbial fuel cells in which the anodes mostly define the fuel cell performance [200,201]. These cells generate electricity by oxidizing biodegradable organic matter, such as glucose or proteins, in the presence of microorganisms [202]. Garcia-Gomez et al. studied TiO_2 -C/C nanofiber mats and found good electrical performance, combined with the ability to host a dense biofilm of electro-activated *Escherichia coli* (Figure 7), which could be used for the bioconversion to electricity in a microbial fuel cell [202]. The nanofiber mats used in their experiments were prepared from co-electrospinning solutions of TiO_2 -PVP-PAani and pure PAN in DMF through two syringes onto an aluminum collector plate. After spinning, $\text{Ti}(\text{O}_i\text{Pr})_4$ hydrolysis was achieved in air, followed by thermal stabilization and carbonization at 1000 °C. Cai et al. prepared a CNT/CNF anode by electrospinning PAN/CNT from DMF, followed by heat pressing and carbonization [203]. They found only few bacteria, used to grow a biofilm, on pure carbon fiber anodes, and a much thicker biofilm on the CNT/CNF anode, which was attributed to the increased roughness and hydrophilicity of the anode due to the introduction of the CNTs. Another material combination was suggested by Jung and Roh who used CNF/polypyrrole (PPy) electrospun nanofiber mats as anodes in microbial fuel cells and found a nearly doubled power density with their optimized anodes in comparison with commercial graphite felt [204]. Massaglia et al. suggested N-doped carbon nanofibers as anodes for microbial fuel cells [205], while Karra et al. investigated activated carbon nanofibers and found them to be superior to anodes prepared from granular activated carbon or carbon cloth [206].

Besides these examples of biotechnological fuel cells, diverse others were shown to be producible with electrospun anodes. Working with urea-contaminated wastewater, Barakat et al. suggested carbon nanofibers with embedded NiSn nanoparticles as anodes in direct urea fuel cells [207]. They showed that adding tin as a co-catalyst to nickel, a high current density for urea oxidation could be achieved, and found an average carbonization temperature of 850 °C to be advantages as compared to higher temperatures where the graphite content decreased, leading to a decrease in the catalytic activity. Mohamed et al. used a glassy-carbon electrode coated with electrospun Ni/Pd-C nanofibers as the anode

for urea fuel cells, in which the nanofibers were prepared by electrospinning PVA with nickel (II) acetate tetrahydrate and palladium (II) acetate, followed by calcination at a temperature of 900 °C in argon atmosphere [208]. Ni/Cd-decorated electrospun carbon nanofibers were investigated as anodes of urea fuel cells by Abdelkareem, who found a significantly improved electrocatalytic activity for urea oxidation, as compared to anodes without Cd [209].

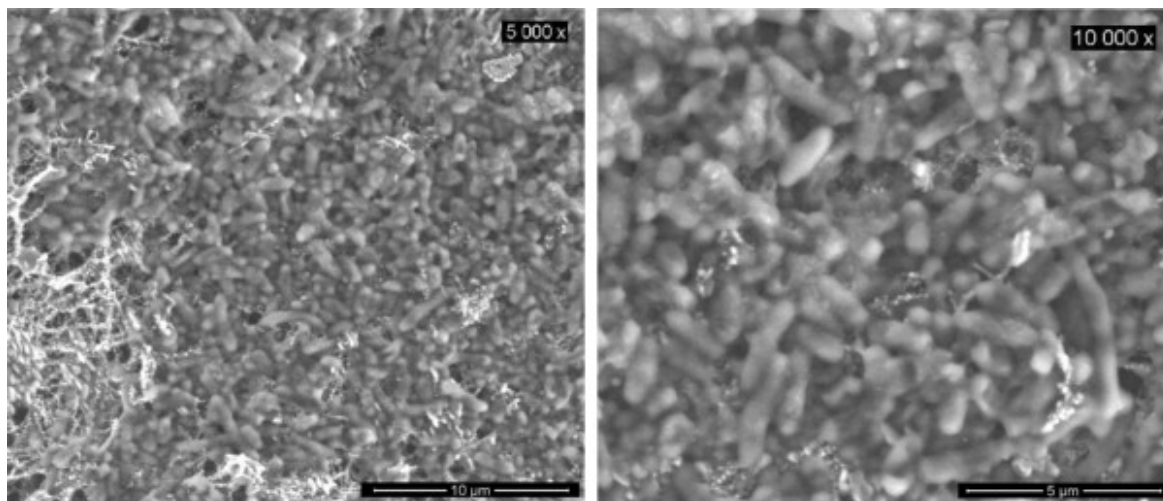


Figure 7. Scanning electron microscope images of electro-activated *Escherichia coli* K12. Reprinted from [202], with permission from Elsevier.

Perovskites were already described before as possible cathodes for solid oxide fuel cells. Similarly, they can be used for the anodes in these cells. Hu et al. recently described $\text{La}_x\text{Sr}_{1-x}\text{TiO}_3\text{-Gd}_y\text{Ce}_{1-y}\text{O}_{2-\delta}$ electrospun nanofiber mats as possible composite anodes for these cells [210]. These nanofiber mats were prepared by dissolving PVP in DMF, adding lanthanum nitrate, strontium nitrate, and tetrabutyl titanate in different molar ratios, needle-based electrospinning the solution and calcinating it at 900 °C, before the nanofibers were partly grinded to obtain nanoparticles. These nanofibers and nanoparticles were mixed with terpeneol solution and in this form coated on both sides of the electrolyte wafers to form cathode and anode, before they were impregnated with $\text{Gd}_y\text{Ce}_{1-y}\text{O}_{2-\delta}$. In this way, a La doping ratio of 0.4 was found to be optimal. Addition of $\text{Gd}_y\text{Ce}_{1-y}\text{O}_{2-\delta}$ was shown to significantly increase the electrochemical performance, with an optimum Gd doping ratio of 0.2. Besides, nanoparticle-based anodes showed a better electrochemical performance than nanofiber-based anodes if only $\text{La}_x\text{Sr}_{1-x}\text{TiO}_3$ was used, while this was reversed for the $\text{Gd}_y\text{Ce}_{1-y}\text{O}_{2-\delta}$ impregnated electrodes [210]. The optimized electrodes were afterwards tested in H_2 and CH_4 fuel gases where they showed good thermal and redox cycling stability [211]. Besides this type of composite [212,213], other material systems as anodes for solid oxide fuel cells are, e.g., Ni-coated yttria-stabilized zirconia nanofiber mats [21–216], $\text{SrCe}_{0.8}\text{Y}_{0.2}\text{O}_{3-\delta}\text{-Ni}$ nanofiber mats [217], and $\text{Sr}_2\text{FeTiO}_{6-\delta}$ nanofiber mats [218].

For direct methanol fuel cells, Chen et al. suggested electrospinning a 3D anodic catalytic layer (Figure 8) to improve catalyst utilization and to reduce charge transfer resistance, in this way significantly increasing the electrochemical performance at simultaneously reduced platinum loading of the electrode [219]. Carbon– CeO_2 composite nanofiber mats were electrospun by Feng et al. who suggested them as a support for a PtRu anode catalyst in direct methanol fuel cells [220]. Thamer et al. used Ni/C nanofibers mixed with Nafion solution as a catalyst layer on glassy carbon anodes and found high electrocatalytic activity in methanol oxidation which was enhanced by nitrogen doping, while the latter also improved the stability of the catalyst [221]. Hanifah et al. suggested electrospun PVDF/Pt-Pd/RGO- CeO_2 nanocomposite nanofibers as anode catalyst in direct methanol fuel cells [222]. These fibers were prepared from a solution containing graphite

oxide, PdCl_2 and $\text{H}_2\text{PtCl}_6 \cdot 6\text{H}_2\text{O}$, mixed with formic acid and $\text{Ce}(\text{NO}_3)_3 \cdot 6\text{H}_2\text{O}$ to reach Pt-Pd/RGO-CeO₂. This was added to a PVDF solution in N-Methyl-2-Pyrrolidone to allow for needle-based electrospinning. In this way, Pt-Pd/RGO-CeO₂ nanocomposites in a PVDF nanofiber matrix could be prepared which could be used as catalyst nanofibers for direct methanol fuel cell anodes. Other materials used to prepare the anodes of direct methanol fuel cells are, e.g., TiO₂/C with platinum and ruthenium catalyst [223,224], PPy nanofiber networks [225], and CeO₂-C nanofibers decorated with Pt-Co nanoparticles [226].

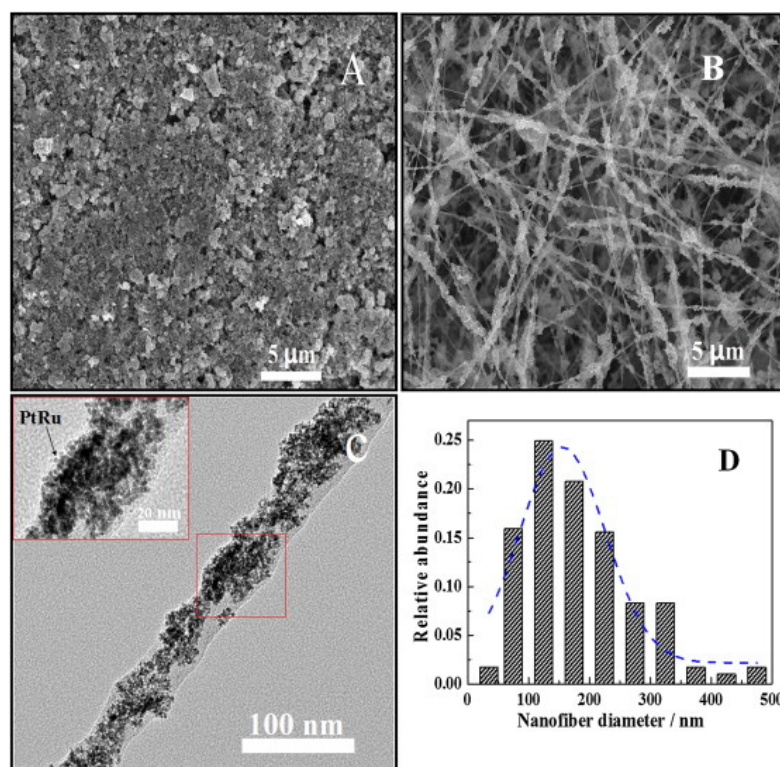


Figure 8. Scanning electron microscopy images of (A) a conventional gas diffusion electrode; (B) an electrospun gas diffusion electrode; (C) transmission electron microscope image of electrospun PtRu-C/Nafion/PVA nanofiber; (D) diameter distribution of the electrospun nanofiber mat. Reprinted from [219], with permission from Elsevier.

Besides these types of fuel cells, electrospun nanofiber mats are only scarcely applied as parts of anodes, e.g., Pt/SnO₂ nanofibers as electrocatalyst in polymer electrolyte membrane fuel cells to support hydrogen oxidation reaction and block oxygen reduction reaction there [227]. Another often reported application of electrospun nanofiber mats is, due to their tailorable porosity, the membrane of different fuel cells.

5.3. Electrospun Membranes

In H₂/Br₂ regenerative fuel cells, Park et al. applied Nafion perfluorosulfonic acid/PVDF electrospun membranes, containing 2–5 nm fine fibril strands from Nafion and PVDF aligned to the fiber axis [215]. The membranes were produced by hot-pressing and subsequent thermal annealing. With increasing PVDF content, a decrease in proton conductivity, water/electrolyte swelling and permeability for Br₂/Br₃[−] was found, making a membrane with 20% PVDF suitable for H₂Br₂ fuel cells and showing nearly 50% higher power output than with a common Nafion 212 membrane [228]. Nafion/polyphenylsulfone nanofiber mats were produced by simultaneous electrospinning of both components and showed good water swelling and mechanical performance as well as proton conductivity [229]. Many other nanofiber mats based on material blends including Nafion are reported in the scientific literature [230–234].

Besides these material combinations, several others are suggested for different fuel cells. Bipolar membranes can be used, e.g., for self-humidifying H_2 /air fuel cells, besides other electrochemical devices [235]. Combining a metal-organic framework (MOF) with sulfonated poly(phthalazinone ether sulfone ketone) (SPPEsk) was suggested by Wu et al. as a possible membrane for high proton conductivity in proton exchange membrane fuel cells, working at high temperatures and under anhydrous conditions [236]. The nanofibers were highly oriented and showed thus high proton conductivity, combined with oxidative stability and resistance of methanol permeability, making them well suitable for direct methanol fuel cells. Similarly, Gong et al. suggested ordered SPPEsk nanofiber mats to reach high tensile strength and cell power density [237]. Another high-temperature membrane was prepared by Muthuraja et al. who used poly(aryl sulfone ether benzimidazole) membranes for proton exchange fuel cells [238]. Electrospinning this material from dimethyl sulfoxide (DMSO) in a needle-based process, they found high proton conductivity and oxidative stability due to the sulfone and ether links in the polymeric backbones as well as a highly porous structure, enabling high acid doping and increasing proton conductivity. Using highly oriented sulfonated PI nanofibers, Tamura and Kawakami produced proton exchange membranes for fuel cells with high chemical and mechanical stability as well as high proton conductivity parallel to the nanofibers [239]. Electrospun nanofiber mats with pore size gradients were suggested by Balakrishnan et al. for polymer-electrolyte membrane fuel cells [240], who also studied degradation of such electrospun gas diffusion layers [241], while Kallem et al. highlight some possible strategies for nanofiber-based proton exchange membranes with aligned nanofiber mats [242].

Finally, a theoretical approach should be mentioned. DeGostin et al. developed a fiber network model to predict the conductivity of electrospun nanofiber mats [243]. They modeled the 3D nanofibrous morphology to approximate fiber layering and membrane swelling in water. By translating the fiber network into a resistor network, as shown in Figure 9, they found similar conductivity as experimentally measured in electrospun proton and anion exchange membranes in fuel cells.

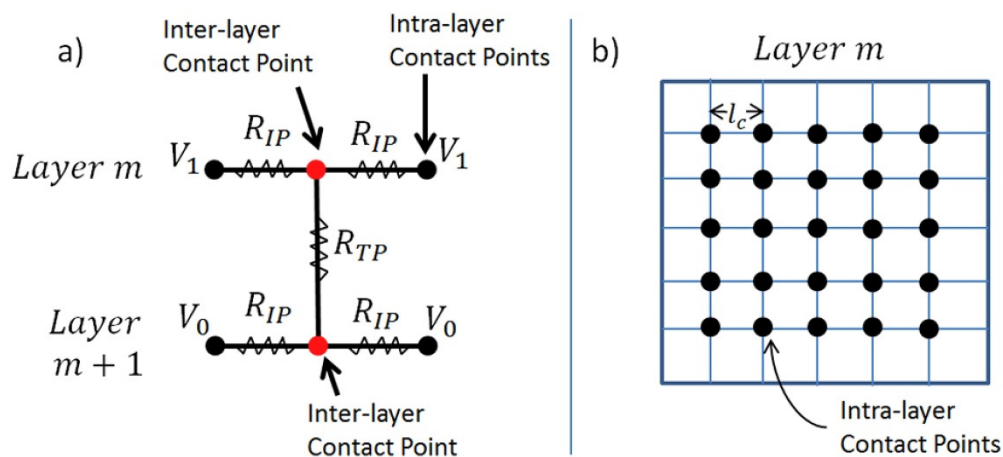


Figure 9. Resistor network of a nanofiber mat: (a) conductivity between layers; (b) formation of contact points inside a single layer. Reprinted from [243], with permission from Elsevier.

In all aforementioned applications in the research area or electrospun elements for fuel cells, the fiber and mat morphologies are again of high interest. Most of the aforementioned papers investigate these properties by SEM, partly by TEM, and aim at providing porous nanofiber structures to further improve the SSA of the corresponding nanofiber mats.

Generally, electrospun nanofiber mats can be applied as cathodes, anodes, or membranes of fuel cells. The possibilities to tailor the morphology of nanofibers and mats, in this way creating the desired nano- and micropores to reach a high SSA, and the physical and chemical material properties, e.g., by varying the carbonization/calcination process,

offer a broad range of available properties which can be optimized towards the respective applications.

6. Supercapacitors

Supercapacitors, also called electrochemical capacitor, double layer capacitors and ultra-capacitors, are considered as one of the novel electrical energy storage methods. Compared to batteries, they deliver higher power rates and life times. However, they suffer from lower stored energy than batteries. So, their practical usage is limited by their poor energy density ($4\text{--}5 \text{ Wh}\cdot\text{kg}^{-1}$), whilst batteries display energy output in the range of 100 to $200 \text{ Wh}\cdot\text{kg}^{-1}$. Supercapacitors could be applied in different electronic equipment, including hybrid vehicles, portable devices, and many more. They are mainly comprised of active and inert components. Electrode and electrolyte are classified as the active materials, whilst current collector, binder, and separator are categorized as the inactive ones [175,244]. Figure 10 schematically illustrates the basic structure of various supercapacitors.

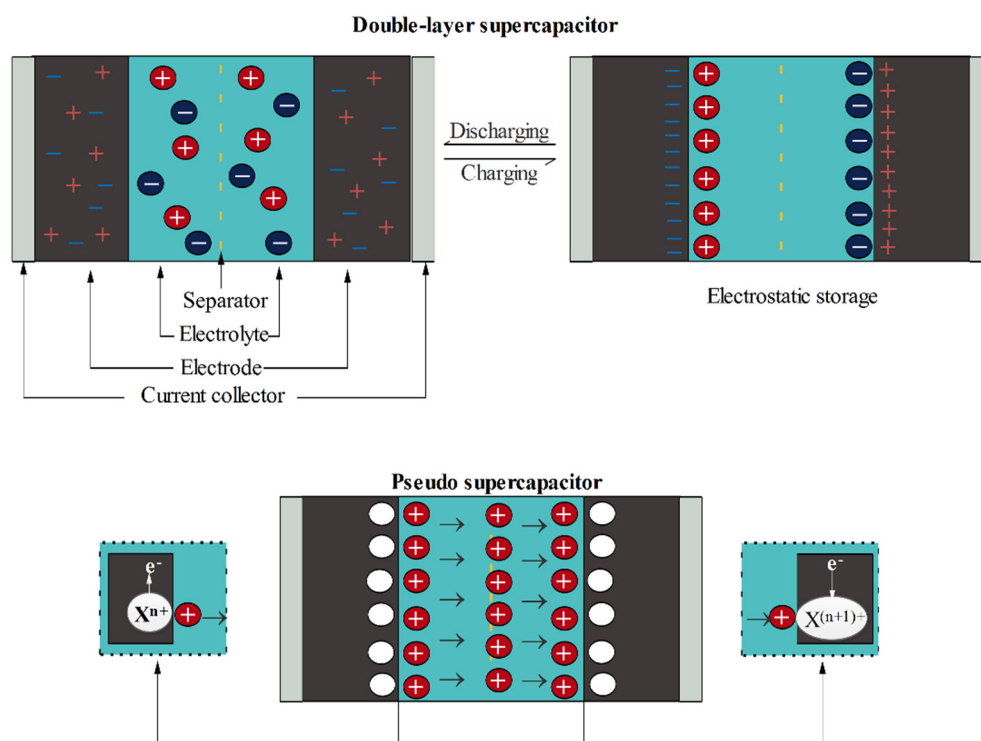


Figure 10. Schematic illustration of various supercapacitor types.

Electrospun Fibers as Supercapacitor Electrode Materials

Based upon the operational mechanism, supercapacitors can be classified into electrochemical double layer capacitance (EDLCs) and pseudo capacitance classes. In the EDLC category, physical accumulation of the charge carriers and ions on the electrode-electrolyte interfacial layer results in the energy storage. Carbon-based materials such as carbon aerogel, graphene, CNT, and many more belong to the EDLC materials, whereas metal oxides and conducting polymers have shown pseudo capacitance behavior as they store energy through physio-chemical reactions [245,246].

Carbon-based materials are frequently described for fabrication of the EDLC electrodes. These materials have revealed numerous advantages such as great electrical conductivity, proper specific surface area, appropriate chemical stability, low cost, and so on. According to their operating mechanism, surface area and morphology parameters influence the capacitor performance. In addition, existence of the functional groups on the carbon-based materials increases the ion adsorption, stemming from the wettability enhancement. Therefore, numerous researches have illustrated that optimized pore size

and surface area factors as well as the existence of functional groups on the material surface could lead to performance enhancement of the carbon-based electrodes. However, contact resistance of the carbon particles is a serious weakness associated with the carbon-based materials. The reason is attributed to increment of the electrode resistance and therefore reduction of the capacitance efficiency [245,246].

Recent evidences suggest that carbon-based nanofibrous materials can enhance ion migration into the active surfaces and improve interfacial charge transportation. This could be linked with the highly porous structure of the nanofibrous materials and their great electrical conductivity. As an example, carbon nanofibers (CNFs) display high electrical and thermal conductivities as well as excellent mechanical and chemical stabilities. Commonly, CNFs are fabricated through electrospinning of a host polymer followed by a carbonization procedure at high temperatures. PAN, PVP, and PI belong to the notable host polymers. Moreover, several guest polymers such as PMMA and polystyrene (PS) could be applied to fabricate porous CNFs. The porous CNF structures are produced as a result of guest polymer removing after the heat treatment step [245,246]. Figure 11 displays the applied procedure for fabrication of hollow-porous CNF by He et al. [247]. It is worth noting that increasing the calcination temperature leads to a reduction of the obtained carbon fiber diameter and results in superior electrochemical behavior as it is declared by Pech and Maensiri [248]. Several attempts applied for synthesis of the CNF structures by using the electrospinning procedure are listed in Table 5.

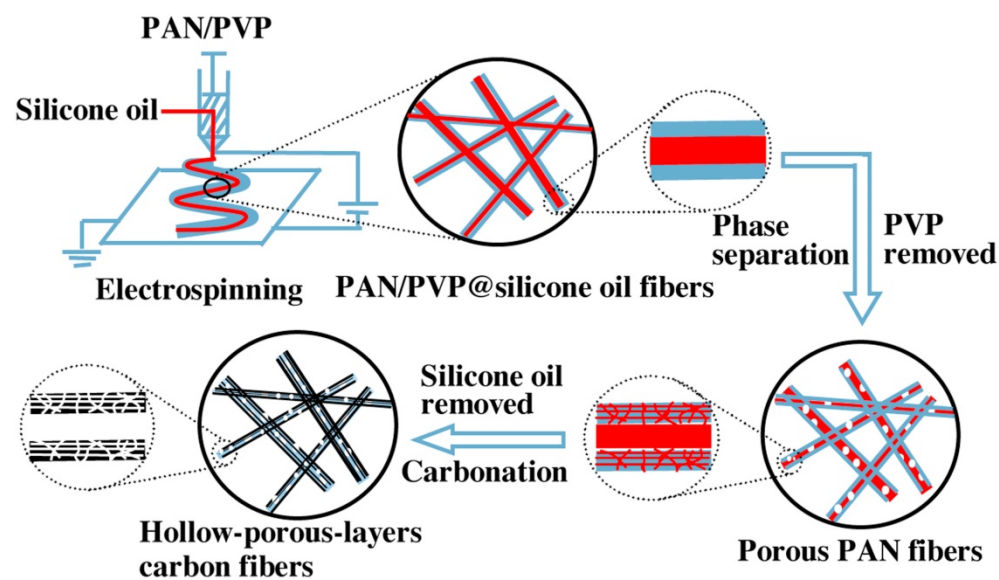


Figure 11. Preparation steps of hollow-porous multilayered ultrafine carbon fibers. Reprinted from [247], with permission from Elsevier.

Table 5. Electrospun carbon nanofibers as supercapacitor electrode material.

Host [Guest] Components	Thermal Treatment	SSA (m ² ·g ⁻¹)	Electrochemical Performance			Author (Year)	Ref.
			Specific Capacity (F·g ⁻¹)	Energy Density (Wh·kg ⁻¹)	Capacity Retention		
PAN	Stabilized at 280 °C for 1 h, carbonized at 700–800 °C, and activated by N ₂ and steam for 30 min	1230	173 at 0.01 A·g ⁻¹	-	-	Kim & Yang (2003)	[249]
Polybenzimidazole	Activated by N ₂ and steam at 750–850 °C for 30 min	1220	178 at 0.007 A	-	-	Kim et al. (2004)	[250]
PVDF/PVP	Dehydrofluorinated at 60 °C for 1 h and heated to 800 °C in N ₂	1084	331 F·g ⁻¹ at 1 A·g ⁻¹	13.1	89.2% after 2000 cycles	Ma et al. (2019)	[251]

Table 5. Cont.

Host [Guest] Components	Thermal Treatment	SSA (m ² ·g ⁻¹)	Electrochemical Performance			Author (Year)	Ref.
			Specific Capacity (F·g ⁻¹)	Energy Density (Wh·kg ⁻¹)	Capacity Retention		
PAN/PMMA	Stabilized at 250 °C for 4 h and carbonized at 800 °C for 1 h in N ₂	224	210 F·g ⁻¹ at 1 A·g ⁻¹	-	100% after 2000 cycles	Lai et al. (2015)	[252]
PAN/PVP	Stabilized at 300 °C for 2 h, carbonized at 300 to 970 °C for 3 h in N ₂ , and activated by CO ₂ at 850 °C for 1.5 h	531	220 F·g ⁻¹	-	-	Niu et al. (2011)	[253]
Polyamic acid (PAA)/PVP	Stabilized at 280 °C for 2 h, carbonized at 280 to 900 °C for 7 h in Ar, and activated by KOH at 850 °C for 2 h	743.5	211.7 F·g ⁻¹	23.1	-	He et al. (2020)	[254]
poly(styrene-co-acrylonitrile)/PAN/PVP	Stabilized at 250 °C for 2 h and carbonized at 800 °C for 1 h in N ₂	26	239 F·g ⁻¹ at 1 A·g ⁻¹	15	92.33% after 10,000 cycles	Kim et al. (2020)	[255]
Lignin/PVA	Stabilized at 250 °C in N ₂ for 2 h and carbonized at 900 °C for 2 h in N ₂	2005	205 F·g ⁻¹ at 1 A·g ⁻¹	-	83% after 1500 cycles	Ago et al. (2016)	[256]
PAN [PVP/Silicone oil]	Stabilized at 300 °C for 2 h, carbonized at 300 to 970 °C for 3 h in Ar, and activated by KOH at 850 °C for 1.5 h	1120.3	231.6 F·g ⁻¹	15.1	99.7% after 2000 cycles	Ishita & Singhal (2020)	[257]
PAN [PS]	Stabilized at 280 °C for 2 h and carbonized at 800 °C for 1 h in N ₂	432	271.6 F·g ⁻¹ at 0.5 A·g ⁻¹	18.8	100% after 5000 cycles	Ishita & Singhal (2020)	[257]

High electrical conductivity, wide operational potential window, and low cost belong to the main advantages of conducting polymers. In such electrode materials, energy is stored through oxidation or reduction reactions. PANi, PPy, poly(3,4-ethylenedioxythiophene) (PEDOT), polyindophenine, and p-phenylenevinylene (PPV) are common examples of conducting polymers. However, poor cycling performance and mechanical degradation are the major drawbacks associated with these electrode materials. The reason may be linked with the surface area reduction and thus specific capacitance decrement by increment of the mass loading. Therefore, porous conducting polymers with improved specific surface area could be great candidates for being applied in such electrochemical devices. Obtained data from several researches has illustrated that the nano-sized conducting polymers could reveal boosted electrochemical behaviors caused by their highly porous structures and superior surface-to-volume ratios. In fact, ion diffusion into the bulk of the electrode material is accelerated in the nanostructured conductive polymers as a result of stronger participation of the applied materials in the redox reactions [258,259]. Chaudhari et al. demonstrated specific capacitance of 267 F·g⁻¹ at a current density of 0.35 A·g⁻¹ for the electrospun PANi fibers. However, the synthesized PANi particles showed lower specific capacitance of 208 F·g⁻¹ [260]. In addition, Maio et al. reported specific capacitance of 601 F·g⁻¹ at a current density of 1 A·g⁻¹ for the fabricated hollow PANi nanofibers [261]. Sahoo et al. reported the highest specific capacitance of 284 F·g⁻¹ at a current density of 1 A·g⁻¹ for the PPy nanofibers [262]. Moreover, Liu et al. presented a specific capacitance of 463 F·g⁻¹ for the synthesized Ppy nanotubes at a current density of 0.3 A·g⁻¹, while the electrospun PANi exhibited much lower specific capacitance of 243 F·g⁻¹ at similar current density [263]. Furthermore, the enhanced electrochemical performance of other electrospun conductive polymers such as PPV [264], polyindophenine [265], and PEDOT [266] has been widely reported.

Compared with the carbon-based materials and conducting polymers, metal oxides have illustrated superior energy storage efficiency, along with higher cycling stability. These materials are able to store energy through both physical accumulation and redox reaction. RuO_2 , MnO_2 , NiO , and CoO_x are of the widely studied electrode metal oxides. However, several challenges such as low electrical conductivity and high cost have restricted their development. As claimed by numerous researchers, the mentioned drawbacks could be addressed through synthesis of the nano-sized transition metal oxides [267,268]. For example, Hyun et al. displayed high specific capacitance of $889 \text{ F}\cdot\text{g}^{-1}$ and 30% capacity loss after 2000 cycles for the fabricated RuO_2 nanofibers [269]. Kolathodi et al. reported higher ionic and electrical kinetics as well as improved capacity retention for the MnO_2 transition metal oxide in the nanofiber formation due to higher surface-to-volume ratio [270]. NiO nanofibers also exhibited a specific capacitance of $182 \text{ F}\cdot\text{g}^{-1}$ at a current density of $2 \text{ A}\cdot\text{g}^{-1}$ and maintained 98.2% of their capacity after 5000 cycles [271]. In addition, high specific capacitance of $700 \text{ F}\cdot\text{g}^{-1}$ and great cycling stability of 96% were illustrated by applying electrospun hollow NiO fibers as the supercapacitor electrode [272]. Moreover, electrospun Co_3O_4 fibers have shown a specific capacitance of $407 \text{ F}\cdot\text{g}^{-1}$ and retained 94% of their capacitance after 1000 cycles [273].

It is extensively reported that graphene has the highest theoretical specific capacity in comparison with the other carbon-based materials. Proper chemical stability, high surface area, and low cost are some appealing characteristics of graphene-based electrodes, while restacking of the graphene layers has blocked approaching to the reported theoretical capacity value. In addition, the evaluated single-phased nanofibrous materials have not been ideal for being applied in the practical usages. As an example, limited specific capacity and low energy density are some of poor properties of nano-structured EDLC materials. In the case of pseudocapacitive nanofibers, poor electrical conductivity and low cycle stability are identified as the main disadvantages. So, nanocomposite materials, composed of several electrode materials, such as carbon-based structures, metal oxides, conducting polymers, etc., have been widely developed to enhance electrochemical performance of the electrodes [245,246]. To date, numerous studies have been devoted to figure out various electrochemical characteristics of the electrospun nanocomposites. For instance, electrospinning of the combination of PANi with various carbon-based materials including CNT [274,275], graphene [276,277], and CNFs [278,279] has resulted in the improved specific capacity as well as enriched cycling durability. Table 6 summarizes recent attempts for synthesis of electrospun nanocomposite materials as supercapacitor electrodes.

Table 6. Electrospun composites applied as electrode in supercapacitor devices.

Electrospun Hybrid Materials	Thermal Treatment	Electrochemical Performance			Author (Year)	Ref.
		Specific Capacity ($\text{F}\cdot\text{g}^{-1}$)	Energy Density ($\text{Wh}\cdot\text{kg}^{-1}$)	Capacity Retention		
PAni/CNF	Stabilized at 280°C for 4 h and carbonized at 800°C in N_2	439 at $1 \text{ mA}\cdot\text{cm}^{-2}$	68.6	90% after 5000 cycles	Anand et al. (2020)	[280]
PAni/heteroatom-doped CNF	Annealed at 250°C for 2 h and pyrolysed at 900°C for 1 h in N_2	680.8 at $0.5 \text{ A}\cdot\text{g}^{-1}$	27.7	93.5% after 3000 cycles	Zhu et al. (2020)	[281]
PAni/ MnO_2 /CNF	Stabilized at 280°C for 2 h and carbonized at 800°C for 0.5 h in N_2	937.66 at $1 \text{ A}\cdot\text{g}^{-1}$	66.12	97.6% after 5000 cycles	Jalil et al. (2020)	[282]
Graphene/CNT/CNF	Stabilized, maintained at 500°C for 1 h, and kept at 700°C	218 at $1 \text{ A}\cdot\text{g}^{-1}$	62.13	94.98% after 10,000 cycles	Kshetri et al. (2020)	[283]
MoS_2 /graphene/CNF	Pretreated at 450°C for 1.5 h and carbonized at 800°C for 2 h in H_2	334 at $0.5 \text{ A}\cdot\text{g}^{-1}$	-	83.8% after 5000 cycles	Fu et al. (2020)	[284]
Nitrogen-oxygen co-doped CNF	Stabilized at 200°C for 1 h, annealed at 1000°C for 0.5 h in N_2 , and maintained at 600°C for 1 h	320 at $1 \text{ A}\cdot\text{g}^{-1}$	17.92	94.5% after 5000 cycles	Dai et al. (2020)	[285]

Table 6. Cont.

Electrospun Hybrid Materials	Thermal Treatment	Electrochemical Performance			Author (Year)	Ref.
		Specific Capacity ($F \cdot g^{-1}$)	Energy Density ($Wh \cdot kg^{-1}$)	Capacity Retention		
PI/CNF	Solvothermal treatment at 200 °C for 12 h	1139 at 5 $A \cdot g^{-1}$	94	90% after 10000 cycles	Zhang et al. (2020)	[286]
$Co_3O_4/C/CNF$	Stabilized at 250 °C for 4 h and carbonized at 950 °C for 1 h	1632 at 5 $A \cdot g^{-1}$	36.6	82.5% after 7000 cycles	Mukhiya et al. (2020)	[287]
MnO_2/TiO_2	Calcinated at 500 °C for 1 h	111.5 at 1 $A \cdot g^{-1}$	62	87.2% after 5000 cycles	Kolathodi et al. (2020)	[288]
MnO_2 /porous CNF	Oxidized at 280 °C for 1 h and carbonized at 280 °C for 1 h in N_2	228 at 1 $A \cdot g^{-1}$	25.3	94% after 10,000 cycles	Jeong et al. (2020)	[289]
$ZnFe_2O_4$ /carbon	Stabilized at 250 °C, carbonized at 600 °C, and annealed at 280 °C	237 at 1 $A \cdot g^{-1}$	-	93.1% after 10,000 cycles	Yang et al. (2020)	[290]
Fe_2MoC /carbon	Stabilized at 250 °C for 2 h and carbonized at 800 °C for 2 h in Ar	347 at 1 $A \cdot g^{-1}$	14.5	93% after 5000 cycles	Hao et al. (2020)	[291]
PAni/ MnO_2 /CNF	stabilized at 280 °C for 5.5 h and carbonized at 700 °C for 2 h	289 at 1 $A \cdot g^{-1}$	119	91% after 1000 cycles	Dirican et al. (2020)	[292]
$NiCo_2S_4$ /graphite	Carbonized at 2000 °C	1175.2 at 10 $A \cdot g^{-1}$	52.3	94.7% after 10,000 cycles	He et al. (2020)	[293]
$NiCo_2O_4$ /CNF	Carbonized	111 at 1 $A \cdot g^{-1}$	40.3	92% after 5000 cycles	Yang et al. (2020)	[294]

To date, supercapacitors have been recognized as high power density energy storage devices. Nevertheless, synthesis of appropriate electrodes for commercialization of supercapacitors has remained as a challenge. Electrospun structures have widely shown their great potentials as electrode materials of supercapacitors due to providing higher conductivity as well as appropriate structural stability and great porosity. Despite numerous successful efforts in the field of electrospun supercapacitor fabrication, there are several downsides (e.g., nonsufficient electrical conductivity) that must be addressed in the future. Evaluation of selenides/CNF and tellurides/CNF composites for conductivity enhancement, synthesis of metal oxides with complex interior for improvement of electrochemical behavior, and synthesis of one-dimensional porous electrospun fibers for boosting the electrical conductivity could be valuable explorations for elimination of drawbacks associated with supercapacitors.

7. Electrochemical Solar Cells

Remembering the definition from the abstract section that electrochemical devices convert chemical reactions into electrical energy or vice versa, actually all solar cells could be described as electrochemical solar cells. Indeed, there are several different definitions of electrochemical solar cells. Most often, however, solar cells are differentiated into solid state solar cells [295,296] and photoelectrochemical solar cells in which chemical reaction with ions or water take place [297,298]. In the latter, the contact potential between a semiconductor and an electrolyte leads to the separation of charge carriers which were photoinduced [299,300], or in other words, the potential barrier which is necessary for charge separation in solar cells is realized here by the semiconductor-electrolyte junction [301]. The principle of such cells is depicted in Figure 12 [302].

Recently, dye-sensitized solar cells (DSSCs) and perovskite solar cells belong to the often investigated so-called third-generation photovoltaic cells which can be described as electrochemical solar cells. This is why diverse review papers are available, giving a good overview of DSSCs [302–306] as well as perovskite solar cells [307–311]. Nevertheless, research on other electrochemical solar cells and specialized devices is still going on.

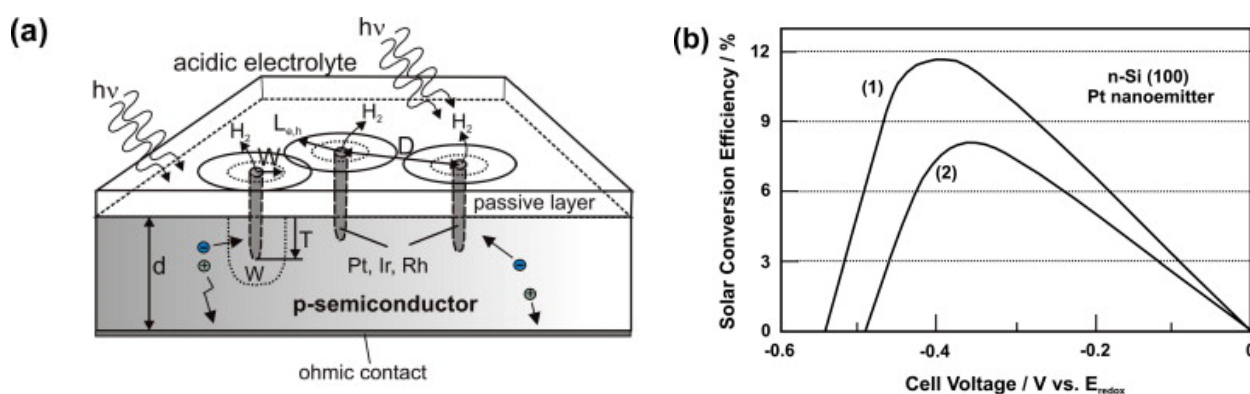


Figure 12. (a) Electrochemical solar cell design for protruding emitter noble metals in the electrolyte; (b) exemplary solar conversion efficiency at the redox electrolyte contact under an illumination of 100 mW cm^{-2} after different pre-treatments: (1) after photocurrent oscillation in $0.1 \text{ M NH}_4\text{F}$ followed by electrochemical pore deepening in 1 M NaOH ; and (2) after emersion at the decreasing branch of a photocurrent oscillation only. Reprinted from [300], with permission from Elsevier.

Vijayaraghavan et al., for example, used spray pyrolysis to deposit CdTe thin films on a TiO_2 nanoparticle layer as photo-active semiconductor in combination with iodine/triiodide electrolyte and found an efficiency of 0.4% for an optimized CdTe layer thickness [312]. A CdSeS composite film was applied by Hazra et al. in their electrochemical cell, leading to reduced photo degradation which is a severe problem in electrochemical cells [313]. The ternary alloy $\text{Cd}_{1-x}\text{Zn}_x\text{Se}$ was suggested by Kissinger to prepare an electrochemical solar cell with $\text{Na}_2\text{S-S-NaOH}$ as redox electrolyte, reaching efficiencies of up to 4.5% [314]. Another often reported material is WSe_2 which was shown to have high efficiencies of about 14–17% [315–317].

Aljafari et al. suggested combining an electrochemical solar cell with a supercapacitor into a single device, including a PVA/hydrochloric acid-based gel electrolyte, multi-walled CNT, and fluorine-doped tin oxide as counter and working electrodes, respectively, where the working electrode consists of a composite of a conducting polymer and synthetic dyes, such as methylene blue, methyl orange, or Prussian blue [318]. They reported strong photo-electrochemical reaction especially for methylene blue. In the aforementioned papers, crystallinity of the active components is regarded as more important than the surface morphology.

Besides these and a few other reports found in the recent scientific literature, electrochemical solar cells mostly refer to DSSCs for which the reader is referred to the aforementioned or other specialized review papers.

8. Sensors

Sensors are devices required for authentic detections in various fields of chemical analysis, food assessment, clinical diagnosis, and many more. They have been developed based upon several detection technologies including fluoro-photometry, chemoluminescence, liquid chromatography, spectrophotometry, and electrochemistry [319,320]. Among them, electrochemical sensors received tremendous attention resulting from their wide detection range as well as high selectivity [321]. This kind of sensors was first introduced by Clark in 1962 [322]. They are commonly comprised of a receptor and a signal transducer (Figure 13). In such devices, the interactions between the sensitive receptor and analyte are measured. Then, an electrical signal is applied to clarify the level of interaction. Through analysis of the reported signal, information about the material content could be obtained.

According to the mentioned operational mechanism, such sensors mainly contain an electrode connected to a sensitive component. Materials with specific performance are deposited on the electrode surface. By applying an external voltage, the utilized specific materials take part in a redox reaction which results in generation of a current. Then, the produced current is transferred to a signal analysis system to report the binding effi-

ciency. An ideal electrochemical sensor should reveal low detection limit and appropriate selectivity. In addition, it is vital to report the result in a short response time [321].

Electrospun membranes are great candidates to design highly efficient electrochemical devices, especially electrochemical sensors. This could be attributed to the unique characteristics of the nanofibrous mats, such as high SSA, proper porosity structure, tiny pores, interconnected fibers, etc. In recent decades, great performance features of different electrospun electrochemical sensors have been extensively reported. The evaluated nanofibrous structures have been mainly obtained through electrospinning of various kinds of polymeric, carbon-based, and metal oxide materials [323,324].

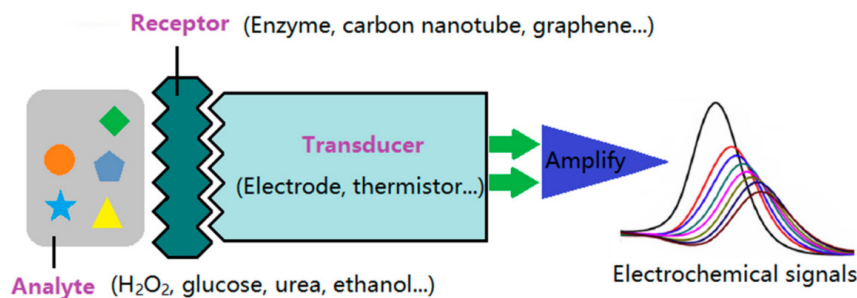


Figure 13. Schematic diagram of an electrochemical sensor. Reproduced from [325], originally published under a CC-BY license.

8.1. Electrochemical Sensors Based on Electrospun Polymeric Fibers

Enzymes are able to catalyze numerous interactions due to their catalytic activity characteristics. They are widely utilized on the electrode surfaces for sensing activity regarding to their proper sensitivity along with great selectivity. Notably, stabilizing of the enzymes on the surface of the electrodes is considered as a critical step in sensor fabrication procedure. Physical adsorption, sol–gel, and self-assembly are some of the commonly applied routes for enzyme stabilization. Meanwhile, unique characteristics of the polymeric nanofibers have facilitated immobilization of the enzymes on the surface of the electrodes. This could be carried out through direct and indirect methods. In the prior technique, enzymes are embedded into the polymeric nanofibers by direct loading of enzymes into the electrospinning solutions, whereas enzymes could be added to the electrospun polymeric nanofibers by using the post-modification processes [324,325]. As an example, Ren et al. immobilized glucose oxidase (GOx) by direct electrospinning of PVA/GOx on the surface of an electrode followed by a cross-linking procedure. The as-spun structure showed linear response in the range from 1 to 10 mM and detection limit of 0.05 mM [326]. In another attempt, Arecchi et al. displayed linear response range of 1 to 10 mM and detection limit of 6 μ M by covalent stabilization of GOx on a Nylon-6 electrospun membrane [327]. Several recent approaches focusing on modification of the electrodes by using the electrospun polymeric fibers are summarized in Table 7.

Table 7. Polymeric nanofibers utilized for modification of the electrochemical sensors.

Support Materials	Target	Linear Response Range	Detection Limit	Author (Year)	Ref.
PAN/PPy/PPy ₃ COOH	Glucose	20 nM–2 μ M	2 nM	Sapountzi et al. (2020)	[328]
Cellulose acetate/chitosan	Glucose	5 μ M–0.75 mM	4.8 μ M	Yezer & Demirkol (2020)	[329]
PAN/montmorillonite	Glucose	1.0×10^{-5} – 2.45×10^{-3} M and 2.45×10^{-3} – 15×10^{-3} M	2.4 μ M	Apetrei & Camurlu (2020)	[330]
Chitosan/GO	Glucose	0.05–20 mM	0.02 mM	Mehdizadeh et al. (2020)	[331]
Chitosan/sodium dodecyl sulfate/hemoglobin	Hydrogen peroxide	3–2940 μ M	0.16 μ M	Kholosi et al. (2020)	[332]
PVA/chitosan	Urea	0.023–0.23 mM	-	Kutlu et al. (2020)	[333]
PAni/GO	Breast cancer biomarker	10^{-15} – 10^{-7} M	3.01×10^{-16} M	Su et al. (2020)	[120]

8.2. Electrochemical Sensors Based on Carbon Nanofibers

Wide potential window, cost effectiveness, and inertness are well-known intrinsic features of the carbon-based electrodes. Carbon materials have been mainly applied in various forms including carbon fibers, carbon powder, graphite, and many more. With development of nano-sized materials, CNFs have been applied in fabrication of several electrochemical applications, specifically sensing and electro-analysis. CNFs are introduced as an efficient matrix for immobilization of enzymes due to several advantages such as excellent mechanical strength, appropriate conductivity, and high SSA. In addition to their performance as ideal matrixes, proper electrical conductivity has provided their potential for acting as transducers. This may be attributed to the existence of more edge planes in the CNF structure [334]. CNF-based electrochemical sensors are commonly fabricated using an electrospinning method followed by a carbonization technique. Wu et al. investigated catalytic activity of an electrochemical glucose sensor designed by CNFs which resulted in linear response range of 0.1 to 78 μM and low detection limit of 0.07 μM [335]. Based on a study performed by Bae et al., increasing the porosity, crystallinity, and orientation of the carbon nanofibers could result in higher current and superior sensitivity [336]. In addition, Liu et al. reported linear range of 1 to 800 μM with a low detection limit of 0.6 μM for a H_2O_2 electrochemical sensor for an electrode loaded by Pt nanoparticles and CNFs [337]. A sensitivity down to 1 nM and high selectivity for glucose molecules was presented by Kim et al., using cobalt-oxide-incorporated multichannel carbon nanotubes [338], while Simsek et al. reached a detection limit of 0.3 μM glucose with Ni nanoparticles adhered to a CNF network [339].

A summary of the most recent fabricated sensors based on CNFs is provided in Table 8.

Table 8. Catalytic activity of the electrochemical sensors based on carbon nanofibers.

Support Materials	Target	Linear Response Range	Detection Limit	Author (Year)	Ref.
CNF	Malachite green	0.1–22.1 μM	0.05 μM	Yang et al. (2020)	[340]
CNF	Tramadol	0.05–100 nM	0.05 nM	Jahromi et al. (2020)	[341]
CNF	Cadmium (II)	2–100 ppb	0.11 ppb	Fakude et al. (2020)	[342]
CNF	Paracetamol	2.0×10^{-9} – 5.0×10^{-8} and 1.0×10^{-7} – 2.0×10^{-6} M	5.4×10^{-10} M	Sasal et al. (2020)	[343]
CNF/GO	Uric acid	100–700 μM	0.14 $\mu\text{A} \cdot \mu\text{M}^{-1}$	Aryal & Jeong et al. (2020)	[344]
CNF/ β -cyclodextrin	Ascorbic acid	0.9 μM	100–400 μM	Aryal & Jeong et al. (2020)	[345]
CNF/poly(L-aspartic acid)/nanodiamond particles	L-ascorbic acid	0.2 μM –1.8 mM	0.1 μM	Kacer & Erden (2020)	[346]
CNF/PEDOT	neurotransmitters	0.1–9 μM	0.045 μM	Saunier et al. (2020)	[347]
CNF/zeolitic imidazolate framework-8	dihydroxybenzene isomers	0.06 μM	2–400 μM	Yang et al. (2020)	[348]

8.3. Electrochemical Sensors Based on Metal and Metal Oxide Nanofibers

Distinctive characteristics of the electrospun metals and metal oxides, such as high specific surface area, interconnected pores, proper porosity, fast response, high sensitivity, etc., have made them a great candidate for fabrication of various electrospun sensors. Nanofibrous metal oxides are commonly produced through the following procedures: (a) electrospinning of polymer solution embedded with metal oxide precursor, and (b) dipping the electrospun fibers into a metal oxide precursor solution. Both methods are followed by a calcination step. During the calcination process, the utilized polymer content is degraded, while metal-oxide crystals are grown and nucleated by temperature increment. Numerous literatures have reported excellent performance of the mentioned electrospun fibers for sensing of different targets, including glucose, ascorbic acid, cholesterol, uric acid, and so on. These kinds of electrospun fibers are applied in synthesis of enzyme and non-enzyme electrochemical sensors. The non-enzyme sensors act based on catalyzed reactions. So, electro-catalytic materials (e.g., metals and metal oxides) play a key role

in providing the aforementioned reactions. The non-enzyme electrochemical sensors could reveal superior cycling stability compared with the enzyme ones. In addition, they are synthesized through easier processes as they do not require an immobilization procedure. Notably, the combination of nano-dimensional metals and metal oxides with carbon-based materials has been broadly applied to enhance the performance of signal transduction in the non-enzyme electrochemical sensors. Nano-sized metals and metal oxides display significantly superior transducer activity as compared to the micro-sized ones [349–351]. Table 9 lists several recent studies which have explored electrochemical behavior of electrospun sensors through fabrication of metal and metal oxide nanofibers and their combination with CNFs.

Table 9. Electrospun electrochemical sensors based on metals and metal oxides.

Materials	Target	Linear Response Range	Detection Limit	Author (Year)	Ref.
CuCr ₂ O ₄ /CuO	Methotrexate	0.1–300 µM	25 nM	Salandari-Jolge et al. (2020)	[352]
WO ₃	Catechol	1–100 µM	0.52 µM	Veeralingam & Badhulika (2020)	[353]
L-cysteine/ZnO	Lead ion	10–140 µg·Lit ⁻¹	0.397 µg·L ⁻¹	Oliviera et al. (2020)	[354]
NiCo ₂ S ₄ /graphene/CNF	Pyrimethanil	0.06–800 µM	20 nM	He et al. (2020)	[355]
Co ₃ O ₄ /CNF	Hemoglobin	1–12 mM	0.33 mM	Xie et al. (2020)	[356]
NiMoO ₄ /CNF	Glucose	0.0003–4.5 mM	50 nM	Rani et al. (2020)	[357]
Graphene/gold	Glucose	0.5–9 mM	55 µM	Shamsabadi et al. (2020)	[358]
MnO ₂ /Co ₃ O ₄ /CNF	Glucose	<10.2 mM	0.02 µM	Wei et al. (2020)	[359]
Ferric ceria	Uric acid	0.5–500 µM	0.3 µM	Shekh et al. (2020)	[360]
ZnO/CNT	Atrazine	10 zM–1 µM	5.368 zM	Supraja et al. (2020)	[361]
CNF/Co	Hydrogen peroxide	<50 mM	10 µM	Riaz et al. (2020)	[362]
Au/Pt/CNF	Mercury ion	10 ⁻¹⁵ –10 ⁻⁶ M	3.33 × 10 ⁻¹⁶ M	Xie et al. (2021)	[363]
ZrO ₂ /graphene	Osteopontin	0.01 pg·mLit ⁻¹ –2.0 ng·mLit ⁻¹	4.76 fg·mL ⁻¹	Zhou et al. (2020)	[364]
TiO ₂ /CNT/CNF	Bovine hemoglobin	5–80 mM	1.67 mM	Zhu et al. (2020)	[365]
CoFe ₂ O ₄ /GO	Rutin	0.001–0.1 nM and from 1.0–100 nM	0.94 pM	Ansari et al. (2020)	[366]
CoFe ₂ Se ₄ /CNF	Hydroquinone	0.5–200 µM	0.13 µM	Yin et al. (2020)	[367]
	Catechol	0.5–190 µM	0.15 µM		
	Resorcinol	5–350 µM	1.36 µM		

As a working principal, effective sensing and conversion of the signals are the main features of an ideal electrochemical sensor. In addition, efficiency, size, and price are other critical issues related to an appropriate electrochemical sensor. Applying nanotechnology for the fabrication of electrochemical sensors has led to production of more efficient, smaller, and cheaper electrochemical sensors due to high specific surface area, great electrical conductivity, and so on. Nevertheless, progress and development of technology have a greater demand for increment of sensitivity and specificity. Among various materials applied for synthesis of electrospun non-enzyme sensors, fibrous composites of metal or metal oxides with carbon nanofibers have illustrated desirable features and could be the future trend of most researches. In addition, production of multi-analysis electrochemical sensor systems is of interest to researchers and developers. Any advancement in this area could be beneficial for various medical fields.

9. Conclusions

In this review, the broad range of recent approaches on applications of electrospun fibers in various electrochemical structures has been evaluated. Based on the investigated efforts, electrospun fibers have enhanced various characteristics of electrolytic cells, battery structures, fuel cells, supercapacitors, solar cells, and sensors. The great potential of such structures for being applied as different components of the mentioned cells has been widely illustrated. Regarding the possible materials for nanofiber mats in electrochemical devices,

a broad range of materials can be found in the recent literature, from quite common, easily spinnable ones like PAN along carbon nanofibers, e.g., produced by stabilizing and carbonizing PAN or other precursor fibers, to semiconducting or metallic nanoparticles integrated in a polymer matrix or as pure nanofibers produced by calcination of the electrospun composite fibers. While electrode materials need to be conductive and are thus often produced from carbon nanofibers, partly also from conductive polymers, the mechanical properties and pore sizes are more important for separating membranes which thus often consist of PAN and other reliably spinnable materials. Sensors, on the other hand, necessitate specific metallic or other constituents to reach a high sensitivity towards a desired molecule.

Overall, nanofibrous structures have promising industrial applications in various electrochemical cells regarding their unique and fabulous features. Nevertheless, there is still a lot of challenges to be solved and open questions to be investigated. For electrolytic cells, e.g., research should be broadened beyond electrolytic water splitting and degradation of dyes and other contaminants. Regarding batteries, the main goals are a high efficiency and improved functionality, necessitating further improvements of all battery components, especially in terms of mechanical stability, electrical conductivity, and ionic conductivity. For the diverse kinds of fuel cells in which electrospun nanofiber mats can be applied, the most crucial parameters for the electrodes are specific surface area and conductivity as well as introducing a suitable catalyst, while for membranes, the pore size distribution and possible selectivity governs the choice of materials and structures. In supercapacitors, high conductivity, structural stability, and great porosity of nanofiber mats are again the most important parameters. Especially the electrical conductivity and the electrochemical properties need to be improved further, which may be done by introducing composite materials like selenide/CNF or telluride/CNF nanofibers or metal oxides with complex interior, respectively. Research on electrochemical solar cells is mainly related to DSSCs or perovskite solar cells recently; here, finding non-toxic, abundantly available materials with high efficiency as dyes or for other parts of these solar cells would highly increase the further interest in this topic. Finally, nanofiber mats for applications in electrochemical sensors need further increased sensitivity and specificity, ideally in the form of multi-analysis sensor systems. We hope that our review paper can support future research in all these areas.

Author Contributions: Conceptualization, S.N.B. and A.E.; investigation, S.N.B. and A.E.; writing—original draft preparation, S.N.B. and A.E.; writing—review and editing, S.N.B. and A.E.; visualization, S.N.B. and A.E. Both authors have read and agreed to the published version of the manuscript.

Funding: This research was funded by the Iran National Science Foundation (INSF) with grant number of 98025579 and the German Federal Ministry for Economic Affairs and Energy via the AiF, based on a resolution of the German Bundestag, grant number KK5044902SY0.

Institutional Review Board Statement: Not applicable.

Informed Consent Statement: Not applicable.

Data Availability Statement: No data were generated in this study.

Conflicts of Interest: The authors declare no conflict of interest. The funders had no role in the design of the study; in the collection, analyses, or interpretation of data; in the writing of the manuscript, or in the decision to publish the results.

References

1. Virkar, A.V. A model for degradation of electrochemical devices based on linear non-equilibrium thermodynamics and its application to lithium ion batteries. *J. Power Sources* **2011**, *196*, 5970–5984. [[CrossRef](#)]
2. Molaiyan, P.; Witter, R. Mechanochemical synthesis of solid-state electrolyte $\text{Sm}_{1-x}\text{Ca}_x\text{F}_{3-x}$ for batteries and other electrochemical devices. *Mater. Lett.* **2019**, *244*, 22–26. [[CrossRef](#)]
3. Zhao, L.; Hu, Y.-S.; Li, H.; Wang, Z.X.; Chen, L.Q. Porous $\text{Li}_4\text{Ti}_5\text{O}_{12}$ Coated with N-Doped Carbon from Ionic Liquids for Li-Ion Batteries. *Adv. Mater.* **2011**, *23*, 1385–1388. [[CrossRef](#)]

4. Garcia, E.M.; Taroco, H.A.; Matencio, T.; Domingues, R.Z.; dos Santos, J.A.F.; Ferreira, R.V.; Lorencon, E.; Lima, D.Q.; de Freitas, B.J.G. Electrochemical recycling of cobalt from spent cathodes of lithium-ion batteries: Its application as supercapacitor. *J. Appl. Electrochem.* **2012**, *42*, 361–366. [[CrossRef](#)]
5. Chen, G.Z. Supercapacitor and supercapattery as emerging electrochemical energy stores. *Int. Mater. Rev.* **2017**, *62*, 173–202. [[CrossRef](#)]
6. Zhang, J.T.; Zhao, X.S. On the configuration of supercapacitors for maximizing electrochemical performance. *ChemSusChem* **2012**, *5*, 818–841. [[CrossRef](#)]
7. Lucia, U. Overview on fuel cells. *Renew. Sustain. Energy Rev.* **2014**, *30*, 164–169. [[CrossRef](#)]
8. Jacobson, A.J. Materials for solid oxide fuel cells. *Chem. Mater.* **2010**, *22*, 660–674. [[CrossRef](#)]
9. Elabd, Y.A.; Hickner, M.A. Block copolymers for fuel cells. *Macromolecules* **2011**, *44*, 1–11. [[CrossRef](#)]
10. Kumar, S.; Bukkitgar, S.D.; Singh, S.; Pratibha; Singh, V.; Reddy, K.R.; Shetti, N.P.; Reddy, C.V.; Sadhu, V.; Naveen, S. Electrochemical sensors and biosensors based on graphene functionalized with metal oxide nanostructures for healthcare applications. *Chem. Sel.* **2019**, *4*, 5322–5337. [[CrossRef](#)]
11. Hernández-Rodríguez, J.F.; Rojas, D.; Escarpa, A. Electrochemical sensing directions for next-generation healthcare: Trends, challenges, and frontiers. *Anal. Chem.* **2021**, *93*, 167–183. [[CrossRef](#)] [[PubMed](#)]
12. Bae, C.W.; Toi, P.T.; Kim, B.Y.; Lee, W.I.; Lee, H.B.; Hanif, A.; Lee, E.H.; Lee, N.-E. Fully Stretchable Capillary Microfluidics-Integrated Nanoporous Gold Electrochemical Sensor for Wearable Continuous Glucose Monitoring. *ACS Appl. Mater. Interfaces* **2019**, *11*, 14567–14575. [[CrossRef](#)] [[PubMed](#)]
13. Bay, L.; West, K.; Winther-Jensen, B.; Jacobsen, T. Electrochemical reaction rates in a dye-sensitised solar cell—the iodide/tri-iodide redox system. *Sol. Energy Mater. Sol. Cells* **2006**, *90*, 341–351. [[CrossRef](#)]
14. Ehrmann, A.; Blachowicz, T. Recent coating materials for textile-based solar cells. *Aims Mater. Sci.* **2019**, *6*, 234–251. [[CrossRef](#)]
15. Hatamvand, M.; Kamrani, E.; Lira-Cantú, M.; Madsen, M.; Patil, B.R.; Vivo, P.; Mehmood, M.S.; Numan, A.; Ahmed, I.; Zhan, Y.Q. Recent advances in fiber-shaped and planar-shaped textile solar cells. *Nano Energy* **2020**, *71*, 104609. [[CrossRef](#)]
16. McDowell, M.T.; Cui, Y. Single Nanostructure Electrochemical Devices for Studying Electronic Properties and Structural Changes in Lithiated Si Nanowires. *Adv. Energy Mater.* **2011**, *1*, 894–900. [[CrossRef](#)]
17. Guo, Y.-G.; Hu, J.-S.; Wan, L.-J. Nanostructured materials for electrochemical energy conversion and storage devices. *Adv. Mater.* **2008**, *20*, 2878–2887. [[CrossRef](#)]
18. Zhou, M.; Xu, Y.; Lei, Y. Heterogeneous nanostructure array for electrochemical energy conversion and storage. *Nano Today* **2018**, *20*, 33–57. [[CrossRef](#)]
19. Greiner, A.; Wendorff, J.H. Electrospinning: A Fascinating Method for the Preparation of Ultrathin Fibers. *Angew. Chem. Int. Ed.* **2007**, *46*, 5670–5703. [[CrossRef](#)]
20. Grothe, T.; Großrhode, C.; Hauser, T.; Kern, P.; Stute, K.; Ehrmann, A. Needleless electrospinning of PEO nanofibers mats. *Adv. Eng. Res.* **2017**, *102*, 54–58.
21. Yadav, D.; Amini, F.; Ehrmann, A. Recent advances in carbon nanofibers and their applications—A review. *Eur. Polym. J.* **2020**, *138*, 109963. [[CrossRef](#)]
22. Yarin, A.L.; Zussman, E. Upward needleless electrospinning of multiple nanofibers. *Polymer* **2004**, *45*, 2977–2980. [[CrossRef](#)]
23. Wang, X.; Niu, H.T.; Wang, X.G.; Lin, T. Needleless electrospinning of uniform nanofibers using spiral coil spinnerets. *J. Nanomater.* **2012**, *2012*, 785920. [[CrossRef](#)]
24. Liu, Y.Q.; Zhang, X.P.; Xia, Y.N.; Yang, H. Magnetic-field-assisted electrospinning of aligned straight and wavy polymeric nanofibers. *Adv. Mater.* **2010**, *22*, 2454–2457. [[CrossRef](#)] [[PubMed](#)]
25. Molnar, K.; Nagy, Z.K. Corona-electrospinning: Needleless method for high-throughput continuous nanofiber production. *Eur. Polym. J.* **2016**, *74*, 279–286. [[CrossRef](#)]
26. Klinkhammer, K.; Seiler, N.; Grafahrend, D.; Gerardo-Nava, J.; Mey, J.; Brook, G.A.; Möller, M.; Dalton, P.D.; Klee, D. Deposition of electrospun fibers on reactive substrates for in vitro investigations. *Tissue Eng Part. C* **2009**, *15*, 77–85. [[CrossRef](#)] [[PubMed](#)]
27. Mamun, A. Review of possible applications of nanofibrous mats for wound dressings. *Tekstilec* **2019**, *62*, 89–100. [[CrossRef](#)]
28. Wehlage, D.; Blattner, H.; Mamun, A.; Kutzli, I.; Diestelhorst, E.; Rattenholl, A.; Gudermann, F.; Lütkemeyer, D.; Ehrmann, A. Cell growth on electrospun nanofiber mats from polyacrylonitrile (PAN) blends. *Aims Bioeng.* **2020**, *7*, 43–54. [[CrossRef](#)]
29. Mamun, A.; Trabelsi, M.; Klöcker, M.; Storck, J.L.; Böttjer, R.; Sabantina, L. Needleless electrospun polyacrylonitrile/konjac glucomannan nanofiber mats. *J. Eng. Fibers Fabr.* **2020**, *15*, 1558925020964806.
30. Ippel, B.D.; Van Haaften, E.E.; Bouten, C.V.; Dankers, P.Y. Impact of Additives on Mechanical Properties of Supramolecular Electrospun Scaffolds. *ACS Appl. Polym. Mater.* **2020**, *2*, 3742–3748. [[CrossRef](#)]
31. Topuz, F.; Holtzl, T.; Szekely, G. Scavenging organic micropollutants from water with nanofibrous hypercrosslinked cyclodextrin membranes derived from green resources. *Chem. Eng. J.* **2021**, *419*, 129443. [[CrossRef](#)]
32. Mahdiah, Z.; Mitra, S.; Holian, A. Core-Shell Electrospun Fibers with an Improved Open Pore Structure for Size-Controlled Delivery of Nanoparticles. *Acs Appl. Polym. Mater.* **2020**, *2*, 4004–4015. [[CrossRef](#)]
33. Yim, V.M.-W.; Lo, A.S.-W.; Deka, B.J.; Guo, J.; Kharraz, J.A.; Horváth, I.T.; An, A.K. Molecular engineering low-surface energy membranes by grafting perfluoro-tert-butoxy chains containing fluorosilica aerogels. *Green Chem.* **2020**, *22*, 3283–3295. [[CrossRef](#)]

34. Topuz, F.; Abdulhamid, M.A.; Nunes, S.P.; Szekely, G. Hierarchically porous electrospun nanofibrous mats produced from intrinsically microporous fluorinated polyimide for the removal of oils and non-polar solvents. *Environ. Sci. Nano* **2020**, *7*, 1365–1372. [[CrossRef](#)]
35. Yalcinkaya, F.; Siekierka, A.; Bryjak, M. Surface modification of electrospun nanofibrous membranes for oily wastewater separation. *RSC Adv.* **2017**, *7*, 56704–56712. [[CrossRef](#)]
36. Roche, R.; Yalcinkaya, F. Incorporation of PVDF nanofibre multilayers into functional structure for filtration applications. *Nanomaterials* **2018**, *8*, 771. [[CrossRef](#)] [[PubMed](#)]
37. Kozior, T.; Mamun, A.; Trabelsi, M.; Wortmann, M.; Sabantina, L.; Ehrmann, A. Electrospinning on 3D printed polymers for mechanically stabilized filter composites. *Polymers* **2019**, *11*, 2034. [[CrossRef](#)]
38. Boyraz, E.; Yalcinkaya, F. Hydrophilic surface-modified PAN nanofibrous membranes for efficient oil-water emulsion separation. *Polymers* **2021**, *13*, 197. [[CrossRef](#)]
39. Wu, W.-N.; Yu, H.-F.; Yeh, M.-H.; Ho, K.-C. Incorporating electrospun nanofibers of TEMPO-grafted PVDF-HFP polymer matrix in viologen-based electrochromic devices. *Sol. Energy Mater. Sol. Cells* **2020**, *208*, 110375. [[CrossRef](#)]
40. Haider, A.; Haider, S.; Kang, I.-K. A comprehensive review summarizing the effect of electrospinning parameters and potential applications of nanofibers in biomedical and biotechnology. *Arab. J. Chem.* **2018**, *11*, 1165–1188. [[CrossRef](#)]
41. Ibrahim, H.M.; Klingner, A. A review on electrospun polymeric nanofibers: Production parameters and potential applications. *Polym. Test.* **2020**, *90*, 106647. [[CrossRef](#)]
42. Rodríguez-Tobias, H.; Morales, G.; Grande, D. Comprehensive review on electrospinning techniques as versatile approaches toward antimicrobial biopolymeric composite fibers. *Mater. Sci. Eng. C* **2019**, *101*, 306–322. [[CrossRef](#)]
43. Banitaba, S.N.; Semnani, D.; Heydari-Soureshjani, E.; Rezaei, B.; Ensafi, A.A. The effect of concentration and ratio of ethylene carbonate and propylene carbonate plasticizers on characteristics of the electrospun PEO-based electrolytes applicable in lithium-ion batteries. *Solid State Ion.* **2020**, *347*, 115252. [[CrossRef](#)]
44. Sadek, A.Z.; Baker, C.O.; Powell, D.A.; Wlodarski, W.; Kaner, R.B.; Kalantar-zadeh, K. Polyaniline nanofiber based surface acoustic wave gas sensors—Effect of nanofiber diameter on H₂ response. *IEEE Sens. J.* **2007**, *7*, 213–218. [[CrossRef](#)]
45. Şener, A.G.; Altay, A.S.; Altay, F. Effect of voltage on morphology of electrospun nanofibers. In Proceedings of the 2011 7th International Conference on Electrical and Electronics Engineering (ELECO), Bursa, Turkey, 1–4 December 2011; pp. 1-324–I-328.
46. Shao, H.; Fang, J.; Wang, H.; Lin, T. Effect of electrospinning parameters and polymer concentrations on mechanical-to-electrical energy conversion of randomly-oriented electrospun poly (vinylidene fluoride) nanofiber mats. *RSC Adv.* **2015**, *5*, 14345–14350. [[CrossRef](#)]
47. Beachley, V.; Wen, X. Effect of electrospinning parameters on the nanofiber diameter and length. *Mater. Sci. Eng. C* **2009**, *29*, 663–668. [[CrossRef](#)]
48. Stachewicz, U.; Szewczyk, P.K.; Kruk, A.; Barber, A.H.; Czyrska-Filemonowicz, A. Pore shape and size dependence on cell growth into electrospun fiber scaffolds for tissue engineering: 2D and 3D analyses using SEM and FIB-SEM tomography. *Mater. Sci. Eng. C* **2019**, *95*, 397–408. [[CrossRef](#)] [[PubMed](#)]
49. Tarus, B.; Fadel, N.; Al-Oufy, A.; El-Messiry, M. Effect of polymer concentration on the morphology and mechanical characteristics of electrospun cellulose acetate and poly(vinyl chloride) nanofiber mats. *Alex. Eng. J.* **2016**, *55*, 2975–2984. [[CrossRef](#)]
50. Angamma, C.J.; Jayaram, S.H. Analysis of the effects of solution conductivity on electrospinning process and fiber morphology. *IEEE Trans. Ind. Appl.* **2011**, *47*, 1109–1117. [[CrossRef](#)]
51. Marshall, R.J.; Walsh, F.C. A review of some recent electrolytic cell designs. *Surf. Technol.* **1985**, *24*, 45–77. [[CrossRef](#)]
52. Furuya, N.; Yamazaki, T.; Shibata, M. High performance Ru-Pd catalysts for CO₂ reduction at gas-diffusion electrodes. *J. Electroanal. Chem.* **1997**, *431*, 39–41. [[CrossRef](#)]
53. Hara, K.; Sakata, T. Electrocatalytic formation of CH₄ from CO₂ on a Pt gas diffusion electrode. *J. Electrochem. Soc.* **1997**, *144*, 539–545. [[CrossRef](#)]
54. Yamamoto, T.; Tryk, D.A.; Fujishima, A.; Ohata, H. Production of syngas plus oxygen from CO₂ in a gas-diffusion electrode-based electrolytic cell. *Electrochim. Acta* **2002**, *47*, 3327–3334. [[CrossRef](#)]
55. Issabayeva, G.; Aroua, M.K.; Sulaiman, N.M. Electrodeposition of copper and lead on palm shell activated carbon in a flow-through electrolytic cell. *Desalination* **2006**, *194*, 192–201. [[CrossRef](#)]
56. Bertazzoli, R.; Widner, R.C.; Lanza, M.R.V.; Di Iglia, R.A.; Sousa, M.F.B. Electrolytic removal of metals using a flow-through cell with a reticulated vitreous carbon cathode. *J. Braz. Chem. Soc.* **1997**, *8*, 487–493. [[CrossRef](#)]
57. Brennstainer, A.; Zondlo, J.W.; Stiller, A.H.; Stansberry, P.G.; Tian, D.C.; Xu, Y. Environmental pollution control devices based on novel forms of carbon: Heavy metals. *Energy Fuels* **1997**, *11*, 348–353. [[CrossRef](#)]
58. Abghou, Y.; Sigtryggsson, S.B.; Skúlason, E. Biomimetic nitrogen fixation catalyzed by transition metal sulfide surfaces in an electrolytic cell. *ChemSusChem* **2019**, *12*, 4265–4273. [[CrossRef](#)] [[PubMed](#)]
59. Jeong, J.-Y.; Kim, H.-K.; Kim, J.-H.; Park, J.-Y. Electrochemical removal of nitrate using ZVI packed bed bipolar electrolytic cell. *Chemosphere* **2012**, *89*, 172–178. [[CrossRef](#)] [[PubMed](#)]
60. Huang, Y.H.; Zhang, T.C. Enhancement of nitrate reduction in Fe⁰-packed columns by selected cations. *J. Environ. Eng.* **2005**, *131*, 603–611. [[CrossRef](#)]
61. Zhu, H.B.; Wang, L.; Chen, Y.M.; Li, G.Y.; Li, H.; Tang, Y.; Wang, P.Y. Electrochemical depolymerization of lignin into renewable aromatic compounds in a nondiaphragm electrolytic cell. *RSC Adv.* **2014**, *4*, 29917. [[CrossRef](#)]

62. Manesh, K.M.; Santhosh, P.; Gopalan, A.; Lee, K.-P. Electrospun poly(vinylidene fluoride)/poly(aminophenylboronic acid) composite nanofibrous membrane as a novel glucose sensor. *Anal. Biochem.* **2007**, *360*, 189–195. [[CrossRef](#)]
63. Ignatova, M.; Manolova, N.; Rashkov, I. Novel antibacterial fibers of quaternized chitosan and poly(vinyl pyrrolidone) prepared by electrospinning. *Eur. Polym. J.* **2007**, *43*, 1112–1122. [[CrossRef](#)]
64. Penchev, H.; Paneva, D.; Manolova, N.; Rashkov, I. Hybrid nanofibrous yarns based on *N*-carboxyethylchitosan and silver nanoparticles with antibacterial activity prepared by self-bundling electrospinning. *Carbohydr. Res.* **2010**, *345*, 2374–2380. [[CrossRef](#)]
65. Toncheva, A.; Paneva, D.; Manolova, N.; Rashkov, I.; Mita, L.; Crispi, S.; Damiano, G.M. Dual vs. single spinneret electrospinning for the preparation of dual drug containing non-woven fibrous materials. *Colloids Surf. A Physicochem. Eng. Asp.* **2013**, *439*, 176–183. [[CrossRef](#)]
66. Liu, F.F.; Wang, X.H.; Chen, T.T.; Zhang, N.Y.; Wie, Q.; Tian, J.L.; Wang, Y.B.; Ma, C.; Lu, Y. Hydroxyapatite/silver electrospun fibers for anti-infection and osteoinduction. *J. Adv. Res.* **2020**, *21*, 91–102. [[CrossRef](#)]
67. Soto-Nieto, F.; Fariás, R.; Reyes-López, S.Y. Sol-gel and electrospinning synthesis of silica-hydroxyapatite-silver nanofibers for SEIRAS and SERS. *Coatings* **2020**, *10*, 910. [[CrossRef](#)]
68. Sun, Y.Y.; Wang, G.; Dong, Y.; Yian, B.Q.; Meng, Y.L.; Qiu, J.S. Electrolysis removal of methyl orange dye from water by electrospun activated carbon fibers modified with carbon nanotubes. *Chem. Eng. J.* **2014**, *253*, 73–77. [[CrossRef](#)]
69. Li, L.; Liu, Y.; Li, Y.F. Electrochemical degradation of methylene blue aqueous solution on electrospinning nanofibers (ESF) electrodes. *Adv. Mater. Res.* **2013**, *807–809*, 1362–1367. [[CrossRef](#)]
70. Hwang, I.-H.; Choi, S.-Y.; Lee, S.H.; Lee, Y.-H.; Lee, S.M.; Kim, S.-C.; Kim, S.S. Electrospinning method-based CNF properties analysis and its application to electrode in electrolysis process. *Appl. Chem. Eng.* **2017**, *28*, 257–262.
71. Kim, J.-C.; Oh, S.-I.; Kang, W.H.; Yoo, H.-Y.; Lee, J.S.; Kim, D.-W. Superior anodic oxidation in tailored Sb-doped SnO₂/RuO₂ composite nanofibers for electrochemical water treatment. *J. Catal.* **2019**, *374*, 118–126. [[CrossRef](#)]
72. Chen, Y.Y.; Wrubel, J.A.; Klein, W.E.; Kabir, S.; Smith, W.A.; Neyerlin, K.C.; Deutsch, T.G. High-performance bipolar membrane development for improved water dissociation. *ACS Appl. Polym. Mater.* **2020**, *2*, 4559–4569. [[CrossRef](#)]
73. Wang, Z.M.; Liu, P.; Cao, Y.P.; Ye, F.; Xu, C.; Du, X.Z. Characterization and electrocatalytic properties of electrospun Pt-IrO₂ nanofiber catalysts for oxygen evolution reaction. *Internat. J. Energy Res.* **2021**, *45*, 5841–5851. [[CrossRef](#)]
74. Mugheri, A.Q.; Ali, S.; Narejo, G.S.; Otho, A.A.; Lal, R.; Abro, M.A.; Memon, S.H.; Abbasi, F. Electrospun fibrous active bimetallic electrocatalyst for hydrogen evolution. *Internat. J. Hydrogen Energy* **2020**, *45*, 21502–21511. [[CrossRef](#)]
75. Aljabour, A. Long-lasting electrospun Co₃O₄ nanofibers for electrocatalytic oxygen evolution reaction. *Chem. Sel.* **2020**, *5*, 7482–7487.
76. Zhang, J.X.; Sun, X.P.P.; Wei, P.; Lu, G.C.; Sun, S.X.; Xu, Y.; Fang, C.; Li, Q.; Han, J.T.T. Bimetallic Co/Mo₂C nanoparticles embedded in 3D hierarchical N-doped carbon heterostructures as highly efficient electrocatalysts for water splitting. *ChemCatChem* **2020**, *12*, 3737–3745. [[CrossRef](#)]
77. Sankar, S.S.; Karthick, K.; Sangeetha, K.; Gill, R.S.; Kundu, S. Annexation of nickel vanadate (Ni₃V₂O₈) nanocubes on nanofibers: An excellent electrocatalyst for water oxidation. *ACS Sustain. Chem. Eng.* **2020**, *11*, 4572–4579. [[CrossRef](#)]
78. Xie, L.C.; Shu, Y.; Hu, Y.Y.; Cheng, J.H.; Chen, Y.C. SWNTs-PAN/TPU/PANI composite electrospun nanofiber membrane for point-of-use efficient electrochemical disinfection: New strategy of CNT disinfection. *Chemosphere* **2020**, *251*, 126286. [[CrossRef](#)]
79. Zaher, A.; El Rouby, W.M.A.; Barakat, N.A.M. Influences of tungsten incorporation, morphology and calcination temperature on the electrolytic activity of Ni/C nanostructures toward urea elimination from wastewaters. *Intern. J. Hydrogen Energy* **2020**, *45*, 8082–8093. [[CrossRef](#)]
80. Zheng, X.J.; Zhang, Z.H.; Li, X.M.; Ding, C.F. MnO-carbon nanofiber composite material toward electro-chemical N₂ fixation under ambient conditions. *New J. Chem.* **2019**, *43*, 7932–7935. [[CrossRef](#)]
81. Barré, A.; Deguilhem, B.; Grolleau, S.; Gérard, M.; Suard, F.; Riu, D. A review on lithium-ion battery ageing mechanisms and estimations for automotive applications. *J. Power Sources* **2013**, *241*, 680–689. [[CrossRef](#)]
82. Yoshio, M.; Brodd, R.J.; Kozawa, A. *Lithium-Ion Batteries*; Springer: Berlin/Heidelberg, Germany, 2009; Volume 1.
83. Zhang, X.; Ji, L.; Toprakci, O.; Liang, Y.; Alcoutlabi, M. Electrospun nanofiber-based anodes, cathodes, and separators for advanced lithium-ion batteries. *Polym. Rev.* **2011**, *51*, 239–264. [[CrossRef](#)]
84. Jung, J.-W.; Lee, C.-L.; Yu, S.; Kim, I.-D. Electrospun nanofibers as a platform for advanced secondary batteries: A comprehensive review. *J. Mater. Chem. A* **2016**, *4*, 703–750. [[CrossRef](#)]
85. Banitaba, S.N. Chapter 14—Application of electrospun fibers for the fabrication of high performance all-solid-state fibrous batteries. In *Nanosensors and Nanodevices for Smart Multifunctional Textiles*; Ehrmann, A., Nguyen, T.A., Nguyen Tri, P., Eds.; Elsevier: Amsterdam, The Netherlands, 2021; pp. 229–244.
86. Fergus, J.W. Recent developments in cathode materials for lithium ion batteries. *J. Power Sources* **2010**, *195*, 939–954. [[CrossRef](#)]
87. Manthiram, A. A reflection on lithium-ion battery cathode chemistry. *Nat. Commun.* **2020**, *11*, 1–9. [[CrossRef](#)] [[PubMed](#)]
88. Yu, F.-D.; Que, L.-F.; Xu, C.-Y.; Wang, M.-J.; Sun, G.; Duh, J.-G.; Wang, Z.-B. Dual conductive surface engineering of Li-rich oxides cathode for superior high-energy-density Li-ion batteries. *Nano Energy* **2019**, *59*, 527–536. [[CrossRef](#)]
89. Bao, Y.; Wang, J.; Qian, Y.; Deng, Y.; Yang, X.; Chen, G. An appropriate amount of new spinel phase induced by control synthesis for the improvement of electrochemical performance of Li-rich layered oxide cathode material. *Electrochim. Acta* **2020**, *330*, 135240. [[CrossRef](#)]

90. Shevtsov, A.; Han, H.; Morozov, A.; Carozza, J.C.; Savina, A.A.; Shakhova, I.; Khasanova, N.R.; Antipov, E.V.; Dikarev, E.V.; Abakumov, A.M. Protective Spinel Coating for $\text{Li}_{1.17}\text{Ni}_{0.17}\text{Mn}_{0.50}\text{Co}_{0.17}\text{O}_2$ Cathode for Li-Ion Batteries through Single-Source Precursor Approach. *Nanomaterials* **2020**, *10*, 1870. [[CrossRef](#)] [[PubMed](#)]
91. Gong, Z.; Yang, Y. Recent advances in the research of polyanion-type cathode materials for Li-ion batteries. *Energy Environ. Sci.* **2011**, *4*, 3223–3242. [[CrossRef](#)]
92. Lei, L.; Zhang, B.; Huang, X.-J. A 3.9 V polyanion-type cathode material for Li-ion batteries. *Prog. Nat. Sci. Mater. Int.* **2011**, *21*, 211–215.
93. Moshitev, R.; Johnson, B. State of the art of commercial Li ion batteries. *J. Power Sources* **2000**, *91*, 86–91. [[CrossRef](#)]
94. Joho, F.; Rykart, B.; Imhof, R.; Novák, P.; Spahr, M.E.; Monnier, A. Key factors for the cycling stability of graphite intercalation electrodes for lithium-ion batteries. *J. Power Sources* **1999**, *81*, 243–247. [[CrossRef](#)]
95. Ou, Y.; Wen, J.; Xu, H.; Xie, S.; Li, J. Ultrafine LiCoO_2 powders derived from electrospun nanofibers for Li-ion batteries. *J. Phys. Chem. Solids* **2013**, *74*, 322–327. [[CrossRef](#)]
96. Sun, K.; Lu, H.-W.; Li, D.; Zeng, W.; Li, Y.-S.; Fu, Z.-W. Electrospun manganese oxides nanofibers electrode for lithium ion batteries. *J. Inorg. Mater.* **2009**, *24*, 357–360. [[CrossRef](#)]
97. Lu, H.-W.; Zeng, W.; Li, Y.-S.; Fu, Z.-W. Fabrication and electrochemical properties of three-dimensional net architectures of anatase TiO_2 and spinel $\text{Li}_4\text{Ti}_5\text{O}_{12}$ nanofibers. *J. Power Sources* **2007**, *164*, 874–879. [[CrossRef](#)]
98. Jin, E.M.; Gu, H.-B. Synthesis and electrochemical properties of LiFePO_4 -graphite nanofiber composites as cathode materials for lithium ion batteries. *J. Power Sources* **2013**, *244*, 586–591.
99. Kap, Ö.; Inan, A.; Er, M.; Horzum, N. Li-ion battery cathode performance from the electrospun binary LiCoO_2 to ternary $\text{Li}_2\text{CoTi}_3\text{O}_8$. *J. Mater. Sci. Mater. Electron.* **2020**, *31*, 8394–8402. [[CrossRef](#)]
100. Cao, Z.; Sang, M.; Chen, S.; Jia, J.; Yang, M.; Zhang, H.; Li, X.; Yang, S. In situ constructed (010)-oriented LiFePO_4 nanocrystals/carbon nanofiber hybrid network: Facile synthesis of free-standing cathodes for lithium-ion batteries. *Electrochim. Acta* **2020**, *333*, 135538. [[CrossRef](#)]
101. Ahmadian, A. Design and Fabrication of High Capacity Lithium-Ion Batteries Using Electro-Spun Graphene Modified Vanadium Pentoxide Cathodes. Ph.D. Thesis, Purdue University Graduate School, West Lafayette, IN, USA, 2020.
102. Vu, N.H.; Dao, V.-D.; Van, H.N.; Huy, L.T.; Quang, N.T.; Huu, H.T.; Choi, S.; Im, W.B. Spinel-layered $\text{Li}_2\text{MnTiO}_{4+z}$ nanofibers as cathode materials for Li-ion batteries. *Solid State Sci.* **2020**, *103*, 106178. [[CrossRef](#)]
103. Chen, W.; Xu, D.; Chen, Y.; Tang, T.; Kuang, S.; Fu, H.; Zhou, W.; Yu, X. In situ electrospinning synthesis of N-doped C nanofibers with uniform embedding of Mn doped $\text{MFe}_{1-x}\text{Mn}_x\text{PO}_4$ (M= Li, Na) as a High Performance Cathode for Lithium/Sodium-Ion Batteries. *Adv. Mater. Interfaces* **2020**, *7*, 2000684. [[CrossRef](#)]
104. Yang, J.; Tan, R.; Li, D.; Ma, J.; Duan, X. Ionic liquid-assisted electrospinning of porous $\text{LiFe}_{0.4}\text{Mn}_{0.6}\text{PO}_4/\text{CNFs}$ as free-standing cathodes with pseudocapacitive contribution for high-performance lithium-ion batteries. *Chem. A Eur. J.* **2020**, *26*, 5341–5346. [[CrossRef](#)]
105. Zeng, S.; Zhao, R.; Li, A.; Xue, S.; Lv, D.; Luo, Q.; Shu, D.; Chen, H. MnO/Carbon fibers prepared by an electrospinning method and their properties used as anodes for lithium ion batteries. *Appl. Surf. Sci.* **2019**, *463*, 211–216. [[CrossRef](#)]
106. Ma, X.; Smirnova, A.L.; Fong, H. Flexible lignin-derived carbon nanofiber substrates functionalized with iron (III) oxide nanoparticles as lithium-ion battery anodes. *Mater. Sci. Eng. B* **2019**, *241*, 100–104. [[CrossRef](#)]
107. Kim, C.; Yang, K.S.; Kojima, M.; Yoshida, K.; Kim, Y.J.; Kim, Y.A.; Endo, M. Fabrication of electrospinning-derived carbon nanofiber webs for the anode material of lithium-ion secondary batteries. *Adv. Funct. Mater.* **2006**, *16*, 2393–2397. [[CrossRef](#)]
108. Chen, Y.; Li, X.; Park, K.; Song, J.; Hong, J.; Zhou, L.; Mai, Y.-W.; Huang, H.; Goodenough, J.B. Hollow Carbon-Nanotube/Carbon-Nanofiber Hybrid Anodes for Li-Ion Batteries. *J. Am. Chem. Soc.* **2013**, *135*, 16280–16283. [[CrossRef](#)] [[PubMed](#)]
109. Culebras, M.; Geaney, H.; Beaucamp, A.; Upadhyaya, P.; Dalton, E.D.; Ryan, K.M.; Collins, M.N. Bio-derived carbon nanofibers from lignin as high performance Li-ion anode materials. *ChemSusChem* **2019**, *12*, 1–7. [[CrossRef](#)]
110. Nan, D.; Huang, Z.-H.; Lv, R.; Lin, Y.; Yang, L.; Yu, X.; Ye, L.; Shen, W.; Sun, H.; Kang, F. Silicon-encapsulated hollow carbon nanofiber networks as binder-free anodes for lithium ion battery. *J. Nanomater.* **2014**, *2014*, 139639. [[CrossRef](#)]
111. Peng, Y.-T.; Lo, C.-T. Electrospun porous carbon nanofibers as lithium ion battery anodes. *J. Solid State Electrochem.* **2015**, *19*, 3401–3410. [[CrossRef](#)]
112. Zhang, D.; Li, G.; Fan, J.; Li, B.; Li, L. In Situ Synthesis of Mn_3O_4 nanoparticles on hollow carbon nanofiber as high-performance lithium-ion battery anode. *Chem. A Eur. J.* **2018**, *24*, 9632–9638. [[CrossRef](#)] [[PubMed](#)]
113. Ryu, W.-H.; Shin, J.; Jung, J.-W.; Kim, I.-D. Cobalt(ii) monoxide nanoparticles embedded in porous carbon nanofibers as a highly reversible conversion reaction anode for Li-ion batteries. *J. Mater. Chem. A* **2013**, *1*, 3239–3243. [[CrossRef](#)]
114. Aravindan, V.; Suresh Kumar, P.; Sundaramurthy, J.; Ling, W.C.; Ramakrishna, S.; Madhavi, S. Electrospun NiO nanofibers as high performance anode material for Li-ion batteries. *J. Power Sources* **2013**, *227*, 284–290. [[CrossRef](#)]
115. Jang, B.-O.; Park, S.-H.; Lee, W.-J. Electrospun Co-Sn alloy/carbon nanofibers composite anode for lithium ion batteries. *J. Alloys Compd.* **2013**, *574*, 325–330. [[CrossRef](#)]
116. Jiang, Y.; Chen, S.; Mu, D.; Wu, B.; Liu, Q.; Zhao, Z.; Wu, F. A three-dimensional network structure Si/C anode for Li-ion batteries. *J. Mater. Sci.* **2017**, *52*, 10950–10958. [[CrossRef](#)]
117. Xia, J.; Liu, L.; Jamil, S.; Xie, J.; Yan, H.; Yuan, Y.; Zhang, Y.; Nie, S.; Pan, J.; Wang, X.; et al. Free-standing SnS/C nanofiber anodes for ultralong cycle-life lithium-ion batteries and sodium-ion batteries. *Energy Storage Mater.* **2019**, *17*, 1–11. [[CrossRef](#)]

118. Li, X.; Sun, N.; Tian, X.; Yang, T.; Song, Y.; Xu, B.; Liu, Z. Electrospun coal liquefaction residues/polyacrylonitrile composite carbon nanofiber nonwoven fabrics as high-performance electrodes for lithium/potassium batteries. *Energy Fuels* **2020**, *34*, 2445–2451. [[CrossRef](#)]
119. Zhu, L.; Li, F.; Yao, T.; Liu, T.; Wang, J.; Li, Y.; Lu, H.; Qian, R.; Liu, Y.; Wang, H. Electrospun MnCo_2O_4 nanotubes as high-performance anode materials for lithium-ion batteries. *Energy Fuels* **2020**, *34*, 11574–11580. [[CrossRef](#)]
120. Su, D.; Liu, L.; Liu, Z.; Dai, J.; Wen, J.; Yang, M.; Jamil, S.; Deng, H.; Cao, G.; Wang, X. Electrospun Ta-doped TiO_2/C nanofibers as a high-capacity and long-cycling anode material for Li-ion and K-ion batteries. *J. Mater. Chem. A* **2020**, *8*, 20666–20676. [[CrossRef](#)]
121. Liu, Y.; Chen, J.; Liu, Z.; Xu, H.; Zheng, Y.; Zhong, J.; Yang, Q.; Tian, H.; Shi, Z.; Yao, J.; et al. Facile fabrication of Fe_3O_4 nanoparticle/carbon nanofiber aerogel from Fe-ion cross-linked cellulose nanofibrils as anode for lithium-ion battery with superhigh capacity. *J. Alloys Compd.* **2020**, *829*, 154541. [[CrossRef](#)]
122. Ran, L.; Gentle, I.; Lin, T.; Luo, B.; Mo, N.; Rana, M.; Li, M.; Wang, L.; Knibbe, R. Sn_4P_3 @Porous carbon nanofiber as a self-supported anode for sodium-ion batteries. *J. Power Sources* **2020**, *461*, 228116. [[CrossRef](#)]
123. Liberale, F.; Fiore, M.; Ruffo, R.; Bernasconi, R.; Shiratori, S.; Magagnin, L. Red phosphorus decorated electrospun carbon anodes for high efficiency lithium ion batteries. *Sci. Rep.* **2020**, *10*, 13233. [[CrossRef](#)]
124. Tian, X.; Xu, Q.; Cheng, L.; Meng, L.; Zhang, H.; Jia, X.; Bai, S.; Qin, Y. Enhancing the performance of a self-standing si/pcnf anode by optimizing the porous structure. *ACS Appl. Mater. Interfaces* **2020**, *12*, 27219–27225. [[CrossRef](#)]
125. Yadav, P.; Malik, W.; Dwivedi, P.K.; Jones, L.A.; Shelke, M.V. Electrospun nanofibers of tin phosphide ($\text{SnP}_{0.94}$) nanoparticles encapsulated in a carbon matrix: A tunable conversion-cum-alloying lithium storage anode. *Energy Fuels* **2020**, *34*, 7648–7657. [[CrossRef](#)]
126. Xia, J.; Yuan, Y.; Yan, H.; Liu, J.; Zhang, Y.; Liu, L.; Zhang, S.; Li, W.; Yang, X.; Shu, H.; et al. Electrospun SnSe/C nanofibers as binder-free anode for lithium-ion and sodium-ion batteries. *J. Power Sources* **2020**, *449*, 227559. [[CrossRef](#)]
127. Shaji, N.; Santhoshkumar, P.; Kang, H.S.; Nanthagopal, M.; Park, J.W.; Praveen, S.; Sim, G.S.; Senthil, C.; Lee, C.W. Tin selenide/N-doped carbon composite as a conversion and alloying type anode for sodium-ion batteries. *J. Alloys Compd.* **2020**, *834*, 154304. [[CrossRef](#)]
128. Cho, T.-H.; Tanaka, M.; Ohnishi, H.; Kondo, Y.; Yoshikazu, M.; Nakamura, T.; Sakai, T. Composite nonwoven separator for lithium-ion battery: Development and characterization. *J. Power Sources* **2010**, *195*, 4272–4277. [[CrossRef](#)]
129. Hao, J.; Lei, G.; Li, Z.; Wu, L.; Xiao, Q.; Wang, L. A novel polyethylene terephthalate nonwoven separator based on electrospinning technique for lithium ion battery. *J. Membr. Sci.* **2013**, *428*, 11–16. [[CrossRef](#)]
130. Liang, Y.; Cheng, S.; Zhao, J.; Zhang, C.; Sun, S.; Zhou, N.; Qiu, Y.; Zhang, X. Heat treatment of electrospun Polyvinylidene fluoride fibrous membrane separators for rechargeable lithium-ion batteries. *J. Power Sources* **2013**, *240*, 204–211. [[CrossRef](#)]
131. Cao, L.; An, P.; Xu, Z.; Huang, J. Performance evaluation of electrospun polyimide non-woven separators for high power lithium-ion batteries. *J. Electroanal. Chem.* **2016**, *767*, 34–39. [[CrossRef](#)]
132. Jiang, W.; Liu, Z.; Kong, Q.; Yao, J.; Zhang, C.; Han, P.; Cui, G. A high temperature operating nanofibrous polyimide separator in Li-ion battery. *Solid State Ion.* **2013**, *232*, 44–48. [[CrossRef](#)]
133. Cho, T.-H.; Tanaka, M.; Onishi, H.; Kondo, Y.; Nakamura, T.; Yamazaki, H.; Tanase, S.; Sakai, T. Battery performances and thermal stability of polyacrylonitrile nano-fiber-based nonwoven separators for Li-ion battery. *J. Power Sources* **2008**, *181*, 155–160. [[CrossRef](#)]
134. Evans, T.; Lee, J.-H.; Bhat, V.; Lee, S.-H. Electrospun polyacrylonitrile microfiber separators for ionic liquid electrolytes in Li-ion batteries. *J. Power Sources* **2015**, *292*, 1–6. [[CrossRef](#)]
135. Zhai, Y.; Wang, N.; Mao, X.; Si, Y.; Yu, J.; Al-Deyab, S.S.; El-Newehy, M.; Ding, B. Sandwich-structured PVdF/PMIA/PVdF nanofibrous separators with robust mechanical strength and thermal stability for lithium ion batteries. *J. Mater. Chem. A* **2014**, *2*, 14511–14518. [[CrossRef](#)]
136. Zhu, C.; Nagaiishi, T.; Shi, J.; Lee, H.; Wong, P.Y.; Sui, J.; Hyodo, K.; Kim, I.S. Enhanced wettability and thermal stability of a novel polyethylene terephthalate-based poly(vinylidene fluoride) nanofiber hybrid membrane for the separator of lithium-ion batteries. *ACS Appl. Mater. Interfaces* **2017**, *9*, 26400–26406. [[CrossRef](#)] [[PubMed](#)]
137. Wu, D.; Shi, C.; Huang, S.; Qiu, X.; Wang, H.; Zhan, Z.; Zhang, P.; Zhao, J.; Sun, D.; Lin, L. Electrospun nanofibers for sandwiched polyimide/poly(vinylidene fluoride)/polyimide separators with the thermal shutdown function. *Electrochim. Acta* **2015**, *176*, 727–734. [[CrossRef](#)]
138. Peng, K.; Wang, B.; Ji, C. A poly(ethylene terephthalate) nonwoven sandwiched electrospun polysulfonamide fibrous separator for rechargeable lithium ion batteries. *J. Appl. Polym. Sci.* **2017**, *134*, 44907. [[CrossRef](#)]
139. Cao, C.; Tan, L.; Liu, W.; Ma, J.; Li, L. Polydopamine coated electrospun poly(vinylidene fluoride) nanofibrous membrane as separator for lithium-ion batteries. *J. Power Sources* **2014**, *248*, 224–229. [[CrossRef](#)]
140. Shi, C.; Dai, J.; Huang, S.; Li, C.; Shen, X.; Zhang, P.; Wu, D.; Sun, D.; Zhao, J. A simple method to prepare a polydopamine modified core-shell structure composite separator for application in high-safety lithium-ion batteries. *J. Membr. Sci.* **2016**, *518*, 168–177. [[CrossRef](#)]
141. Park, S.-R.; Jung, Y.-C.; Shin, W.-K.; Ahn, K.H.; Lee, C.H.; Kim, D.-W. Cross-linked fibrous composite separator for high performance lithium-ion batteries with enhanced safety. *J. Membr. Sci.* **2017**, *527*, 129–136. [[CrossRef](#)]

142. Ye, W.; Zhu, J.; Liao, X.; Jiang, S.; Li, Y.; Fang, H.; Hou, H. Hierarchical three-dimensional micro/nano-architecture of polyaniline nanowires wrapped-on polyimide nanofibers for high performance lithium-ion battery separators. *J. Power Sources* **2015**, *299*, 417–424. [[CrossRef](#)]
143. Shen, X.; Li, C.; Shi, C.; Yang, C.; Deng, L.; Zhang, W.; Peng, L.; Dai, J.; Wu, D.; Zhang, P.; et al. Core-shell structured ceramic nonwoven separators by atomic layer deposition for safe lithium-ion batteries. *Appl. Surf. Sci.* **2018**, *441*, 165–173. [[CrossRef](#)]
144. Zainab, G.; Wang, X.; Yu, J.; Zhai, Y.; Ahmed Babar, A.; Xiao, K.; Ding, B. Electrospun polyacrylonitrile/polyurethane composite nanofibrous separator with electrochemical performance for high power lithium ion batteries. *Mater. Chem. Phys.* **2016**, *182*, 308–314. [[CrossRef](#)]
145. Zhao, M.; Wang, J.; Chong, C.; Yu, X.; Wang, L.; Shi, Z. An electrospun lignin/polyacrylonitrile nonwoven composite separator with high porosity and thermal stability for lithium-ion batteries. *RSC Adv.* **2015**, *5*, 101115–101120. [[CrossRef](#)]
146. Zhou, X.; Yue, L.; Zhang, J.; Kong, Q.; Liu, Z.; Yao, J.; Cui, G. A core-shell structured polysulfonamide-based composite nonwoven towards high power lithium ion battery separator. *J. Electrochem. Soc.* **2013**, *160*, A1341. [[CrossRef](#)]
147. Yanilmaz, M.; Lu, Y.; Zhu, J.; Zhang, X. Silica/polyacrylonitrile hybrid nanofiber membrane separators via sol-gel and electrospinning techniques for lithium-ion batteries. *J. Power Sources* **2016**, *313*, 205–212. [[CrossRef](#)]
148. Shayapat, J.; Chung, O.H.; Park, J.S. Electrospun polyimide-composite separator for lithium-ion batteries. *Electrochim. Acta* **2015**, *170*, 110–121. [[CrossRef](#)]
149. Yanilmaz, M.; Zhu, J.; Lu, Y.; Ge, Y.; Zhang, X. High-strength, thermally stable nylon 6,6 composite nanofiber separators for lithium-ion batteries. *J. Mater. Sci.* **2017**, *52*, 5232–5241. [[CrossRef](#)]
150. Ma, X.; Kolla, P.; Yang, R.; Wang, Z.; Zhao, Y.; Smirnova, A.L.; Fong, H. Electrospun polyacrylonitrile nanofibrous membranes with varied fiber diameters and different membrane porosities as lithium-ion battery separators. *Electrochim. Acta* **2017**, *236*, 417–423. [[CrossRef](#)]
151. Dong, T.; Arifeen, W.U.; Choi, J.; Yoo, K.; Ko, T. Surface-modified electrospun polyacrylonitrile nano-membrane for a lithium-ion battery separator based on phase separation mechanism. *Chem. Eng. J.* **2020**, *398*, 125646. [[CrossRef](#)]
152. Wei, Z.; Gu, J.; Zhang, F.; Pan, Z.; Zhao, Y. Core-Shell Structured Nanofibers for Lithium Ion Battery Separator with Wide Shutdown Temperature Window and Stable Electrochemical Performance. *ACS Appl. Polym. Mater.* **2020**, *2*, 1989–1996. [[CrossRef](#)]
153. Xiao, W.; Song, J.; Huang, L.; Yang, Z.; Qiao, Q. PVA-ZrO₂ multilayer composite separator with enhanced electrolyte property and mechanical strength for lithium-ion batteries. *Ceram. Int.* **2020**, *46*, 29212–29221. [[CrossRef](#)]
154. Jaritphun, S.; Park, J.S.; Chung, O.H.; Nguyen, T.T.T. Sandwiched polyimide-composite separator for lithium-ion batteries via electrospinning and electrospraying. *Polym. Compos.* **2020**, *41*, 4478–4488. [[CrossRef](#)]
155. Xu, Y.; Zhu, J.-W.; Fang, J.-B.; Li, X.; Yu, M.; Long, Y.-Z. Electrospun high-thermal-resistant inorganic composite nonwoven as lithium-ion battery separator. *J. Nanomater.* **2020**, *2020*, 3879040. [[CrossRef](#)]
156. Cai, M.; Yuan, D.; Zhang, X.; Pu, Y.; Liu, X.; He, H.; Zhang, L.; Ning, X. Lithium ion battery separator with improved performance via side-by-side bicomponent electrospinning of PVDF-HFP/PI followed by 3D thermal crosslinking. *J. Power Sources* **2020**, *461*, 228123. [[CrossRef](#)]
157. Liang, T.; Liang, W.-H.; Cao, J.-H.; Wu, D.-Y. Enhanced performance of high energy density lithium metal battery with PVDF-HFP/LAGP composite separator. *ACS Appl. Energy Mater.* **2021**, *4*, 2578–2585. [[CrossRef](#)]
158. Chen, Y.; Qiu, L.; Ma, X.; Dong, L.; Jin, Z.; Xia, G.; Du, P.; Xiong, J. Electrospun cellulose polymer nanofiber membrane with flame resistance properties for lithium-ion batteries. *Carbohydr. Polym.* **2020**, *234*, 115907. [[CrossRef](#)] [[PubMed](#)]
159. Fu, Q.; Zhang, W.; Muhammad, I.P.; Chen, X.; Zeng, Y.; Wang, B.; Zhang, S. Coaxially electrospun PAN/HCNFs@PVDF/UiO-66 composite separator with high strength and thermal stability for lithium-ion battery. *Microporous Mesoporous Mater.* **2021**, *311*, 110724. [[CrossRef](#)]
160. Long, L.; Wang, S.; Xiao, M.; Meng, Y. Polymer electrolytes for lithium polymer batteries. *J. Mater. Chem. A* **2016**, *4*, 10038–10069. [[CrossRef](#)]
161. Murata, K.; Izuchi, S.; Yoshihisa, Y. An overview of the research and development of solid polymer electrolyte batteries. *Electrochim. Acta* **2000**, *45*, 1501–1508. [[CrossRef](#)]
162. Wang, F.; Li, L.; Yang, X.; You, J.; Xu, Y.; Wang, H.; Ma, Y.; Gao, G. Influence of additives in a PVDF-based solid polymer electrolyte on conductivity and Li-ion battery performance. *Sustain. Energy Fuels* **2018**, *2*, 492–498. [[CrossRef](#)]
163. Kim, J.-W.; Ji, K.-S.; Lee, J.-P.; Park, J.-W. Electrochemical characteristics of two types of PEO-based composite electrolyte with functional SiO₂. *J. Power Sources* **2003**, *119*, 415–421. [[CrossRef](#)]
164. Joge, P.N.; Kanchan, D.; Sharma, P.L. Effect of Al₂O₃ on crystallinity and conductivity of PVA-PEO-EC-LiCF₃SO₃ blend electrolyte system. *AIP Conf. Proc.* **2014**, *1591*, 356.
165. Abdel-Samiea, B.; Basyouni, A.; Khalil, R.; Sheha, E.M.; Tsuda, H.; Matsui, T. The role of TiO₂ anatase nano-filler to enhance the physical and electrochemical properties of PVA-based polymer electrolyte for magnesium battery applications. *J. Mater. Sci. Eng. A* **2013**, *3*, 678–689.
166. Freitag, K.M.; Kirchhain, H.; Wullen, L.V.; Nilges, T. Enhancement of Li ion conductivity by electrospun polymer fibers and direct fabrication of solvent-free separator membranes for Li ion batteries. *Inorg. Chem.* **2017**, *56*, 2100–2107. [[CrossRef](#)]
167. Freitag, K.; Walke, P.; Nilges, T.; Kirchhain, H.; Spranger, R.; van Wüllen, L. Electrospun sodiumtetrafluoroborate-polyethylene oxide membranes for solvent-free sodium ion transport in solid state sodium ion batteries. *J. Power Sources* **2018**, *378*, 610–617. [[CrossRef](#)]

168. Banitaba, S.N.; Semnani, D.; Fakhrli, A.; Ebadi, S.V.; Heydari-Soureshjani, E.; Rezaei, B.; Ensafi, A.A. Electrospun PEO nanofibrous membrane enabled by LiCl, LiClO₄, and LiTFSI salts: A versatile solvent-free electrolyte for lithium-ion battery application. *Ionics* **2020**, *26*, 3249–3260. [[CrossRef](#)]
169. Banitaba, S.N.; Semnani, D.; Heydari-Soureshjani, E.; Rezaei, B.; Ensafi, A.A.; Taghipour-Jahromi, A. Novel electrospun polymer electrolytes incorporated with Keggin-type hetero polyoxometalate fillers as solvent-free electrolytes for lithium ion batteries. *Polym. Int.* **2020**, *69*, 675–687. [[CrossRef](#)]
170. Banitaba, S.N.; Semnani, D.; Rezaei, B.; Ensafi, A.A. Morphology and electrochemical and mechanical properties of polyethylene-oxide-based nanofibrous electrolytes applicable in lithium ion batteries. *Polym. Int.* **2019**, *68*, 746–754. [[CrossRef](#)]
171. Walke, P.; Freitag, K.M.; Kirchhain, H.; Kaiser, M.; van Wüllen, L.; Nilges, T. Electrospun Li (TFSI)@polyethylene oxide membranes as solid electrolytes. *Z. Für Anorg. Und Allg. Chem.* **2018**, *644*, 1863–1874. [[CrossRef](#)]
172. Banitaba, S.N.; Semnani, D.; Heydari-Soureshjani, E.; Rezaei, B.; Ensafi, A.A. Electrospun Polyethylene Oxide-Based Membranes Incorporated with Silicon Dioxide, Aluminum Oxide and Clay Nanoparticles as Flexible Solvent-Free Electrolytes for Lithium-Ion Batteries. *JOM* **2019**, *71*, 4537–4546. [[CrossRef](#)]
173. Fu, K.K.; Gong, Y.; Dai, J.; Gong, A.; Han, X.; Yao, Y.; Wang, C.; Wang, Y.; Chen, Y.; Yan, C. Flexible, solid-state, ion-conducting membrane with 3D garnet nanofiber networks for lithium batteries. *Proc. Natl. Acad. Sci. USA* **2016**, *113*, 7094–7099. [[CrossRef](#)] [[PubMed](#)]
174. Liu, W.; Liu, N.; Sun, J.; Hsu, P.-C.; Li, Y.; Lee, H.-W.; Cui, Y. Ionic conductivity enhancement of polymer electrolytes with ceramic nanowire fillers. *Nano Lett.* **2015**, *15*, 2740–2745. [[CrossRef](#)]
175. Liu, W.; Lee, S.W.; Lin, D.; Shi, F.; Wang, S.; Sendek, A.D.; Cui, Y. Enhancing ionic conductivity in composite polymer electrolytes with well-aligned ceramic nanowire. *Nat. Energy* **2017**, *2*, 1–7. [[CrossRef](#)]
176. Ormerod, R.M. Solid oxide fuel cells. *Chem. Soc. Rev.* **2003**, *32*, 17–28. [[CrossRef](#)] [[PubMed](#)]
177. Mekhilef, S.; Saidur, R.; Safari, A. Comparative study of different fuel cell technologies. *Renew. Sustain. Energy Rev.* **2012**, *16*, 981–989. [[CrossRef](#)]
178. Kirubakaran, A.; Jain, S.; Nema, R.K. A review on fuel cell technologies and power electronic interfaces. *Renew. Sustain. Energy Rev.* **2009**, *13*, 2430–2440. [[CrossRef](#)]
179. Lin, G.; Nguyen, T.V. Effect of thickness and hydrophobic polymer content of the gas diffusion layer on electrode flooding level in a PEMFC. *J. Electrochem. Soc.* **2005**, *152*, A1942–A1948. [[CrossRef](#)]
180. Chung, S.; Shin, D.Y.; Choun, M.H.; Kim, J.S.; Yang, S.G.; Choi, M.; Kim, J.W.; Lee, J.Y. Improved water management of Pt/C cathode modified by graphitized carbon nanofiber in proton exchange membrane fuel cell. *J. Power Sources* **2018**, *399*, 350–356. [[CrossRef](#)]
181. Slack, J.J.; Brodt, M.; Cullen, D.A.; Reeves, K.S.; More, K.L.; Pintauro, P.N. Impact of polyvinylidene fluoride on nanofiber cathode structure and durability in proton exchange membrane fuel cells. *J. Electrochem. Soc.* **2020**, *167*, 054517. [[CrossRef](#)]
182. Slack, J.J.; Gumeci, C.; Dale, N.; Parrondo, J.; Macauley, N.; Mukundan, R.; Cullen, D.; Sneed, B.; More, K.; Pintauro, P.N. Nanofiber fuel cell MEAs with a PtCo/C cathode. *J. Electrochem. Soc.* **2019**, *166*, F3202. [[CrossRef](#)]
183. Khandavalli, S.; Sharma-Nene, N.; Kabir, S.; Sur, S.; Rothstein, J.P.; Neyerlin, K.C.; Mauger, S.A.; Ulsh, M. Towards optimizing electrospun nanofiber fuel cell catalyst layers: Polymer-particle interactions and spinnability. *ACS Appl. Polym. Mater.* **2021**, *3*, 2374–2384. [[CrossRef](#)]
184. Zhang, W.J.; Brodt, M.W.; Pintauro, P.N. Nanofiber cathodes for low and high humidity hydrogen fuel cell operation. *ECS Trans.* **2011**, *41*, 891. [[CrossRef](#)]
185. Wei, M.; Jiang, M.; Liu, X.B.; Wang, M.; Mu, S.C. Graphene-doped electrospun nanofiber membrane electrodes and proton exchange membrane fuel cell performance. *J. Power Sources* **2016**, *327*, 384–393. [[CrossRef](#)]
186. Li, Y.; Hui, J.; Kawchuk, J.; O'Brien, A.; Jiang, Z.; Hoorfar, M. Composite membranes of PVDF nanofibers impregnated with Nafion for increased fuel concentrations in direct methanol fuel cells. *Fuel Cells* **2019**, *19*, 43–50. [[CrossRef](#)]
187. Liu, X.P.; Yang, Z.H.; Zhang, Y.F.; Li, C.C.; Dong, J.M.; Liu, Y.; Cheng, H.S. Electrospun multifunctional sulfonated carbon nanofibers for design and fabrication of SPEEK composite proton exchange membranes for direct methanol fuel cell application. *Int. J. Hydrogen Energy* **2017**, *42*, 10275–10284. [[CrossRef](#)]
188. Jindal, A.; Basu, S.; Chauhan, N.; Ukai, T.; Kumar, D.S.; Samudhyatha, K.T. Application of electrospun CN_x nanofibers as cathode in microfluidic fuel cell. *J. Power Sources* **2017**, *342*, 165–174. [[CrossRef](#)]
189. Jindal, A.; Basu, S. Improvement in electrocatalytic activity of oxygen reduction of electrospun carbon nitride/polyacrylonitrile nanofibers by addition of carbon black and nafion® fillers. *Int. J. Hydrogen Energy* **2016**, *41*, 11624–11633. [[CrossRef](#)]
190. Mei, R.G.; Xi, J.J.; Ma, L.; An, L.; Wang, F.; Sun, H.Y.; Luo, Z.K.; Wu, Q.X. Multi-scaled porous Fe-N/C nanofibrous catalysts for the cathode electrodes of direct methanol fuel cells. *J. Electrochem. Soc.* **2017**, *164*, F1556. [[CrossRef](#)]
191. Zhi, M.J.; Lee, S.W.; Miller, N.; Menzler, N.H.; Wu, N.Q. An intermediate-temperature solid oxide fuel cell with electrospun nanofiber cathode. *Energy Environ. Sci.* **2012**, *5*, 7066–7071. [[CrossRef](#)]
192. Zhi, M.J.; Mariani, N.; Gemmen, R.; Gerdes, K.; Wu, N.Q. Nanofiber scaffolds for cathode of solid oxide fuel cell. *Energy Environ. Sci.* **2011**, *4*, 417–420. [[CrossRef](#)]
193. Enrico, A.; Zhang, W.J.; Traulsen, M.L.; Sala, E.M.; Costamagna, P.; Holtappels, P. La_{0.6}Sr_{0.4}Co_{0.2}Fe_{0.8}O_{3-δ} nanofiber cathode for intermediate-temperature solid oxide fuel cells by water-based sol-gel electrospinning: Synthesis and electrochemical behaviour. *J. Eur. Ceram. Soc.* **2018**, *38*, 2677–2686. [[CrossRef](#)]

194. Zhao, E.Q.; Ma, C.; Yang, W.; Xiong, Y.P.; Li, J.Q.; Sun, C.W. Electrospinning $\text{La}_{0.8}\text{Sr}_{0.2}\text{Co}_{0.2}\text{Fe}_{0.8}\text{O}_{3-\delta}$ tubes impregnated with $\text{Ce}_{0.8}\text{Gd}_{0.2}\text{O}_{1.9}$ nanoparticles for an intermediate temperature solid oxide fuel cell cathode. *Int. J. Hydrogen Energy* **2013**, *38*, 6821–6829. [CrossRef]
195. Ahn, M.W.; Cho, J.; Lee, W.Y. One-step fabrication of composite nanofibers for solid oxide fuel cell electrodes. *J. Power Sources* **2019**, *434*, 226749. [CrossRef]
196. Sammes, N.; Bove, R.; Stahl, K. Phosphoric acid fuel cells: Fundamentals and applications. *Curr. Opin. Solid State Mater. Sci.* **2004**, *8*, 372–378. [CrossRef]
197. Skupov, K.M.; Ponomarev, I.I.; Razorenov, D.Y.; Zhigalina, V.G.; Zhigalina, O.M.; Ponomarev, I.I.; Volkova, Y.A.; Volkovich, Y.M.; Sosenkin, V.E. Carbon nanofiber paper cathode modification for higher performance of phosphoric acid fuel cells on polybenzimidazole membrane. *Russ. J. Electrochem.* **2017**, *53*, 728–733. [CrossRef]
198. Ponomarev, I.I.; Skupov, K.M.; Razorenov, D.Y.; Zhigalina, V.G.; Zhigalina, O.M.; Ponomarev, I.I.; Volkova, Y.A.; Kondratenko, M.S.; Bukalov, S.S.; Davydova, E.S. Electrospun nanofiber pyropolymer electrodes for fuel cells on polybenzimidazole membranes. *Russ. J. Electrochem.* **2016**, *52*, 735–739. [CrossRef]
199. Uhm, S.H.; Jeong, B.G.; Lee, J.Y. A facile route for preparation of non-noble CNF cathode catalysts in alkaline ethanol fuel cells. *Electrochim. Acta* **2011**, *56*, 9186–9190. [CrossRef]
200. Sun, J.J.; Zhao, H.Z.; Yang, Q.Z.; Song, J.; Xue, A. A novel layer-by-layer self-assembled carbon nanotube-based anode: Preparation, characterization, and application in microbial fuel cell. *Electrochim. Acta* **2010**, *55*, 3041–3047. [CrossRef]
201. Zhang, B.-G.; Zhou, S.-G.; Zhao, H.-Z.; Shi, C.-H.; Kong, L.-C.; Sun, J.-J.; Yang, Y.; Ni, J.-R. Factors affecting the performance of microbial fuel cells for sulfide and vanadium (V) treatment. *Bioprocess. Biosyst. Eng.* **2010**, *33*, 187–194. [CrossRef]
202. Gardia-Gomez, N.A.; Balderas-Renteria, I.; Garcia-Gutierrez, D.I.; Mosqueda, H.A.; Sánchez, E.M. Development of mats composed by TiO_2 and carbon dual electrospun nanofibers: A possible anode material in microbial fuel cells. *Mater. Sci. Eng. B* **2015**, *193*, 130–136. [CrossRef]
203. Cai, T.; Huang, M.H.; Huang, Y.X.; Zheng, W. Enhanced performance of microbial fuel cells by electrospinning carbon nanofibers hybrid carbon nanotubes composite anode. *Int. J. Hydrogen Energy* **2019**, *44*, 3088–3098. [CrossRef]
204. Jung, H.-Y.; Roh, S.-H. Carbon nanofiber/polypyrrole nanocomposite as anode material in microbial fuel cells. *J. Nanosci. Nanotechnol.* **2017**, *17*, 5830–5833. [CrossRef]
205. Massaglia, G.; Margaria, V.; Fiorentin, M.R.; Pasha, K.; Sacco, A.; Castellino, M.; Chiodoni, A.; Bianco, S.; Pirri, F.C.; Quaglio, M. Nonwoven mats of N-doped carbon nanofibers as high-performing anodes in microbial fuel cells. *Mater. Today Energy* **2020**, *16*, 100385. [CrossRef]
206. Karra, U.; Manickam, S.S.; McCutcheon, J.R.; Patel, N.; Li, B. Power generation and organics removal from wastewater using activated carbon nanofiber (ACNF) microbial fuel cells (MFCs). *Int. J. Hydrogen Energy* **2013**, *38*, 1588–1597. [CrossRef]
207. Barakat, N.A.M.; Amen, M.T.; Al-Mubaddel, F.S.; Karim, M.R.; Alrashed, M. NiSn nanoparticle-incorporated carbon nanofibers as efficient electrocatalysts for urea oxidation and working anodes in direct urea fuel cells. *J. Adv. Res.* **2019**, *16*, 43–53. [CrossRef]
208. Mohamed, I.M.A.; Kanagaraj, P.; Yasin, A.S.; Iqbal, W.; Liu, C.K. Electrochemical impedance investigation of urea oxidation in alkaline media based on electrospun nanofibers towards the technology of direct-urea fuel cells. *J. Alloys Comp.* **2020**, *816*, 152513. [CrossRef]
209. Abdelkareem, M.A.; Al Haj, Y.; Alajami, M.; Alawadhi, H.; Barakat, N.A.M. Ni-Cd carbon nanofibers as an effective catalyst for urea fuel cell. *J. Environ. Chem. Eng.* **2018**, *6*, 332–337. [CrossRef]
210. Hu, Q.J.; Fan, L.Q.; Wang, Y.W.; Wang, Z.; Xiong, Y.P. Nanofiber-based $\text{La}_x\text{Sr}_{1-x}\text{TiO}_3\text{-Gd}_y\text{Ce}_{1-y}\text{O}_{2-\delta}$ composite anode for solid oxide fuel cells. *Ceram. Int.* **2017**, *43*, 12145–12153. [CrossRef]
211. Hu, Q.J.; Liu, C.J.; Fan, L.Q.; Wang, Y.W.; Xiong, Y.P. Nanofiber-based $\text{La}_{0.4}\text{Sr}_{0.6}\text{TiO}_3\text{-Gd}_{0.2}\text{Ce}_{0.8}\text{O}_{1.9}\text{-Ni}$ composite anode for solid oxide fuel cells. *Electrochim. Acta* **2018**, *265*, 1–9. [CrossRef]
212. Fan, L.Q.; Xiong, Y.P.; Liu, L.B.; Wang, Y.W.; Kishimoto, H.; Yamaji, K.; Horita, T. Performance of $\text{Gd}_{0.2}\text{Ce}_{0.8}\text{O}_{1.9}$ infiltrated $\text{La}_{0.2}\text{Sr}_{0.8}\text{TiO}_3$ nanofiber scaffolds as anodes for solid oxide fuel cells. *J. Power Sources* **2014**, *265*, 125–131. [CrossRef]
213. Fan, L.Q.; Xiong, Y.P.; Wang, Y.W.; Kishimoto, H.; Yamaji, K.; Horita, T. Performance of $\text{Gd}_{0.2}\text{Ce}_{0.8}\text{O}_{1.9}$ infiltrated $\text{La}_{0.2}\text{Sr}_{0.8}\text{TiO}_3$ nanofiber scaffolds as anodes for solid oxide fuel cells: Redox stability and effects of electrolytes. *J. Power Sources* **2015**, *294*, 452–459. [CrossRef]
214. Li, L.P.; Zhang, P.G.; Liu, R.R.; Guo, S.M. Preparation of fibrous Ni-coated YSZ anodes for solid oxide fuel cells. *J. Power Sources* **2011**, *196*, 1242–1247. [CrossRef]
215. Ahn, M.W.; Han, S.W.; Lee, J.S.; Lee, W.Y. Electrospun composite nanofibers for intermediate-temperature solid oxide fuel cell electrodes. *Ceram. Int.* **2020**, *46*, 6006–6011. [CrossRef]
216. Yu, G.S.; Li, T.S.; Xu, M.; Andersson, M.; Li, B.H.; Tang, H.; Parbey, J.; Shao, J. Fabrication of nickel-YSZ cermet nanofibers via electrospinning. *J. Alloys Comp.* **2017**, *693*, 1214–1219. [CrossRef]
217. Lee, K.-R.; Tseng, C.J.; Chang, J.-K.; Wang, K.-W.; Huang, Y.-S.; Chou, T.-C.; Tsai, L.-D.; Lee, S.-W. Nano-fibrous $\text{SrCe}_{0.8}\text{Y}_{0.2}\text{O}_{3-\delta}\text{-Ni}$ anode functional layer for proton-conducting solid oxide fuel cells. *J. Power Sources* **2019**, *436*, 226863. [CrossRef]
218. Li, W.D.; Cheng, Y.; Zhou, Q.J.; Wei, T.; Li, Z.P.; Yan, H.Y.; Wang, Z.; Han, X. Evaluation of double perovskite $\text{Sr}_2\text{FeTiO}_{6-\delta}$ as potential cathode or anode materials for intermediate-temperature solid oxide fuel cells. *Ceram. Int.* **2015**, *41*, 12393–12400. [CrossRef]

219. Chen, P.; Wu, H.J.; Yuan, T.; Zou, Z.Q.; Zhang, H.F.; Zheng, J.W.; Yang, H. Electrospun nanofiber network anode for a passive direct methanol fuel cell. *J. Power Sources* **2014**, *255*, 70–75. [[CrossRef](#)]
220. Feng, C.; Takeuchi, T.; Abdelkareem, M.A.; Tsujiguchi, T.; Nakagawa, N. Carbon–CeO₂ composite nanofibers as a promising support for a PtRu anode catalyst in a direct methanol fuel cell. *J. Power Sources* **2013**, *242*, 57–64. [[CrossRef](#)]
221. Thamer, B.M.; El-Newehy, M.H.; Barakat, N.A.M.; Abdelkareem, M.A.; Al-Deyab, S.S.; Kim, H.Y. Influence of nitrogen doping on the catalytic activity of Ni-incorporated carbon nanofibers for alkaline direct methanol fuel cells. *Electrochim. Acta* **2014**, *142*, 228–239. [[CrossRef](#)]
222. Hanifah, M.F.R.; Jaafar, J.; Othman, M.H.D.; Ismail, A.F.; Rahman, M.A.; Yusof, N.; Aziz, F. Electro-spun of novel PVDF-Pt-Pd/RGO-CeO₂ composite nanofibers as the high potential of robust anode catalyst in direct methanol fuel cell: Fabrication and characterization. *Inorg. Chem. Commun.* **2019**, *107*, 107487. [[CrossRef](#)]
223. Abdullah, N.; Kamarudin, S.K.; Shyuan, L.K.; Karim, N.A. Fabrication and characterization of new composite TiO₂ carbon-nanofiber anodic catalyst support for direct methanol fuel cell via electrospinning method. *Nanoscale Res. Lett.* **2017**, *12*, 613. [[CrossRef](#)] [[PubMed](#)]
224. Ito, Y.; Takeuchi, T.; Tsujiguchi, T.; Nakagawa, N. Ultrahigh methanol electro-oxidation activity of PtRu nanoparticles prepared on TiO₂-embedded carbon nanofiber support. *J. Power Sources* **2013**, *242*, 280–288. [[CrossRef](#)]
225. Wu, H.J.; Yuan, T.; Huang, Q.H.; Zhang, H.F.; Zou, Z.Q.; Zheng, J.W.; Yang, H. Polypyrrole nanowire networks as anodic micro-porous layer for passive direct methanol fuel cells. *Electrochim. Acta* **2014**, *141*, 1–5. [[CrossRef](#)]
226. Zheng, Y.P.; Zhang, Z.Y.; Zhang, X.; Ni, H.M.; Sun, Y.M.; Lou, Y.B.; Li, X.J.; Lu, Y. Application of Pt-Co nanoparticles supported on CeO₂-C as electrocatalyst for direct methanol fuel cell. *Mater. Lett.* **2018**, *221*, 301–304. [[CrossRef](#)]
227. Suryamas, A.B.; Anilkumar, G.M.; Sago, S.; Ogi, T.; Okuyama, K. Electrospun Pt/SnO₂ nanofibers as an excellent electrocatalysts for hydrogen oxidation reaction with ORR-blocking characteristic. *Catal. Commun.* **2013**, *33*, 11–14. [[CrossRef](#)]
228. Park, J.W.; Wycisk, R.; Lin, G.G.; Chong, P.Y.; Powers, D.; van Nguyen, T.; Dowd, R.P., Jr.; Pintauro, P.N. Electrospun Nafion/PVDF single-fiber blended membranes for regenerative H₂/Br₂ fuel cells. *J. Membr. Sci.* **2017**, *541*, 85–92. [[CrossRef](#)]
229. Ballengee, J.B.; Pintauro, P.N. Preparation of nanofiber composite proton-exchange membranes from dual fiber electrospun mats. *J. Membr. Sci.* **2013**, *442*, 187–195. [[CrossRef](#)]
230. Park, J.W.; Wycisk, R.; Pintauro, P.N. Nafion/PVDF nanofiber composite membranes for regenerative hydrogen/bromine fuel cells. *J. Membr. Sci.* **2015**, *490*, 103–112. [[CrossRef](#)]
231. Park, J.W.; Wycisk, R.; Pintauro, P.N.; Yarlagadda, V.; van Nguyen, T. Electrospun Nafion®/polyphenylsulfone composite membranes for regenerative hydrogen bromine fuel cells. *Materials* **2016**, *9*, 143. [[CrossRef](#)]
232. Shahgaldi, S.; Ghasemi, M.; Wan Daud, W.R.; Yaakob, Z.; Sedighi, M.; Alam, J.; Ismail, A.F. Performance enhancement of microbial fuel cell by PVDF/Nafion nanofiber composite proton exchange membrane. *Fuel Process. Technol.* **2014**, *124*, 290–295. [[CrossRef](#)]
233. Zhang, S.K.; He, G.H.; Gong, X.; Zhu, X.P.; Wu, X.M.; Sun, X.Y.; Zhao, X.Y.; Li, H. Electrospun nanofiber enhanced sulfonated poly (phthalazinone ether sulfone ketone) composite proton exchange membranes. *J. Membr. Sci.* **2015**, *493*, 58–65. [[CrossRef](#)]
234. Vezzù, K.; Nawn, G.; Negro, E.; Crivellaro, G.; Park, J.W.; Wycisk, R.; Pintauro, P.N.; di Noto, V. Electric response and conductivity mechanism of blended polyvinylidene fluoride/Nafion electrospun nanofibers. *J. Am. Chem. Soc.* **2020**, *142*, 801–814. [[CrossRef](#)]
235. Shen, C.H.; Wycisk, R.; Pintauro, P.N. High performance electrospun bipolar membrane with a 3D junction. *Energy Environ. Sci.* **2017**, *10*, 1435–1442. [[CrossRef](#)]
236. Wu, B.; Pan, J.F.; Ge, L.; Wu, L.; Wang, H.T.; Xu, T.W. Oriented MOF-polymer composite nanofiber membranes for high proton conductivity at high temperature and anhydrous condition. *Sci. Rep.* **2014**, *4*, 4334. [[CrossRef](#)]
237. Gong, X.; He, G.H.; Wu, Y.; Zhang, S.K.; Chen, B.; Dai, Y.; Wu, X.M. Aligned electrospun nanofibers as proton conductive channels through thickness of sulfonated poly (phthalazinone ether sulfone ketone) proton exchange membranes. *J. Power Sources* **2017**, *358*, 134–141. [[CrossRef](#)]
238. Muthuraja, P.; Prakash, S.; Shanmugam, V.M.; Manisankar, P. Stable nanofibrous poly(aryl sulfone ether benzimidazole) membrane with high conductivity for high temperature PEM fuel cells. *Solid State Ion.* **2018**, *317*, 201–209. [[CrossRef](#)]
239. Tamura, T.; Kawakami, H. Aligned electrospun nanofiber composite membranes for fuel cell electrolytes. *Nano Lett.* **2010**, *10*, 1324–1328. [[CrossRef](#)]
240. Balakrishnan, M.; Shrestha, P.; Ge, N.; Lee, C.H.; Fahy, K.F.; Zeis, R.; Schulz, V.P.; Hatton, B.J.; Bazylak, A. Designing tailored gas diffusion layers with pore size gradients via electrospinning for polymer electrolyte membrane fuel cells. *ACS Appl. Energy Mater.* **2020**, *3*, 2695–2707. [[CrossRef](#)]
241. Balakrishnan, M.; Shrestha, P.; Lee, C.H.; Ge, N.; Fahy, K.F.; Messerschmidt, M.; Scholta, J.; Eifert, L.; Maibach, J.; Zeis, R.; et al. Degradation characteristics of electrospun gas diffusion layers with custom pore structures for polymer electrolyte membrane fuel cells. *ACS Appl. Mater. Interfaces* **2021**, *13*, 2414–2427. [[CrossRef](#)]
242. Kallem, P.; Yanar, N.; Choi, H. Nanofiber-based proton exchange membranes: Development of aligned electrospun nanofibers for polymer electrolyte fuel cell applications. *ACS Sustain. Chem. Eng.* **2019**, *7*, 1808–1825. [[CrossRef](#)]
243. DeGostin, M.B.; Peracchio, A.A.; Myles, T.D.; Cassenti, B.N.; Chiu, W.K.S. Charge transport in the electrospun nanofiber composite membrane's three-dimensional fibrous structure. *J. Power Sources* **2016**, *307*, 538–551. [[CrossRef](#)]
244. Liang, J.; Zhao, H.; Yue, L.; Fan, G.; Li, T.; Lu, S.; Chen, G.; Gao, S.; Asiri, A.M.; Sun, X. Recent advances in electrospun nanofibers for supercapacitors. *J. Mater. Chem. A* **2020**, *8*, 16747–16789. [[CrossRef](#)]

245. Lu, X.; Wang, C.; Favier, F.; Pinna, N. Electrospun nanomaterials for supercapacitor electrodes: Designed architectures and electrochemical performance. *Adv. Energy Mater.* **2017**, *7*, 1601301. [[CrossRef](#)]
246. Mao, X.; Hatton, T.A.; Rutledge, G.C. A review of electrospun carbon fibers as electrode materials for energy storage. *Curr. Org. Chem.* **2013**, *17*, 1390–1401. [[CrossRef](#)]
247. He, T.; Su, Q.; Yildiz, Z.; Cai, K.; Wang, Y. Ultrafine carbon fibers with hollow-porous multilayered structure for supercapacitors. *Electrochim. Acta* **2016**, *222*, 1120–1127. [[CrossRef](#)]
248. Pech, O.; Maensiri, S. Effect of Calcining Temperature on Electrospun Carbon Nanofibers for Supercapacitor. *J. Mater. Eng. Perform.* **2020**, *29*, 2386–2394. [[CrossRef](#)]
249. Kim, C.; Yang, K. Electrochemical properties of carbon nanofiber web as an electrode for supercapacitor prepared by electrospinning. *Appl. Phys. Lett.* **2003**, *83*, 1216–1218. [[CrossRef](#)]
250. Kim, C.; Park, S.-H.; Lee, W.-J.; Yang, K.-S. Characteristics of supercapacitor electrodes of PBI-based carbon nanofiber web prepared by electrospinning. *Electrochim. Acta* **2004**, *50*, 877–881. [[CrossRef](#)]
251. Ma, S.; Wang, Y.; Liu, Z.; Huang, M.; Yang, H.; Xu, Z.-L. Preparation of carbon nanofiber with multilevel gradient porous structure for supercapacitor and CO₂ adsorption. *Chem. Eng. Sci.* **2019**, *205*, 181–189. [[CrossRef](#)]
252. Lai, C.-C.; Lo, C.-T. Preparation of nanostructural carbon nanofibers and their electrochemical performance for supercapacitors. *Electrochim. Acta* **2015**, *183*, 85–93. [[CrossRef](#)]
253. Niu, H.; Zhang, J.; Xie, Z.; Wang, X.; Lin, T. Preparation, structure and supercapacitance of bonded carbon nanofiber electrode materials. *Carbon* **2011**, *49*, 2380–2388. [[CrossRef](#)]
254. He, T.-S.; Yu, X.-D.; Bai, T.-J.; Li, X.-Y.; Fu, Y.-R.; Cai, K.-D. Porous carbon nanofibers derived from PAA-PVP electrospun fibers for supercapacitor. *Ionics* **2020**, *26*, 4103–4111. [[CrossRef](#)]
255. Kim, J.-G.; Kim, H.-C.; Kim, N.D.; Khil, M.-S. N-doped hierarchical porous hollow carbon nanofibers based on PAN/PVP@SAN structure for high performance supercapacitor. *Compos. Part. B Eng.* **2020**, *186*, 107825. [[CrossRef](#)]
256. Ago, M.; Borghei, M.; Haataja, J.S.; Rojas, O.J. Mesoporous carbon soft-templated from lignin nanofiber networks: Microphase separation boosts supercapacitance in conductive electrodes. *RSC Adv.* **2016**, *6*, 85802–85810. [[CrossRef](#)]
257. Ishita, I.; Singhal, R. Porous multi-channel carbon nanofiber electrodes using discarded polystyrene foam as sacrificial material for high-performance supercapacitors. *J. Appl. Electrochem.* **2020**, *50*, 809–820. [[CrossRef](#)]
258. Lu, C.; Chen, X. Electrospun polyaniline nanofiber networks toward high-performance flexible supercapacitors. *Adv. Mater. Technol.* **2019**, *4*, 1900564. [[CrossRef](#)]
259. Miao, F.; Shao, C.; Li, X.; Lu, N.; Wang, K.; Zhang, X.; Liu, Y. Polyaniline-coated electrospun carbon nanofibers with high mass loading and enhanced capacitive performance as freestanding electrodes for flexible solid-state supercapacitors. *Energy* **2016**, *95*, 233–241. [[CrossRef](#)]
260. Chaudhari, S.; Sharma, Y.; Archana, P.S.; Jose, R.; Ramakrishna, S.; Mhaisalkar, S.; Srinivasan, M. Electrospun polyaniline nanofibers web electrodes for supercapacitors. *J. Appl. Polym. Sci.* **2013**, *129*, 1660–1668. [[CrossRef](#)]
261. Miao, Y.-E.; Fan, W.; Chen, D.; Liu, T. High-performance supercapacitors based on hollow polyaniline nanofibers by electrospinning. *ACS Appl. Mater. Interfaces* **2013**, *5*, 4423–4428. [[CrossRef](#)] [[PubMed](#)]
262. Sahoo, S.; Dhivar, S.; Das, C. Facile synthesis of polypyrrole nanofiber and its enhanced electrochemical performances in different electrolytes. *Express Polym. Lett.* **2012**, *6*, 965–974. [[CrossRef](#)]
263. Liu, J.; An, J.; Ma, Y.; Li, M.; Ma, R.; Yu, M.; Li, S. Electrochemical properties comparison of the polypyrrole nanotube and polyaniline nanofiber applied in supercapacitor. *Eur. Phys. J. Appl. Phys.* **2012**, *57*, 30702. [[CrossRef](#)]
264. Okuzaki, H.; Takahashi, T.; Miyajima, N.; Suzuki, Y.; Kuwabara, T. Spontaneous formation of poly(p-phenylenevinylene) nanofiber yarns through electrospinning of a precursor. *Macromolecules* **2006**, *39*, 4276–4278. [[CrossRef](#)]
265. Okuzaki, H.; Yan, H. *Uniaxially Aligned Poly(p-Phenylene Vinylene) and Carbon Nanofiber Yarns through Electrospinning of a Precursor*; Coondoo, I., Ed.; IntechOpen: London, UK, 2010; pp. 139–154.
266. Balakrishnan, K.; Kumar, M.; Angaiah, S. Synthesis of polythiophene and its carbonaceous nanofibers as electrode materials for asymmetric supercapacitors. *Adv. Mater. Res.* **2014**, *938*, 151–157. [[CrossRef](#)]
267. Jiang, H.; Ma, J.; Li, C. Mesoporous carbon incorporated metal oxide nanomaterials as supercapacitor electrodes. *Adv. Mater.* **2012**, *24*, 4197–4202. [[CrossRef](#)] [[PubMed](#)]
268. Kim, C.H.; Kim, B.-H. Zinc oxide/activated carbon nanofiber composites for high-performance supercapacitor electrodes. *J. Power Sources* **2015**, *274*, 512–520. [[CrossRef](#)]
269. Hyun, T.-S.; Tuller, H.L.; Youn, D.-Y.; Kim, H.-G.; Kim, I.-D. Facile synthesis and electrochemical properties of RuO₂ nanofibers with ionically conducting hydrous layer. *J. Mater. Chem.* **2010**, *20*, 9172–9179. [[CrossRef](#)]
270. Kolathodi, M.S.; Hanumantha Rao, S.N.; Natarajan, T.S.; Singh, G. Beaded manganese oxide (Mn₂O₃) nanofibers: Preparation and application for capacitive energy storage. *J. Mater. Chem. A* **2016**, *4*, 7883–7891. [[CrossRef](#)]
271. Kolathodi, M.S.; Palei, M.; Natarajan, T.S. Electrospun NiO nanofibers as cathode materials for high performance asymmetric supercapacitors. *J. Mater. Chem. A* **2015**, *3*, 7513–7522. [[CrossRef](#)]
272. Zhang, M.; Li, Q.; Fang, D.; Ayhan, I.A.; Zhou, Y.; Dong, L.; Xiong, C.; Wang, Q. NiO hierarchical hollow nanofibers as high-performance supercapacitor electrodes. *RSC Adv.* **2015**, *5*, 96205–96212. [[CrossRef](#)]
273. Kumar, M.; Subramania, A.; Balakrishnan, K. Preparation of electrospun Co₃O₄ nanofibers as electrode material for high performance asymmetric supercapacitors. *Electrochim. Acta* **2014**, *149*, 152–158. [[CrossRef](#)]

274. Simotwo, S.K.; DelRe, C.; Kalra, V. Supercapacitor electrodes based on high-purity electrospun polyaniline and polyaniline-carbon nanotube nanofibers. *ACS Appl. Mater. Interfaces* **2016**, *8*, 21261–21269. [[CrossRef](#)]
275. Sivakkumar, S.; Kim, W.J.; Choi, J.-A.; MacFarlane, D.R.; Forsyth, M.; Kim, D.-W. Electrochemical performance of polyaniline nanofibres and polyaniline/multi-walled carbon nanotube composite as an electrode material for aqueous redox supercapacitors. *J. Power Sources* **2007**, *171*, 1062–1068. [[CrossRef](#)]
276. Rose, A.; Prasad, K.G.; Sakthivel, T.; Gunasekaran, V.; Maiyalagan, T.; Vijayakumar, T. Electrochemical analysis of graphene oxide/polyaniline/polyvinyl alcohol composite nanofibers for supercapacitor applications. *Appl. Surf. Sci.* **2018**, *449*, 551–557. [[CrossRef](#)]
277. Rose, A.; Raghavan, N.; Thangavel, S.; Maheswari, B.U.; Nair, D.P.; Venugopal, G. Investigation of cyclic voltammetry of graphene oxide/polyaniline/polyvinylidene fluoride nanofibers prepared via electrospinning. *Mater. Sci. Semicond. Process.* **2015**, *31*, 281–286. [[CrossRef](#)]
278. Yanilmaz, M.; Dirican, M.; Asiri, A.M.; Zhang, X. Flexible polyaniline-carbon nanofiber supercapacitor electrodes. *J. Energy Storage* **2019**, *24*, 100766. [[CrossRef](#)]
279. Zhou, Z.; Wu, X.-F.; Hou, H. Electrospun carbon nanofibers surface-grown with carbon nanotubes and polyaniline for use as high-performance electrode materials of supercapacitors. *RSC Adv.* **2014**, *4*, 23622–23629. [[CrossRef](#)]
280. Anand, S.; Ahmad, M.W.; Ali Al Saidi, A.K.; Yang, D.-J.; Choudhury, A. Polyaniline nanofiber decorated carbon nanofiber hybrid mat for flexible electrochemical supercapacitor. *Mater. Chem. Phys.* **2020**, *254*, 123480. [[CrossRef](#)]
281. Zhu, J.; Zhang, Q.; Chen, H.; Zhang, R.; Liu, L.; Yu, J. *Setaria viridis*-inspired electrode with polyaniline decorated on porous heteroatom-doped carbon nanofibers for flexible supercapacitors. *ACS Appl. Mater. Interfaces* **2020**, *12*, 43634–43645. [[CrossRef](#)] [[PubMed](#)]
282. Jalil, N.A.; Mohd Abdah, M.A.A.; Azman, N.H.N.; Sulaiman, Y. Polyaniline and manganese oxide decorated on carbon nanofibers as a superior electrode material for supercapacitor. *J. Electroanal. Chem.* **2020**, *867*, 114188. [[CrossRef](#)]
283. Kshetri, T.; Tran, D.T.; Nguyen, D.C.; Kim, N.H.; Lau, K.-T.; Lee, J.H. Ternary graphene-carbon nanofibers-carbon nanotubes structure for hybrid supercapacitor. *Chem. Eng. J.* **2020**, *380*, 122543. [[CrossRef](#)]
284. Fu, H.; Zhang, X.; Fu, J.; Shen, G.; Ding, Y.; Chen, Z.; Du, H. Single layers of MoS₂/graphene nanosheets embedded in activated carbon nanofibers for high-performance supercapacitor. *J. Alloys Compd.* **2020**, *829*, 154557. [[CrossRef](#)]
285. Dai, Z.; Ren, P.-G.; He, W.; Hou, X.; Ren, F.; Zhang, Q.; Jin, Y.-L. Boosting the electrochemical performance of nitrogen-oxygen co-doped carbon nanofibers based supercapacitors through esterification of lignin precursor. *Renew. Energy* **2020**, *162*, 613–623. [[CrossRef](#)]
286. Zhang, X.; Cui, X.; Lu, C.-H.; Li, H.; Zhang, Q.; He, C.; Yang, Y. Conjugated polyimide-coated carbon nanofiber aerogels in a redox electrolyte for binder-free supercapacitors. *Chem. Eng. J.* **2020**, *401*, 126031. [[CrossRef](#)]
287. Mukhiya, T.; Ojha, G.P.; Dahal, B.; Kim, T.; Chhetri, K.; Lee, M.; Chae, S.-H.; Muthurasu, A.; Tiwari, A.P.; Kim, H.Y. Designed assembly of porous cobalt oxide/carbon nanotentacles on electrospun hollow carbon nanofibers network for supercapacitor. *ACS Appl. Energy Mater.* **2020**, *3*, 3435–3444. [[CrossRef](#)]
288. Kolathodi, M.S.; Palei, M.; Natarajan, T.S.; Singh, G. MnO₂ encapsulated electrospun TiO₂ nanofibers as electrodes for asymmetric supercapacitors. *Nanotechnology* **2020**, *31*, 125401. [[CrossRef](#)] [[PubMed](#)]
289. Jeong, J.H.; Kim, Y.A.; Kim, B.-H. Electrospun polyacrylonitrile/cyclodextrin-derived hierarchical porous carbon nanofiber/MnO₂ composites for supercapacitor applications. *Carbon* **2020**, *164*, 296–304. [[CrossRef](#)]
290. Yang, S.; Ai, J.; Han, Z.; Zhang, L.; Zhao, D.; Wang, J.; Yang, C.; Cao, B. Electrospun ZnFe₂O₄/carbon nanofibers as high-rate supercapacitor electrodes. *J. Power Sources* **2020**, *469*, 228416. [[CrossRef](#)]
291. Hao, X.; Bi, J.; Wang, W.; Yan, W.; Gao, X.; Sun, X.; Liu, R. Electrospun Fe₂MoC/C nanofibers as an efficient electrode material for high-performance supercapacitors. *J. Power Sources* **2020**, *451*, 227802. [[CrossRef](#)]
292. Dirican, M.; Yanilmaz, M.; Asiri, A.M.; Zhang, X. Polyaniline/MnO₂/porous carbon nanofiber electrodes for supercapacitors. *J. Electroanal. Chem.* **2020**, *861*, 113995. [[CrossRef](#)]
293. He, Y.; Liu, L.; Tao, S.; Ye, J.; Wu, J.; Xu, C.; Guo, Q. Hierarchically hollow NiCo₂S₄/graphitic nanofiber film with ultrahigh-rate capability and long-term cycling durability for asymmetrical supercapacitor. *Ionics* **2020**, *27*, 305–314. [[CrossRef](#)]
294. Yang, X.; Mao, L.; Peng, W.; Jin, J.; Yang, S.; Li, G. Synthesis of double-layered NiCo₂O₄-nanosheet-loaded PAN/lignin-based hollow carbon nanofibers for high-performance supercapacitor. *Chem. Sel.* **2020**, *5*, 2602–2609.
295. Chapin, M.; Fuller, C.S.; Pearson, G.L. A new silicon *p-n* junction photocell for converting solar radiation into electrical power. *J. Appl. Phys.* **1954**, *25*, 676. [[CrossRef](#)]
296. Veith, B.; Ohrdes, T.; Werner, F.; Brendel, R.; Altermatt, P.P.; Harder, N.-P.; Schmidt, J. Injection dependence of the effective lifetime of *n*-type Si passivated by Al₂O₃: An edge effect? *Sol. Energy Mater. Sol. Cells* **2014**, *120A*, 436–440. [[CrossRef](#)]
297. Gerischer, H. Electrochemical photo and solar cells principles and some experiments. *J. Electroanal. Chem. Interfacial Electrochem.* **1975**, *58*, 263–274. [[CrossRef](#)]
298. Lewerenz, H.J.; Goslowsky, H.; Husemann, K.-D.; Fiechter, S. Efficient solar energy conversion with CuInS₂. *Nature* **1986**, *321*, 687–688. [[CrossRef](#)]
299. Stempel, T.; Aggour, M.; Skorupska, K.; Munoz, A.; Lewerenz, H.-J. Efficient photoelectrochemical nanoemitter solar cell. *Electrochem. Commun.* **2008**, *10*, 1184–1186. [[CrossRef](#)]

300. Lewerenz, H.J. Operational principles of electrochemical nanoemitter solar cells for photovoltaic and photoelectrocatalytic applications. *J. Electroanal. Chem.* **2011**, *662*, 184–195. [[CrossRef](#)]
301. Kar, S.; Rajeshwar, K.; Singh, P.; DuBow, J. On the design and operation of electrochemical solar cells. *Sol. Energy* **1979**, *23*, 129–139. [[CrossRef](#)]
302. Shalini, S.; Balasundaraprabhu, R.; Satish Kumar, T.; Prabavathy, N.; Senthilarasu, S.; Prasanna, S. Status and outlook of sensitizers/dyes used in dye sensitized solar cells (DSSC): A review. *Int. J. Energy Res.* **2016**, *40*, 1303–1320. [[CrossRef](#)]
303. Kumara, N.T.R.N.; Lim, A.; Lim, C.M.; Petra, M.I.; Ekanayake, P. Recent progress and utilization of natural pigments in dye sensitized solar cells: A review. *Renew. Sustain. Energy Rev.* **2017**, *78*, 301–317. [[CrossRef](#)]
304. Boro, B.; Gogoi, B.; Rajbongshi, B.M.; Ramchiary, A. Nano-structures TiO₂/ZnO nanocomposite for dye-sensitized solar cells application: A review. *Renew. Sustain. Energy Rev.* **2018**, *81*, 2264–2270. [[CrossRef](#)]
305. Zainudin, S.N.F.; Abdullah, H.; Markom, M. Electrochemical studies of tin oxide based-dye-sensitized solar cells (DSSC): A review. *J. Mater. Sci. Mater. Electron.* **2019**, *30*, 5342–5356. [[CrossRef](#)]
306. Kumar, D.K.; Kriz, J.; Bennett, N.; Chen, B.X.; Upadhayaya, H.; Reddy, K.R.; Sadhu, V. Functionalized metal oxide nanoparticles for efficient dye-sensitized solar cells (DSSCs): A review. *Mater. Sci. Energy Technol.* **2020**, *3*, 472–481. [[CrossRef](#)]
307. Petrus, M.L.; Schlipf, J.; Li, C.; Gujar, T.P.; Giesbrecht, N.; Müller-Buschbaum, P.; Thelakkat, M.; Bein, T.; Hüttner, S.; Docampo, P. Capturing the sun: A review of the challenges and perspectives of perovskite solar cells. *Adv. Energy Mater.* **2017**, *7*, 1700264. [[CrossRef](#)]
308. Ansari, M.I.H.; Qurashi, A.; Nazeeruddin, M.K. Frontiers, opportunities, and challenges in perovskite solar cells: A critical review. *J. Photochem. Photobiol. C Photochem. Rev.* **2018**, *35*, 1–24. [[CrossRef](#)]
309. Uddin, A.; Upama, M.B.; Yi, H.M.; Duan, L.P. Encapsulation of organic and perovskite solar cells: A review. *Coatings* **2019**, *9*, 65. [[CrossRef](#)]
310. Roy, P.; Sinha, M.K.; Tiwari, S.; Khare, Y. A review on perovskite solar cells: Evolution of architecture, fabrication techniques, commercialization issues and status. *Sol. Energy* **2020**, *198*, 665–688. [[CrossRef](#)]
311. Urbina, A. The balance between efficiency, stability and environmental impacts in perovskite solar cells: A review. *J. Phys. Energy* **2020**, *2*, 022001. [[CrossRef](#)]
312. Vijayaraghavan, S.N.; Ashok, A.; Gopakumar, G.; Menon, H.; Nair, S.V.; Shanmugam, M. All spray pyrolysis-coated CdTe–TiO₂ heterogeneous films for photo-electrochemical solar cells. *Mater. Renew. Sustain. Energy* **2018**, *7*, 12. [[CrossRef](#)]
313. Hazra, M.; Jana, A.; Datta, J. Improved stability toward photo-electrochemical behavior of multi-chalcogenide CdSeS thin films. *Appl. Surf. Sci.* **2018**, *454*, 334–342. [[CrossRef](#)]
314. Kissinger, S. Structural and photo electrochemical (PEC) cell properties of Cd_{1-x}Zn_xSe films. *J. Environ. Nanotechnol.* **2020**, *9*, 5–10.
315. Tenne, R.; Wold, A. Passivation of recombination centers in *n*-WSe₂ yields high efficiency (>14%) photo-electrochemical cell. *Appl. Phys. Lett.* **1985**, *47*, 707. [[CrossRef](#)]
316. Prasad, G.; Srivastava, O.N. The high-efficiency (17.1%) WSe₂ photo-electrochemical solar cell. *J. Phys. D* **1988**, *21*, 1028. [[CrossRef](#)]
317. Huang, S.H.; Li, Q.N.; Chi, D.; Meng, X.Q.; He, L. Simulation approach for optimization of ZnO/c-WSe₂ heterojunction solar cells. *J. Semicond.* **2017**, *38*, 044008. [[CrossRef](#)]
318. Aljafari, B.; Ram, M.K.; Takshi, A. Integrated electrochemical energy storage and photovoltaic device with a gel electrolyte. *Proc. SPIE* **2019**, *10913*, 1091318.
319. Lashgari, N.; Badiie, A.; Mohammadi Ziarani, G. Modification of mesoporous silica SBA-15 with different organic molecules to gain chemical sensors: A review. *Nanochem. Res.* **2016**, *1*, 127–141.
320. Samokhvalov, A. Analysis of various solid samples by synchronous fluorescence spectroscopy and related methods: A review. *Talanta* **2020**, *216*, 120944. [[CrossRef](#)]
321. Wei, F.; Patel, P.; Liao, W.; Chaudhry, K.; Zhang, L.; Arellano-Garcia, M.; Hu, S.; Elashoff, D.; Zhou, H.; Shukla, S. Electrochemical sensor for multiplex biomarkers detection. *Clin. Cancer Res.* **2009**, *15*, 4446–4452. [[CrossRef](#)] [[PubMed](#)]
322. Clark, L.C., Jr.; Wolf, R.; Granger, D.; Taylor, Z. Continuous recording of blood oxygen tensions by polarography. *J. Appl. Physiol.* **1953**, *6*, 189–193. [[CrossRef](#)]
323. Mondal, K.; Sharma, A. Recent advances in electrospun metal-oxide nanofiber based interfaces for electrochemical biosensing. *RSC Adv.* **2016**, *6*, 94595–94616. [[CrossRef](#)]
324. Vamvakaki, V.; Tsagaraki, K.; Chaniotakis, N. Carbon nanofiber-based glucose biosensor. *Anal. Chem.* **2006**, *78*, 5538–5542. [[CrossRef](#)] [[PubMed](#)]
325. Chen, K.; Chou, W.; Liu, L.; Cui, Y.; Xue, P.; Jia, M. Electrochemical sensors fabricated by electrospinning technology: An overview. *Sensors* **2019**, *19*, 3676. [[CrossRef](#)]
326. Ren, G.; Xu, X.; Liu, Q.; Cheng, J.; Yuan, X.; Wu, L.; Wan, Y. Electrospun poly(vinyl alcohol)/glucose oxidase biocomposite membranes for biosensor applications. *React. Funct. Polym.* **2006**, *66*, 1559–1564. [[CrossRef](#)]
327. Arecchi, A.; Scampicchio, M.; Brenna, O.V.; Mannino, S. Biocatalytic nylon nanofibrous membranes. *Anal. Bioanal. Chem.* **2010**, *398*, 3097–3103. [[CrossRef](#)]
328. Sapountzi, E.; Chateaux, J.-F.; Lagarde, F. Combining electrospinning and vapor-phase polymerization for the production of polyacrylonitrile/polypyrrole core-shell nanofibers and glucose biosensor application. *Front. Chem.* **2020**, *8*, 678. [[CrossRef](#)] [[PubMed](#)]

329. Yezer, I.; Demirkol, D.O. Cellulose acetate—Chitosan based electrospun nanofibers for bio-functionalized surface design in biosensing. *Cellulose* **2020**, *27*, 10183–10197. [[CrossRef](#)]
330. Apetrei, R.-M.; Camurlu, P. The effect of montmorillonite functionalization on the performance of glucose biosensors based on composite montmorillonite/PAN nanofibers. *Electrochim. Acta* **2020**, *353*, 136484. [[CrossRef](#)]
331. Mehdizadeh, B.; Maleknia, L.; Amirabadi, A.; Shabani, M. Glucose sensing by a glassy carbon electrode modified with glucose oxidase/chitosan/graphene oxide nanofibers. *Diam. Relat. Mater.* **2020**, *109*, 108073. [[CrossRef](#)]
332. Kholosi, F.; Afkhami, A.; Hashemi, P.; Madrakian, T.; Bagheri, H. Bioelectrocatalysis and direct determination of H₂O₂ using the high-performance platform: Chitosan nanofibers modified with SDS and hemoglobin. *J. Iran. Chem. Soc.* **2020**, *17*, 1401–1409. [[CrossRef](#)]
333. Kutlu, N.; İspirli Doğaç, Y.; Deveci, İ.; Teke, M. Urease immobilized electrospun PVA/chitosan nanofibers with improved stability and reusability characteristics: An application for removal of urea from artificial blood serum. *Prep. Biochem. Biotechnol.* **2020**, *50*, 425–437. [[CrossRef](#)]
334. Huang, J.; Liu, Y.; You, T. Carbon nanofiber based electrochemical biosensors: A review. *Anal. Methods* **2010**, *2*, 202–211. [[CrossRef](#)]
335. Wu, L.; Zhang, X.; Ju, H. Amperometric glucose sensor based on catalytic reduction of dissolved oxygen at soluble carbon nanofiber. *Biosens. Bioelectron.* **2007**, *23*, 479–484. [[CrossRef](#)]
336. Bae, T.-S.; Shin, E.; Im, J.S.; Kim, J.G.; Lee, Y.-S. Effects of carbon structure orientation on the performance of glucose sensors fabricated from electrospun carbon fibers. *J. Non-Cryst. Solids* **2012**, *358*, 544–549. [[CrossRef](#)]
337. Liu, Y.; Wang, D.; Xu, L.; Hou, H.; You, T. A novel and simple route to prepare a Pt nanoparticle-loaded carbon nanofiber electrode for hydrogen peroxide sensing. *Biosens. Bioelectron.* **2011**, *26*, 4585–4590. [[CrossRef](#)] [[PubMed](#)]
338. Kim, S.G.; Jun, J.M.; Kim, Y.K.; Kim, J.W.; Lee, J.S.; Jang, J.S. Facile synthesis of Co₃O₄-incorporated multichannel carbon nanofibers for electrochemical applications. *ACS Appl. Mater. Interfaces* **2020**, *12*, 20613–20622. [[CrossRef](#)] [[PubMed](#)]
339. Simsek, M.; Hoecherl, K.; Schlosser, M.; Bäumner, A.J.; Wongkaew, N.N. Printable 3D carbon nanofiber networks with embedded metal nanocatalysts. *ACS Appl. Mater. Interfaces* **2020**, *12*, 39533–39540. [[CrossRef](#)]
340. Yang, B.; Bin, D.; Tian, T.; Liu, Y.; Liu, B. An ordered mesoporous carbon nanofiber array for the sensitive electrochemical detection of malachite green. *ChemElectroChem* **2020**, *7*, 659–664. [[CrossRef](#)]
341. Jahromi, Z.; Mirzaei, E.; Savardashtaki, A.; Afzali, M.; Afzali, Z. A rapid and selective electrochemical sensor based on electrospun carbon nanofibers for tramadol detection. *Microchem. J.* **2020**, *157*, 104942. [[CrossRef](#)]
342. Fakude, C.T.; Arotiba, O.A.; Arduini, F.; Mabuba, N. Flexible Polyester Screen-printed Electrode Modified with Carbon Nanofibers for the Electrochemical Aptasensing of Cadmium (II). *Electroanalysis* **2020**, *32*, 2650–2658. [[CrossRef](#)]
343. Sasal, A.; Tyszczyk-Rotko, K.; Chojceki, M.; Korona, T.; Nosal-Wiercińska, A. Direct determination of paracetamol in environmental samples using screen-printed carbon/carbon nanofibers sensor—experimental and theoretical studies. *Electroanalysis* **2020**, *32*, 1618–1628. [[CrossRef](#)]
344. Aryal, K.P.; Jeong, H.K. Carbon nanofiber modified with reduced graphite oxide for detection of ascorbic acid, dopamine, and uric acid. *Chem. Phys. Lett.* **2020**, *739*, 136969. [[CrossRef](#)]
345. Prasad Aryal, K.; Kyung Jeong, H. Electrochemical detection of ascorbic acid with chemically functionalized carbon nanofiber/β-cyclodextrin composite. *Chem. Phys. Lett.* **2020**, *757*, 137881. [[CrossRef](#)]
346. Kaçar, C.; Erden, P.E. An amperometric biosensor based on poly(l-aspartic acid), nanodiamond particles, carbon nanofiber, and ascorbate oxidase-modified glassy carbon electrode for the determination of l-ascorbic acid. *Anal. Bioanal. Chem.* **2020**, *412*, 5315–5327. [[CrossRef](#)] [[PubMed](#)]
347. Saunier, V.; Flahaut, E.; Blatché, M.-C.; Bergaud, C.; Maziz, A. Carbon nanofiber-PEDOT composite films as novel microelectrode for neural interfaces and biosensing. *Biosens. Bioelectron.* **2020**, *165*, 112413. [[CrossRef](#)]
348. Yang, S.; Yang, M.; Yao, X.; Fa, H.; Wang, Y.; Hou, C. A zeolitic imidazolate framework/carbon nanofiber nanocomposite based electrochemical sensor for simultaneous detection of co-existing dihydroxybenzene isomers. *Sens. Actuators B Chem.* **2020**, *320*, 128294. [[CrossRef](#)]
349. George, J.M.; Antony, A.; Mathew, B. Metal oxide nanoparticles in electrochemical sensing and biosensing: A review. *Microchim. Acta* **2018**, *185*, 1–26. [[CrossRef](#)] [[PubMed](#)]
350. Huang, A.; He, Y.; Zhou, Y.; Zhou, Y.; Yang, Y.; Zhang, J.; Luo, L.; Mao, Q.; Hou, D.; Yang, J. A review of recent applications of porous metals and metal oxide in energy storage, sensing and catalysis. *J. Mater. Sci.* **2019**, *54*, 949–973. [[CrossRef](#)]
351. Li, L.; Mun Lee, P.; Yang, G.; Liu, E. A review on electrospun nanofibers-based electrochemical sensor. *Curr. Nanosci.* **2015**, *11*, 710–721. [[CrossRef](#)]
352. Salandari-Jolge, N.; Ensafi, A.A.; Rezaei, B. A novel three-dimensional network of CuCr₂O₄/CuO nanofibers for voltammetric determination of anticancer drug methotrexate. *Anal. Bioanal. Chem.* **2020**, *412*, 2443–2453. [[CrossRef](#)]
353. Veeralingam, S.; Badhulika, S. Strain engineered biocompatible h-WO₃ nanofibers based highly selective and sensitive chemiresistive platform for detection of Catechol in blood sample. *Mater. Sci. Eng. C* **2020**, *108*, 110365. [[CrossRef](#)]
354. Oliveira, V.H.B.; Rehotnek, F.; da Silva, E.P.; Marques, V.d.S.; Rubira, A.F.; Silva, R.; Lourenço, S.A.; Muniz, E.C. A sensitive electrochemical sensor for Pb²⁺ ions based on ZnO nanofibers functionalized by L-cysteine. *J. Mol. Liq.* **2020**, *309*, 113041. [[CrossRef](#)]
355. He, Y.; Wu, T.; Wang, J.; Ye, J.; Xu, C.; Li, F.; Guo, Q. A sensitive pyrimethanil sensor based on porous NiCo₂S₄/graphitized carbon nanofiber film. *Talanta* **2020**, *219*, 121277. [[CrossRef](#)]

356. Xie, H.; Luo, G.; Niu, Y.; Weng, W.; Zhao, Y.; Ling, Z.; Ruan, C.; Li, G.; Sun, W. Synthesis and utilization of Co_3O_4 doped carbon nanofiber for fabrication of hemoglobin-based electrochemical sensor. *Mater. Sci. Eng. C* **2020**, *107*, 110209. [[CrossRef](#)] [[PubMed](#)]
357. Rani, S.D.; Ramachandran, R.; Sheet, S.; Aziz, M.A.; Lee, Y.S.; Al-Sehemi, A.G.; Pannipara, M.; Xia, Y.; Tsai, S.-Y.; Ng, F.-L.; et al. NiMoO_4 nanoparticles decorated carbon nanofiber membranes for the flexible and high performance glucose sensors. *Sens. Actuators B Chem.* **2020**, *312*, 127886. [[CrossRef](#)]
358. Shamsabadi, A.S.; Tavanai, H.; Ranjbar, M.; Farnood, A.; Bazarganipour, M. Electrochemical non-enzymatic sensing of glucose by gold nanoparticles incorporated graphene nanofibers. *Mater. Today Commun.* **2020**, *24*, 100963. [[CrossRef](#)]
359. Wei, J.; Yin, Z.; Zeng, X.; Allado, K.; Ji, Z.; Sheardy, A.; Arvapalli, D. Binary $\text{MnO}_2/\text{Co}_3\text{O}_4$ well-aligned electrospun carbon nanofibers for sensitive, nonenzymatic glucose sensing. In Proceedings of the 237th ECS Meeting with the 18th International Meeting on Chemical Sensors (IMCS 2020), Montreal, QC, Canada, 10–14 May 2020.
360. Shekh, M.I.; Amirian, J.; Du, B.; Kumar, A.; Sharma, G.; Stadler, F.J.; Song, J. Electrospun ferric ceria nanofibers blended with MWCNTs for high-performance electrochemical detection of uric acid. *Ceram. Int.* **2020**, *46*, 9050–9064. [[CrossRef](#)]
361. Supraja, P.; Singh, V.; Vanjari, S.R.K.; Singh, S.G. Electrospun CNT embedded ZnO nanofiber based biosensor for electrochemical detection of Atrazine: A step closure to single molecule detection. *Microsyst. Nanoeng.* **2020**, *6*, 1–10. [[CrossRef](#)]
362. Riaz, M.A.; Yuan, Z.; Mahmood, A.; Liu, F.; Sui, X.; Chen, J.; Huang, Q.; Liao, X.; Wei, L.; Chen, Y. Hierarchically porous carbon nanofibers embedded with cobalt nanoparticles for efficient H_2O_2 detection on multiple sensor platforms. *Sens. Actuators B Chem.* **2020**, *319*, 128243. [[CrossRef](#)]
363. Xie, H.; Niu, Y.; Deng, Y.; Cheng, H.; Ruan, C.; Li, G.; Sun, W. Electrochemical aptamer sensor for highly sensitive detection of mercury ion with Au/Pt@carbon nanofiber-modified electrode. *J. Chin. Chem. Soc.* **2021**, *68*, 114–120. [[CrossRef](#)]
364. Zhou, S.; Hu, M.; Huang, X.; Zhou, N.; Zhang, Z.; Wang, M.; Liu, Y.; He, L. Electrospun zirconium oxide embedded in graphene-like nanofiber for aptamer-based impedimetric bioassay toward osteopontin determination. *Microchim. Acta* **2020**, *187*, 1–9. [[CrossRef](#)]
365. Zhu, L.; Wang, Y.; Ai, Z.; Zhang, X.; Li, X.; Zhang, X.; Sun, W. Titanium dioxide nanoparticle and carbon nanotube incorporated carbon nanofiber nanocomposite modified electrode for hemoglobin electrochemistry. *Int. J. Electrochem. Sci.* **2020**, *15*, 4712–4721. [[CrossRef](#)]
366. Ansari, S.H.; Arvand, M. A magnetic nanocomposite prepared from electrospun CoFe_2O_4 nanofibers and graphene oxide as a material for highly sensitive determination of rutin. *Microchim. Acta* **2020**, *187*, 103. [[CrossRef](#)]
367. Yin, D.; Liu, J.; Bo, X.; Guo, L. Cobalt-iron selenides embedded in porous carbon nanofibers for simultaneous electrochemical detection of trace of hydroquinone, catechol and resorcinol. *Anal. Chim. Acta* **2020**, *1093*, 35–42. [[CrossRef](#)] [[PubMed](#)]